BresDefender

The effect of an emergency measure on the phreatic surface of a dike in space and time

D.P. Hommes

TU Delft

BresDefender:

The effect of an emergency measure on the phreatic surface of a dike in space and time

MSc. Thesis

By

D.P. Hommes
4359356

in partial fulfilment of the requirements for the degree of

Master of Science
in Hydraulic Engineering

at the Delft University of Technology,
to be defended publicly on Wednesday August 24, 2022

Graduation committee:

Dr. C. Zwanenburg (Chair)	TU Delft, Deltares
Dr. P.J. Vardon	TU Delft
Dr. R.C. Lanzafame	TU Delft
Ir. D. Janssen	TU Delft

TU Delft

Preface

Before you lies the thesis “Bresdefender: the effect of an emergency measure on the phreatic surface of a dike in space and time” which is written as final part of the master programme Hydraulic Engineering with a specialization in Flood Risk at the Delft University of Technology (TU Delft). This thesis is overseen by Dr. Cor Zwanenburg, Dr. Phil Vardon, Dr. Robert Lanzafame and Ir. Danny Janssen.

This thesis was undertaken as part of a larger study related to a specific emergency measure for dike safety, named the BresDefender. The general topic of this thesis was therefore known, but by developing my own research questions, approach, and method this thesis has found its own path in solving the mysterious ways of the BresDefender. The multi-dimensional approach with both a numerical and physical model on different scales made my research quite extensive, but it has allowed me to formulate a more nuanced answer to the main research question.
This thesis has also broadened my horizon with regards to emergency measures for flood defences. In the past, this field of flood risk management has been abandoned in Dutch hydraulic engineering practice, however, with increase of climate change and the associated increase of flood events, application of emergency measures may become more useful in the future. For this reason, I myself want to keep working during my career as hydraulic engineer towards a future where people are safe against flooding at home and abroad.

First, I would like to thank my graduation committee. Cor Zwanenburg for being the chair of the committee and always making time for our profound discussions regarding soil and groundwater flow. Phil Vardon and Robert Lanzafame for their time and expertise, guiding my start and finalization of my thesis in the right direction. At last, I would like to thank my daily supervisor Danny Janssen, not only for the free cups of coffee during our weekly discussions, but also for your feedback and support especially for the fieldwork at Flood Proof Holland, which would not have been possible without your help.

Furthermore, I want to mention a couple people that helped me during my thesis. First, I would like to thank Jean-Paul de Garde for his assistance during the fieldwork at Flood Proof Holland, especially when the water pump broke down. Second, I also want to thank Enno van Waardenburg and Jelle Molenaar from Deltares for providing the data logger and software to read the sensors during my fieldwork. Last, I would like to thank Jolanda van Haagen for her assistance during my soil investigation at the Geoscience and Engineering Laboratory.

Last but not least, I want to thank my family and friends. My parents and sisters for their unconditional support and interest in my thesis. Also, my grandparents and uncle for coming to see me during my fieldwork. My friends for their interest and distractions whether they were necessary or not. My roommate for his interest and thoughts on my thesis.

I am delighted to present my thesis and hope you enjoy reading it!

Dewa Hommes
Delft, August 2022

Abstract

New solutions for future flooding problems are becoming more important than ever before. Emergency measures against failure of flood defenses may play an important role in flood risk management and is therefore currently being investigated. One of these measures is the BresDefender, which is a submersible floating pontoon that can be placed on the outer slope of a weakened dike section to prevent or delay failure. The application of the BresDefender can be divided into two scenarios: (1) to stop breach formation and (2) to limit water infiltration into the dike. The latter application scenario is expected to influence the development of the phreatic surface inside the dike, which affects dike safety. This study focuses on this scenario by assessing the effect of this seal on the development of the phreatic surface.

A numerical modelling approach is developed to describe this effect using the finite element method program PLAXIS, with add-on module PlaxFlow, to describe transient groundwater flow problems. This numerical modelling process starts off with the development of a model for a laboratory scale dike. In a previous study at the WaterLab, the phreatic surface level of the dike was measured over time for different degrees of sealing using a steel plate. These measurements are used to calibrate the numerical model, where the connection between seal and dike slope is described with a transmissive interface layer. It is concluded that this interface layer approximates the effect of the seal on the phreatic surface adequately.
The next step is to extent the numerical model to a larger scale dike consisting of heterogeneous soils. This model represents the dike located in the Flood Proof Holland test facility, which consists of a permeable core covered by a low-permeability layer. By modelling this transition from simple to complex, influences of permeability, heterogeneity, and damage of the cover on the phreatic surface are identified.

The effect of a seal on the phreatic surface is also studied using physical model tests of the dike at Flood Proof Holland. The position of the phreatic surface is measured by pressure sensors in standpipes, which are spread over the crest and inner slope of the dike. Different scenarios for the seal are examined: stiff plate, flexible textile, and no emergency measure (reference case). For every scenario, experiments are carried out with and without a damaged location in the outer slope of the dike, which lead to a total of six test cases.
The results of the physical model tests show multiple effects of the seal on the phreatic surface. First, the seal shows a delaying effect on the position of the phreatic surface, which implies that the seal delays the rise of the phreatic surface over time. The time until the phreatic surface reached a steady-state over the entire dike was increased with around 15% for plate cases and around 25% for textile cases when compared to the corresponding reference cases. Second, no decreasing effect on the phreatic surface can be observed, which means that the phreatic surface level in its steady-state condition is not affected by the placement of a seal on the outer slope. Third, the delaying effect is larger for a seal that consists of a flexible textile rather than a stiff plate. The connection between seal and dike cover is proved to be important since leakages underneath the seal influence its performance, especially when the dike is locally damaged.
Last, the textile seal has a three-dimensional effect on the development of the phreatic surface. A certain area of influence can be identified where the phreatic surface is affected. The effect of the phreatic surface is seen to be stronger for locations near the textile and this effect diminishes over time. For the textile case on a damaged dike, an initial decrease of the phreatic level is observed directly behind the textile ranging up to 30 cm.

Overall, the effect of a seal on the development of the phreatic surface is concluded to be relatively small. The effect is only of a time-varying nature and, in three dimensions, the effect diminishes for larger distances. The application of a textile in terms of dike safety shows only a marginal improvement, which occurs only in a limited time period.

Table of Contents

1 Introduction 1
1.1 Background 1
1.2 Conceptual model 5
1.3 Research questions 7
1.4 Research method 8
2 Theory 9
2.1 Pore water pressure 9
2.2 Groundwater flow 14
2.3 Phreatic surface in dikes 20
3 Numerical Modelling 22
3.1 Modelling process 22
3.2 Soil parameters 23
3.3 WaterLab experiments 25
3.4 FPH experiments 33
4 Physical Modelling 36
4.1 Model 36
4.2 Materials 38
4.3 Method 39
4.4 Hypothesis 44
5 Results 45
5.1 Data output 45
5.2 Analysis of effects 47
5.3 3D approach 53
6 Calibration and dike safety 56
6.1 Calibration of numerical model 56
6.2 Dike safety analysis 62
7 Discussion 64
7.1 Interpretation of effects 64
7.2 Assumptions and limitations 65
8 Conclusions and recommendations 67
8.1 Conclusions 67
8.2 Recommendations 69

A. Theory 79
A.1 Numerical model selection 79
A.2 Limit Equilibrium Methods 80
B. Soil Investigation 81
B.1 Goal 81
B.2 KSAT experiments 81
B.3 HYPROP experiments 81
B.4 WaterLab experiments 81
C. Physical modelling 82
C.1 Sensor specifications 82
C.2 Data logger 83
C.3 Infiltrometer 84
D. Dike Safety 88
D.1 Macro stability 88
D.2 Micro stability 89
E. Flood Proof Holland 91
E.1 Leakage paths 91
E.2 After-construction state of dike 94

1 Introduction

In section 1.1, the background of the BresDefender as emergency measure is discussed to explain the concept, its use and effect. In section 1.2, a conceptual model is proposed of the intended effects based on physical reasoning. In section 1.3, the main research question is formed based on multiple sub questions, which will give a direction for this thesis. In section 1.4, the outline of this thesis is discussed with the different components that will form this thesis.

1.1 Background

1.1.1 Current state of emergency measures

The Netherlands has a global reputation in its expertise in the field of Hydraulic Engineering and, more specifically, its success in flood control. After the devastating North Sea flood of 1953, the Netherlands developed an integral flood defense system, which is known as the Delta Works.
This battle against flooding matured over the years. Laws and regulations such as The Water Act integrate different authorities and organizations to prevent flooding. The national High Water Protection Program (NL: Hoogwaterbeschermingsprogramma) mainly focuses on strengthening existing dikes and hydraulic structures to fulfill the safety requirements that are imposed by climate change. (Rijkswaterstaat, 2022) The need for protection of valuable low-lying land is assessed from a flood risk approach, which aims to set acceptable limits for flooding based on fatalities, economic damages, and the probability of occurrence of floodings. (Jonkman, Kok, & Vrijling, 2008)
This current approach will most likely result in strengthening and enlarging the current water defense structures to meet future demands. Besides the implementation of preventive measures, spatial planning and disaster control have more recently been added to the Dutch water safety strategy (Fokkens, 2006). Some large-scale measures regarding spatial planning have already been carried out, such as Room for the River (Rijkswaterstaat, 2021), but measures for disaster control are rarely used nowadays.

One of the applications for disaster control is the implementation of emergency response measures for dike failure. These measures can be applied when an imminent threat of flooding is present and these measures must be taken in a short time frame. The aim of these interventions is to stop the dike from failing or to increase the time until failure occurs. By increasing the time to failure, the dike will still fail but evacuation of the hinterland may be more successful. For extreme conditions with a short duration, extending the time to failure beyond the duration of that extreme event may limit the chance of dike failure and may even prevent flooding.

1.1.2 Failure

When assessing stability of flood defences, it is useful to distinguish between failure and collapse of the structure. We speak of failure when the flood defense system does not fulfill one or more of its functions and of collapse when a structure loses cohesion or deforms severely. (De Bruijn, De Vries, & `t Hart, 2018)
A flood defense can thus fail without collapsing and vice-versa. For example, water can flow over a barrier and let the hinterland flood, which indicates failure of the structure to perform its function, but the barrier itself does not have to collapse. Besides failure for cases with high-water conditions, a barrier can also fail at low water levels without the structure collapsing. A ship can for example damage the structure locally in case of a collision, which compromises the safety of the structure but will not induce collapse necessarily.
On the contrary, a hydraulic structure can also collapse without failure. For example, when a dike experiences a rapid drawdown condition after a long period of high-water part of the outer slope can slide down due to excess pore water pressures. (Deltares, n.d.) The deformed dike may in

such case still be capable of performing its functions initially, but eventually such deformations are expected to lead to failure if no repair works are done.

Whether a flood defense system fails or collapses, is determined by the geometry and material properties of the barrier on the one hand and the threats and loads on the other hand. The primary threat to the functioning of flood defenses are high water levels and waves. Numerous physical, biological, and human factors can affect the water retaining capacity and thus pose a threat. (Schiereck, 1998)
The application of the BresDefender is mainly intended as emergency measure for damaged dikes where high-water conditions are expected at short notice. The focus of this study is to relate the application of the BresDefender to changes in phreatic surface of the dike for extreme conditions. The phreatic surface is mostly influenced by external water levels rather than wave overtopping. A study to determine the phreatic surface for the Afsluitdijk by De Raadt, Jaspers Focks, Van Hoven, & Regeling (2015) models wave overtopping (with overtopping discharge: $\mathrm{q} = 10\,\mathrm{l/s/m}$) numerically by applying a constant hydraulic head of 1 cm over the entire inner slope of the dike, which was calibrated by standpipe measurements of the phreatic surface. The effect of waves is thus small compared to the effect and wave overtopping can only occur when a high-water level is present outside the dike. The influence of waves will therefore not be considered and the threat of a high-water level at the outer slope will be further studied.

A failure mechanism describes the way in which the water-retaining capacity of a structure falls short. The first step in assessing the safety of a flood defense system is to evaluate all threats and associated failure mechanisms. Once a mechanism is known, an attempt is made to model it. Such a model can be either experimental or mathematical in nature. The model must help the designer gain insight in the circumstances under which the flood defense system functions properly and under what circumstances it does not. Thereafter it can be estimated how often the circumstances, that lead to insufficient functioning, will occur. This estimation can be used to determine whether the construction (existing or in design) can be considered safe or not.
The most encountered failure mechanisms that are considered in the Dutch safety assessment and design standards are shown in Figure 1.

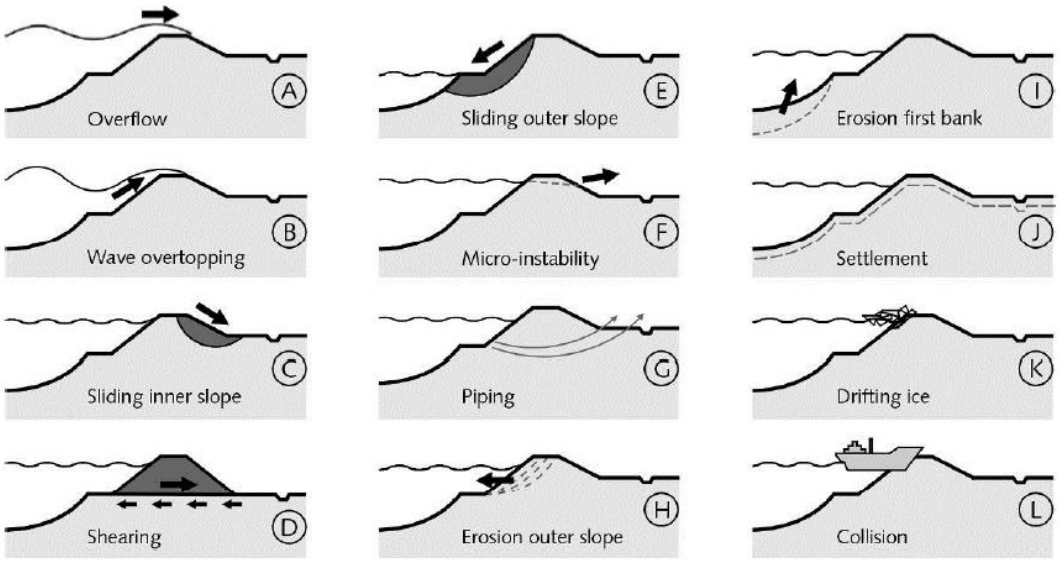

Figure 1: Overview of failure mechanisms of flood defences (Schiereck, 1998)

In this study, a dike will be tested under high-water conditions for different cases to assess how well an emergency measure (in this case BresDefender) performs. The phreatic surface level will be measured in these experiments, but this level by itself does not say much. The failure mechanisms can therefore provide insight to what extent the BresDefender helps to increase the

safety of a dike. Out of these failure mechanisms two failure mechanisms seem relevant for this study: macro stability (C) and micro stability (F).

1.1.3 BresDefender

The Dutch Ministry of Defence (nl: Defensie) plays a critical role in the implementation of emergency measures. Therefore, a study has been initiated by the Faculty of Military Sciences at the Netherlands Defence Academy (nl: Faculteit Militaire Wetenschappen aan de Nedelandse Defensie Academie) and the TU Delft to investigate the use of existing military resources to be integrated in the emergency response strategy for dike breaching.

One of these military sources are watertight pontoons that can normally used as elements to form temporary bridges, which is shown in Figure 2. However, these pontoons may also aid in counteracting dike failure. The BresDefender can be placed on the outer slope of a dike to prevent the dike from breaching, hence the name BresDefender. The pontoon will first be transported afloat to the designated location. The pontoon will then be sunk on the outer slope of the dike and anchored in place. An overview of this procedure can be seen in Figure 3.

Figure 2: Pontoon used as temporary bridge element

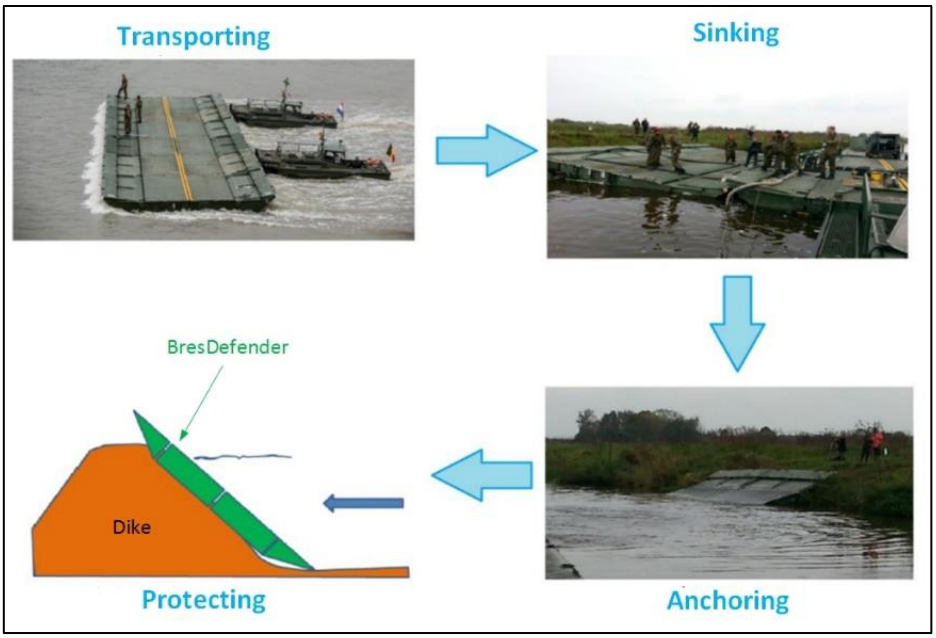

Figure 3: Phases leading to implementation of BresDefender

The main purpose of the BresDefender is to delay the time to (potential) failure of a dike. In this case, the criterium for dike failure is its ability to prevent flooding of a polder. The application of the BresDefender may have a beneficial effect in terms of dike safety for two scenarios: external erosion

(scenario 1) and phreatic surface (scenario 2). (Janssen, Schmets, Hofland, Dado, & Jonkman, 2021)
Both scenarios are explained in further detail below and are illustrated in Figure 4.

Scenario 1: Stop breach formation

The crest of the dike has been damaged by overflowing or overtopping, which results in a lower crest level. The decrease of crest level results in an increase of overflow over the dike, which leads to erosion of the inner slope and eventually core of the dike. The BresDefender can be used on the outer slope to decrease the overflow and thus the breach formation, which improves dike safety.

Scenario 2: Stabilize weakened section

In the early stages of dike instability, the crest level has been reduced e.g. due to macro-instability. The BresDefender can be placed on the outer slope to restore the initial crest level and to decrease seepage into the dike, which stabilizes the dike and increases dike safety.

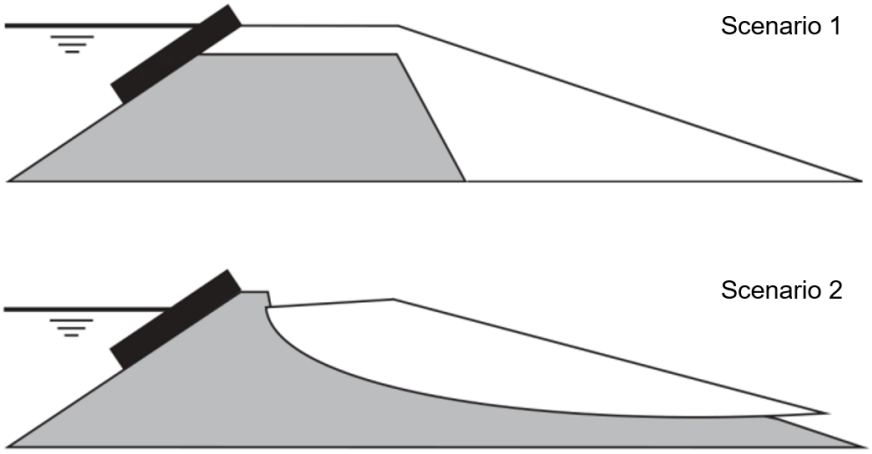

Figure 4: Application scenarios for BresDefender
(Modified from Janssen, Schmets, Hofland, Dado, & Jonkman, 2021)

1.1.4 Previous study

Previous experiments regarding this subject are carried out at the Hydraulic Engineering Laboratory (WaterLab) of the TU Delft. This is part of the study conducted by Bart van der Wilt at the Netherlands Defence Academy (supervisors: Alexander Schmets and Danny Janssen)
The study focuses on the effect of a seal on the development of the phreatic surface. In the laboratory experiments, a small-scale dike has been tested to study the behavior of the phreatic surface by implementing a seal on the outer slope of the dike. Cases have been studied where the degree of sealing on the outer slope of the dike has been varied for unsaturated and saturated initial conditions of the dike.

The results suggest that for a saturated dike the effects of sealing are negligible and for an unsaturated dike the sealing can affect the time until a steady-state condition of the phreatic surface is reached. Especially, the difference between the reference case (no plate) and the case where the entire outer slope is sealed (where also the sides are taped) gives most insight in the effect of the seal, which can be seen in Figure 5.
The conclusion of this study seems promising, but more research should indicate whether the effect of a seal on the phreatic surface is present for more complex problems.

Figure 5: Physical model without plate (left) and with plate (right)

1.2 Conceptual model

The application of a BresDefender as a sort of seal seems quite interesting. It is important, however, to first conceptualize the physical mechanisms behind the application of the BresDefender.
In this research case, the BresDefender will be applied as intervention for the case in which a weakened dike section will be subjected to high-water conditions. The BresDefender will cover part of the outer slope of the dike to limit seepage into the dike and the development of the phreatic surface in the dike may be suppressed as a consequence. The phreatic surface, or free water surface, in the dike is related to dike safety, where a higher phreatic surface is considered less safe.

In this study, two conditions of the dike are considered: with and without a damaged location in the dike cover. When the dike is undamaged, the BresDefender can be used as a preventative measure to reduce seepage into the dike by covering part of the outer slope. The BresDefender itself is a thick steel floating pontoon, which is watertight and contains air pockets that can be filled with water to sink itself. This pontoon can be transported afloat towards the desired location, and it can there be sunk on the outer slope of a dike before a flood wave has arrived. It is expected that the water can still flow underneath the BresDefender since the connection between grass cover of the dike and stiff bottom of the BresDefender is not watertight. Due to the weight of the pontoon and its water filled pockets, however, the pontoon exerts a downward pressure on the outer slope, which compresses the grass cover and restricts a certain amount of water flow.
When the dike is locally damaged, the BresDefender can be used as a temporary repair measure to limit water flow directly into the hole in the dike cover. The typical Dutch Riverine dike consists of a permeable core and a low-permeability cover layer that is covered by grass. When the cover layer is locally damaged, the permeable core is directly exposed to outside water levels which increases seepage into the dike and accelerates the rise of the phreatic surface. Similar to the undamaged condition, the free flow from water into the dike will thereby be partly obstructed because the connection between the BresDefender and the grass cover is assumed to not be fully watertight. Water is therefore expected to flow around the BresDefender towards the hole in the cover layer due to the water pressure difference between these two locations. The water pressure distribution on the edges of the BresDefender are varying leading to differences in flow velocity at each side. It is expected that the relatively large pressure located at the bottom side will induce a large part of the total flow towards the hole in the dike cover, which is depicted in Figure 6.

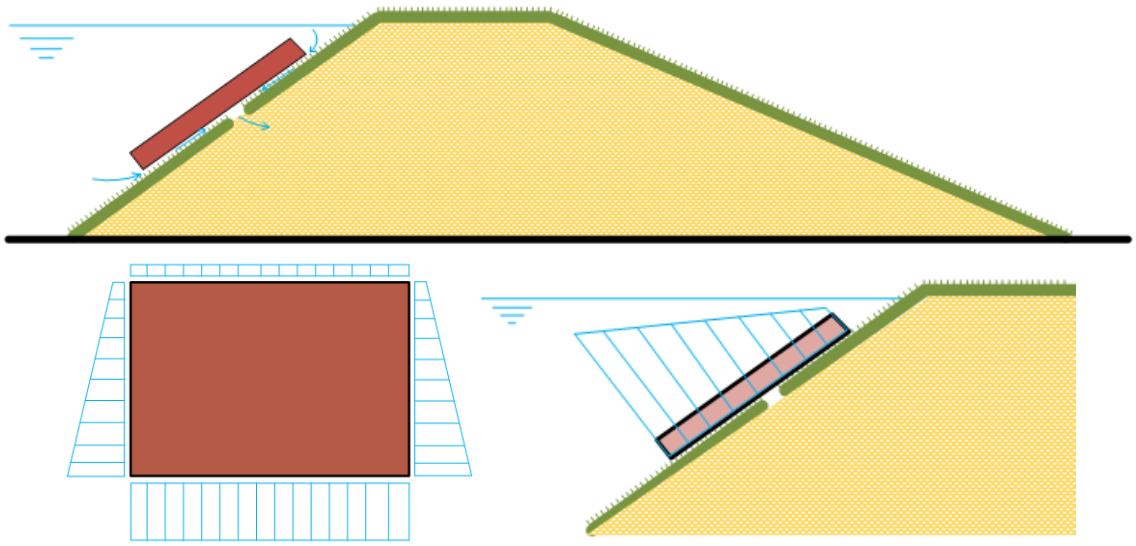

Figure 6: Conceptual model of the BresDefender (with a damaged location in the cover). Top: Flow in-between plate and grass cover. Bottom: Pressure distribution around plate

Due to the obstruction of free flow of water, the BresDefender may influence the development of phreatic surface level of the dike. Based on the previous study described in section 1.1.4, it can be hypothesized that the BresDefender may in this study have two similar effects on the phreatic surface level:

1. Decrease:
   The phreatic surface level in the steady-state condition may be lower due to the partial obstruction of water flow.

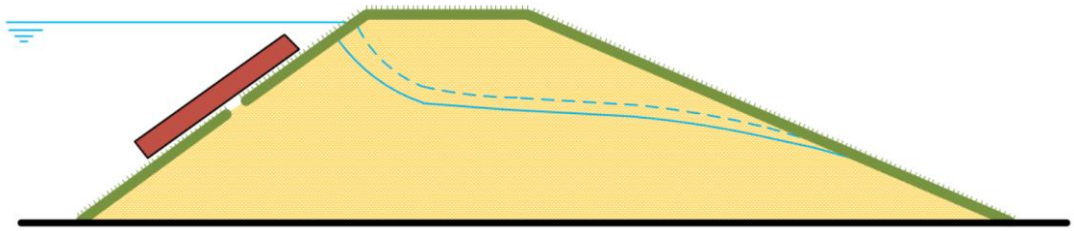

Figure 7: Assumed phreatic surface level decrease in steady-state due to sealing during high-water conditions

2. Delay:
   The time until a certain phreatic surface level is reached may increase by applying the BresDefender and the time may also increase until the steady-state condition is reached.

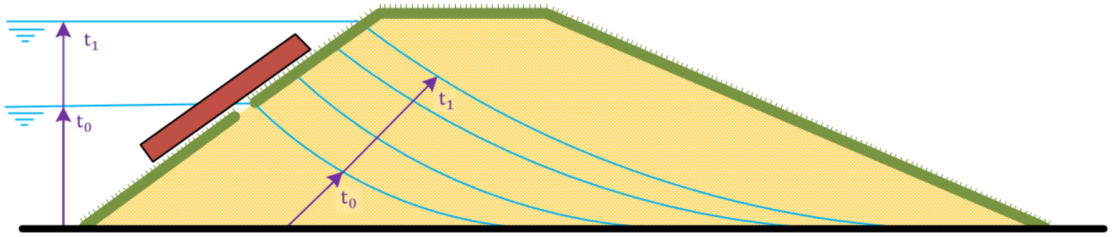

Figure 8: Expected phreatic surface development over time for increasing water level

1.3 Research questions

The objective of this study is to provide more insight in the effect of a BresDefender when applied in scenario 2 as described in section 1.1.3. In order to fulfill this objective, research questions have been formulated which will be answered in this study.
The main research question is based on a few elements that surround the proposed emergency measure, the BresDefender. First, the BresDefender can more generically be seen as a seal on a dike and will be referred to as *seal* or *sealing* throughout this thesis and the term *BresDefender* will only be used to indicate the real BresDefender pontoon (as seen in Figure 2). Second, the effect of this seal will have to be measured in relation to changes in a dike which may occur in space and/or time. Third, the hydrodynamic behavior of the dike is narrowed down to changes in the phreatic surface, which is a quite intuitive and easily measurable approach. Last, the emergency measure will be used in case of extreme conditions and expectancy of (imminent) dike failure, which will in this study be schematized as a dike that is loaded by high-water conditions.
By combining these elements, the main research question for this thesis can be formulated as:

> "What is the effect of a seal on the phreatic surface of a dike in space and time under extreme conditions?"

To answer the main research question, the following research questions have been formulated:

1. "What type of effects of a seal on the phreatic surface can be distinguished?"
   Different effects of a seal are expected which can be examined by a numerical model and physical model. If these effects are found in both models, the validity of the proposed effect is strong, however, due to limitations of each model, some effects can only be observed for a certain model.

2. "How can the effect of a seal on the phreatic surface be described by a numerical model?"
   The outcomes of the previous study at the WaterLab are used to learn lessons to develop a numerical model that describes the development of the phreatic surface adequately for this small-case homogeneous dike. Based on these lessons, a numerical model can be developed for an intermediate-scale heterogeneous dike and can be calibrated based on physical measurements.

3. "What is the effect of leakages around a seal on the phreatic surface?
   The connection between seal and dike slope is of interest and is examined based on numerical and physical models. The degree of leakage can aid in determining the effectivity of such a seal.

4. "What effect does a seal have on the phreatic surface for real-scale dikes with heterogeneous soils?"
   Physical model tests have been carried out for an intermediate-scale test dike with a heterogeneous soil profile. These experiments aim to determine the effect of a seal on the phreatic surface in space and time by taking measurements at discrete locations.

5. "What is the effect of a seal on the safety of a dike for various failure mechanisms?"
   From the literature study, failure mechanisms related to macro stability and micro stability have been discussed. The corresponding failure criteria are used to indicate the potential effect that a seal can have on dike safety based on the results from the physical measurements.

1.4 Research method

Since the research questions are formulated, a general heading for this study can be set. This is captured in the research method that consist of the following parts.

Theory (Chapter 2)

This study starts off with a literature study. It is necessary to attain more understanding of the subject and its components first. The following concepts form a theoretical framework for this study: (1) pore water pressure, (2) groundwater flow and (3) the phreatic surface in dikes. Additionally, based on literature on groundwater flow, a selection is made for a specific software program to develop a numerical model.

Numerical modelling (Chapter 3)

Once a theoretical framework has been established a numerical model can be developed. The numerical model will have to capture the behavior of the phreatic surface of a dike and the effect of the seal. This numerical model can be used eventually to form predictions of the outcomes of the physical modelling.

Physical modelling (Chapter 4)

In order to verify the numerical model, a physical model can be used. This model will be tested at the facility of Flood Proof Holland. An intermediate-scale test dike is present that consists of heterogeneous layers. The dike is situated in a basin that can be filled with water to model the water level that is present at the outer slope of a dike. Pressure sensors, located inside standpipes, are present over the length and width of the dike to monitor the phreatic surface level changes. By testing different cases with and without a seal on the outer slope, the effect of the seal on the phreatic surface can be empirically investigated.

Results (Chapter 5)

The results from the physical experiments are discussed where the different effects that a seal can have on the phreatic surface are analyzed by comparing different test cases. These effects are related to the type of sealing, the steady-state times, the development of the phreatic surface over time, and the dike safety.

Calibration and dike safety (Chapter 6)

The results of the physical model are first analyzed to calibrate of the proposed numerical model, which helps in understanding the performance and limitations of the applied sealing. Besides calibration, the results of the physical model can be used to analyze the effects of the seal in terms of dike safety, which is based on criteria for macro stability and micro stability.

2 Theory

Section 2.1 of the theory is dedicated to pore water pressure. Section 2.2 describes groundwater flow and its equations. Section 2.3 focuses on the definition and influence factors for the phreatic surface in dikes.

2.1 Pore water pressure

Soil is a porous medium consisting of particles, air and water. Various parameters are used to describe the relation between these three elements. A typical soil parameter is porosity n which is defined as the ratio between the volume of the pores and the total volume of the soil: $n = V_p/V$. When the porosity is large the soil is loosely packed and vice versa. (Verruijt, 2012)
The pores may consist of air and water and the ratio between these two is expressed as the degree of saturation S. This parameter relates the volume of water to the total volume of the pore space: $S = V_w/V_p$. If $S = 0$ the soil is completely dry, if $S = 1$ the soil is (fully) saturated, and if $0 < S < 1$ the soil is unsaturated (partially saturated).
The pores in a soil can thus be filled with water and air. The structure of pores in normal soils is such that these are interconnected and water can travel through this complex pore structure. Within this body of water, a pressure is present, which is called the pore pressure u. Under normal conditions, the pore pressure in a soil is mainly influenced by the location of the phreatic surface and the flow conditions. (Smith, 2014)

2.1.1 Saturated and unsaturated zones

The phreatic surface is defined as the hypothetical location in a body of soil where the pore water pressure is equal to the atmospheric pressure. (TAW, 2004) For dike analysis, this can be seen as the free groundwater surface level in the dike body. The phreatic surface forms the border between the unsaturated zone (or vadose zone), located above the phreatic surface, and saturated zone, located below the phreatic surface, for groundwater flow. The pores in the saturated zone are filled with water and the pores in the unsaturated zone are filled with water and air.
Under hydrostatic conditions in the saturated zone, the pore water pressure follows a hydrostatic pressure distribution $u = \gamma_w z$, where γ_w is the density of water and z is the depth below the phreatic surface. The pore pressure in the saturated zone is positive and increases linearly with depth.
For the unsaturated zone, however, the pore water pressure distribution is negative in the region directly above the phreatic surface, which is called the capillary zone. In this zone the pore pressure decreases linearly, following to the same expression of u in the negative direction, and the pressure in this zone may be below atmospheric pressure. This phenomenon, called capillarity, is present in soils with fine pores where water may rise above the phreatic surface due to surface tension. This soil suction in the capillary zone is caused by the interaction of particles, air and water. (Verruijt, 2012) In the capillary zone, the soil is (almost) saturated and the pore water pressure can be described by a nonlinear function. (Kaliakin, 2017)
A schematic overview of the pore water distribution in both zones is presented in Figure 9.

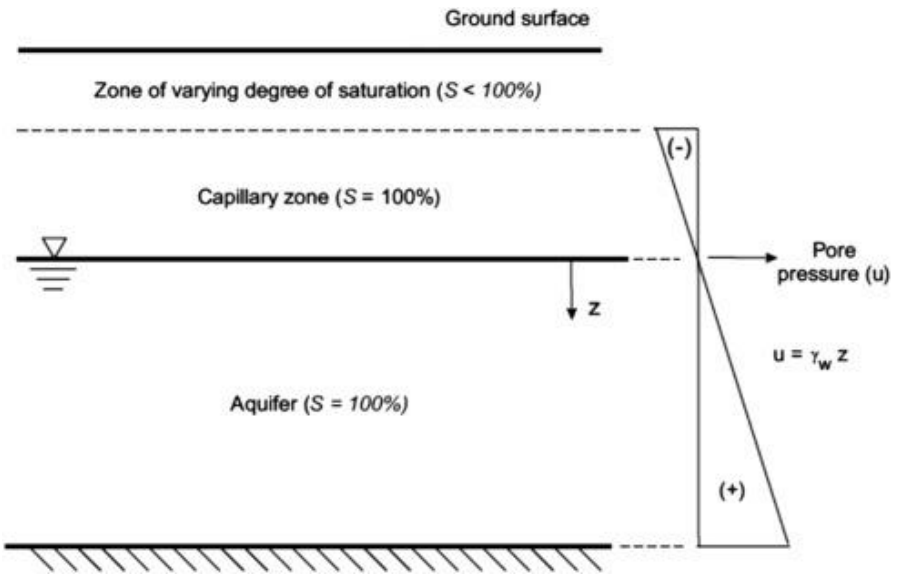

Figure 9: Pore water pressure distribution with capillary rise above the phreatic surface. (Kaliakin, 2017)

Pore water pressure influences the storage of water. In the saturated zone, all pores in the soil are filled with water (saturation). The volume of water stored in this zone is equal to the volume of pores in the soil, which depend on the type of soil material. The storage over depth does not change due to the isotropic behavior of water.
In the unsaturated zone, the soil contains air and water. The negative pore pressure (which is below atmospheric pressure) in this zone leads to soil suction and thus the retention of water. The relationship between soil suction and water storage in the unsaturated zone can be described by the soil-water characteristic curve (SWCC), which will be further discussed in section 2.2.3. (Fredlund & Xing, 1994)

2.1.2 Macro stability

2.1.2.1 Process

Macro instability, or more specifically slope instability, is generally caused by hydrological conditions where the pore water pressure in a dike is influenced by an external forcing. Two types of slope failure can be distinguished: inner slope and outer slope failure. (Ciria, 2013)
On the one hand, instability of the inner slope can occur. This failure mechanism is driven by the infiltration of water into the body and foundation of the dike. This causes an increase of pore water pressure which leads to a diminishing effective stress and shear strength of the soil. Especially, for flood events of prolonged periods, this condition may result in failure of the inner slope.
On the other hand, if a dike is saturated during long periods of flood and is able to withstand the load, a very quick decrease of the outside water level may lead to outer slope failure. As can be seen on the left side in Figure 10, the pore pressure in the dike body is still high when the horizontal water pressure from the river is reduced due to the rapid drawdown. The mechanism of outer slope failure can be categorized more as maintenance problem rather than a flood risk problem. When the dike fails due to outer slope failure, the water level is normally too low to cause flooding of the hinterland. Damages should be repaired nonetheless before the next flood arrives.

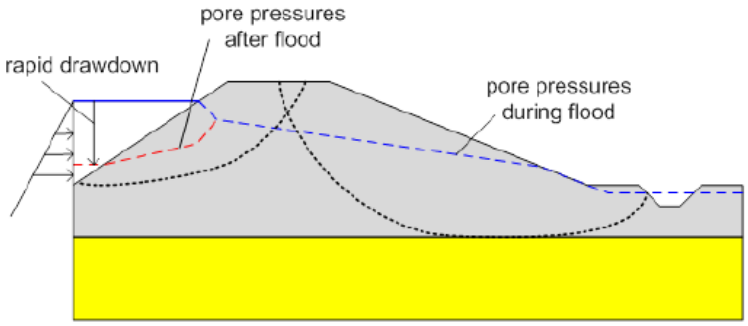

Figure 10: Schematic illustration of inner and outer slope failure (Ciria, 2013)

For this study inner slope stability is important to consider. The main goal of the BresDefender is to aid in reducing the water infiltration into the dike body when the dike is (almost) starting to fail. Outer slope failure is less relevant to consider because the weight of the BresDefender helps to resist the pore pressures inside of the dike and the BresDefender will be removed once the (extreme) high water level decreases again.

2.1.2.2 Assessment

In the lecture notes of Flood Defences (Jonkman, Jorissen, Schweckendiek, & Van Den Bos, Flood Defences - lecture notes, 2018), two approaches to macro stability assessment are mentioned: rules of thumb and limit equilibrium methods. Rules of thumb are too simplified for this study however, so these will not be considered.

Limit equilibrium methods (LEMs) compare the loads and resistances at the maximum mobilizable capacity for force and moment equilibria. This method assumes that the soil of a structure will fail along a slip circle as presented in Figure 11. The soil above this surface is divided into vertical slices which each have a specific weight and shear stress at the bottom.
The factor of safety (FoS) is defined as the ratio between the resisting moment M_r and the driving moment M_s, which is presented in the generic form in equation 1. The driving moment depends on effects located from the water-side as seen from the center point, which depends on the soil weight in this region. The resisting moment depends on the effects from the land-side, which are the soil weight and the shear strength of the soil along the sliding surface. The shear stress of a slice τ depends on the the normal stress of a slice σ_n, which consists of the weight of the slice with respect to the angle perpendicular to the slip surface α. In the resisting moment of the FoS, the normal effective stress σ_n' is used, which is the normal stress minus the pore pressure. An increase in pore pressure leads to a decrease in normal effective stress, which lowers the resisting moment and thus may lead to macro instability.

$$FoS = \frac{M_r}{M_s} \tag{1}$$

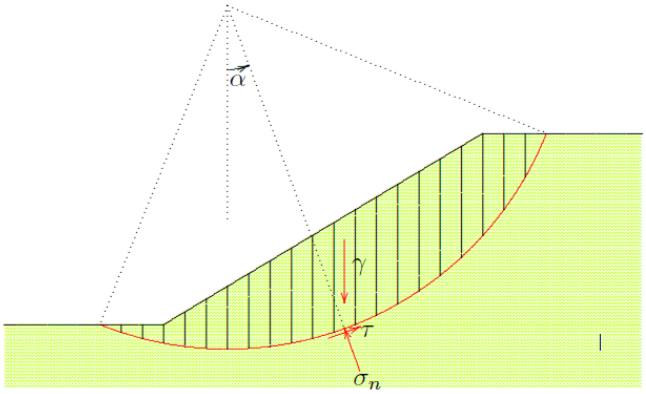

Figure 11: Schematic illustration of a slip circle modelled using the method of slices (Verruijt, 2012)

2.1.3 Micro stability

2.1.3.1 Process

Besides the above-mentioned macro-stability issues, micro-stability can also play an important role in the safety of a dike. In general, micro-instability occurs when seepage water infiltrates a dike with a permeable core. For dikes with impermeable cover layers on the inner slope, the pore pressure inside the dike body builds up and can eventually push off that cover layer if the pressure at the inner slope exceeds a certain threshold.

A schematic overview of the failure process from micro instability until dike breach is presented in Figure 12, where the following phases can be distinguished:

- Dike under normal conditions (0)
- Rise of phreatic surface level in the dike due to high-water conditions. The water tension at the inner toe is high (1).
- Start of micro instability at the toe and erosion of the inner slope (2)
- Ongoing erosion and settlement of material above the phreatic level (3)
- Crest level decreases and overtopping increases, which aggravates erosion of the inner slope (4)
- Start of dike breach due to overflow: the dike fails (5)

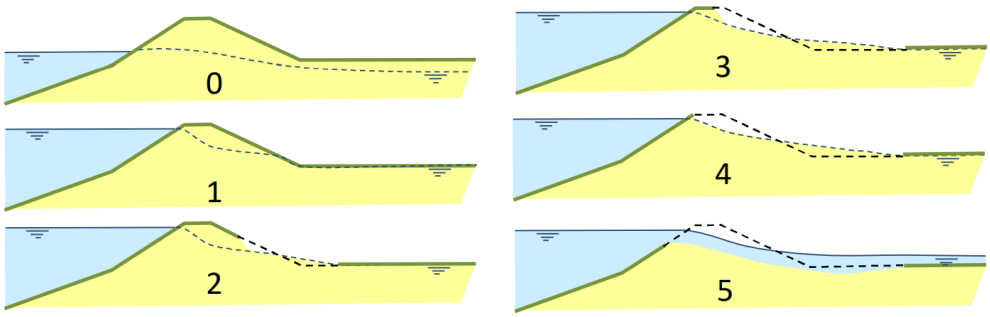

Figure 12: Failure process due to micro-instability (De Bruijn, De Vries, & `t Hart, 2018)

2.1.3.2 Assessment

Micro instability refers to the loss of stability for soil layers with limited thickness at the surface of the inner slope due to leakage of water through the dike body. (De Bruijn, De Vries, & `t Hart, 2018) In micro instability, the threat is internal: various mechanisms can be triggered by a high phreatic line in the ground body itself. In general, the two main mechanisms are (1) outflow of core material due to seepage and (2) uplift and slip of the cover layer due to excess pore water pressures at the inner toe.

These mechanisms depend strongly on the structure of the dike. (TAW, 2001) For dikes consisting solely of clay, micro-stability issues will play no role since the surface layers are more structured

and permeable than the core, which will therefore cause no pore water pressure build-up inside the dike. For sand dikes either with or without a clay cover, micro-stability should be assessed and is described in detail in the guide *Schematiseringshandleiding microstabiliteit* (2019).
For this study, the case of a sand dike with a clay cover is relevant since the BresDefender is intended to improve the safety of a dike where the cover layer has been locally damaged. For a sand dike with clay cover, the assessment is based on the following three failure modes:

1. Uplift of clay cover
2. Wash out of sand through clay cover
3. Sliding of clay cover

The failure mode with the lowest factor of safety will determine which mechanism is normative, however it can be argued that some modes have not to be considered for this study. First, in practice, the guide states that the second failure mode is only relevant for micro stability when the soil structure at the inner toe has horizontal leakage paths (e.g. due to mole ducts) and when overtopping/overflow conditions are present at the dike. The clay cover may fail in such case due to a combination of (1) the horizontal force exerted by the concentrated flow of the leakage paths and (2) the water flowing along the inner slope due to overtopping/overflow. This is not of interest for this study since this mode occurs only in cases with a combination of a damaged inner toe and wave overtopping.
Second, the guide states that the third failure mode is in general practice not normative for a conventional dike. The third failure mechanism will only occur if the first failure mechanism also occurs since the uplift of the clay cover will decrease the friction at its bottom surface which leads to sliding of this layer down the inner slope.
The first failure mode has therefore been chosen to further assess micro stability in this study.

To determine the safety against uplift of the clay cover, the driving forces and resisting forces need to be compared. A balance of these forces is made for a certain slice of the clay cover (dimensions $\Delta x \cdot d$) which is presented in Figure 13. The driving force consist mainly of water pressure and the resisting force contains soil weight, friction, and cohesion. This specific case treats a dike on a clay foundation, which is applicable for this study.

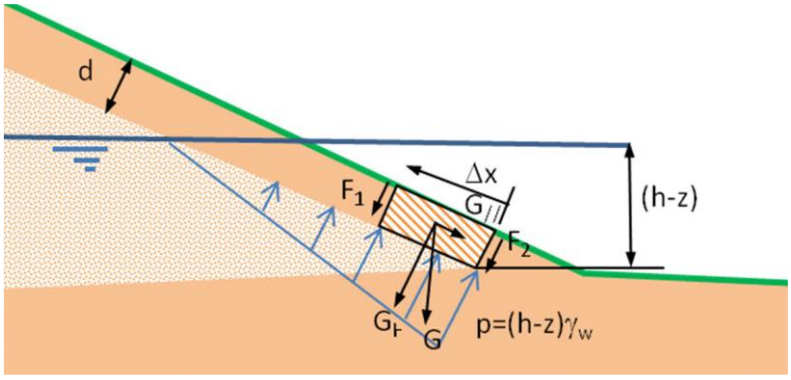

Figure 13: Schematic representation of perpendicular equilibrium soil segment with various forces

The balance of forces can be rewritten to the safety factor presented below:

$$SF = \frac{R}{S} = \frac{1}{\gamma_n \cdot \gamma_d} \cdot \frac{\frac{2c' \cdot d_{klei}}{\gamma_{m,c}} + \frac{\rho_g \cdot g}{\gamma_{m,\rho}} \Delta x \cdot d_{klei} \cdot \cos\alpha + \frac{\rho_g \cdot g}{\gamma_{m,\rho}} \Delta x \cdot d_{klei} \cdot \frac{\tan\phi'}{\gamma_{m,\phi}} \cdot \sin\alpha}{\left(\Delta h - \frac{1}{2}\Delta x \cdot \sin\alpha\right) \frac{\rho_w \cdot g}{\gamma_{m,\rho}} \Delta x} \quad (2)$$

Where:

$\tan\phi'$	Tangent of the effective angle of internal friction	[°]
$\gamma_{m,\phi}$	Partial safety factor for $\tan\varphi'$	[−]
c'	Effective cohesion	[Pa]
$\gamma_{m,c}$	Partial safety factor for c'	[−]
ρ_g	Volumetric weight of saturated soil	$[\mathrm{kg/m^3}]$
ρ_w	Volumetric weight of water	$[\mathrm{kg/m^3}]$
$\gamma_{m,\rho}$	Partial safety factor for volumetric weight	[−]
α	Inner slope angle	[rad]
g	Gravitational acceleration	$[\mathrm{m/s^2}]$
d	Thickness of clay cover	[m]
Δh	$= (h - z)$ Location of the phreatic line in relation to the height of the inner toe	[m]
Δx	Length measure along the inner slope	[m]
γ_d	Model factor	[−]
γ_n	Damage factor	[−]

2.2 Groundwater flow

Groundwater flow can be divided into saturated flow and unsaturated flow. Flow in the saturated zone is located underneath the phreatic surface. Flow in the unsaturated zone is located above the phreatic surface, where water can still be present due to the effects of infiltration and capillary action. Two main principles can be applied for groundwater flow, which are presented below. (Bentley Systems, 2020)

2.2.1 Transient flow

For homogenous, incompressible fluids and isotropic permeability Darcy's law can be used to describe flow through a porous medium by the following equation in three dimensions:

$$\underline{q} = \frac{\mathbf{k}}{\rho_w \underline{g}} \left(\underline{\nabla} p_w + \rho_w \underline{g} \right) \tag{3}$$

Where

$\underline{\mathrm{q}}$	specific discharge vector	$[\mathrm{m/s}]$
$\mathbf{k}$	tensor of permeability coefficient	$[\mathrm{m/s}]$
$\underline{g}$	gravity acceleration vector	$[\mathrm{m/s^2}]$
ρ_w	water density	$[\mathrm{kg/m^3}]$

The term $\underline{\nabla} p_w$ is the gradient of the pore water pressure that causes groundwater flow. The term $\rho_w \underline{g}$ represents the hydrostatic conditions, so when the flow is not affected by the gradient of the pore water pressure in vertical direction.

$$\underline{\mathrm{q}} = \begin{bmatrix} q_x \\ q_y \\ q_z \end{bmatrix} \tag{4}$$

$$\underline{\nabla} = \begin{bmatrix} \partial/\partial \mathrm{x} \\ \partial/\partial \mathrm{y} \\ \partial/\partial \mathrm{z} \end{bmatrix} \tag{5}$$

$$\underline{g} = \begin{bmatrix} 0 \\ -g \\ 0 \end{bmatrix} \tag{6}$$

The permeability coefficient $\mathbf{k}$ for saturated and unsaturated soils given as:

$$\mathbf{k} = \mathrm{k}_{rel}\mathbf{k}^{sat} \tag{7}$$

Where

$$\mathbf{k}^{sat} = \begin{bmatrix} {k_x}^{sat} & 0 & 0 \\ 0 & {k_y}^{sat} & 0 \\ 0 & 0 & {k_z}^{sat} \end{bmatrix} \tag{8}$$

and the relative permeability k_{rel} is the ratio of permeability at a given saturation compared to the permeability in the saturated state $\mathbf{k}^{sat}$. The absolute permeability (also known as intrinsic permeability or specific permeability) of a soil describes the permeability for fully saturated conditions, while the relative permeability takes the degree of saturation of the soil into account. The relative permeability is thus a function of saturation and many models have been formulated to determine unsaturated parameters such as permeability. In this study, the model proposed by Fredlund, Xing & Huang (1994) is used and will be discussed in section 2.2.3.

2.2.2 Continuity equation

For an elemental volume of a medium, the mass concentration is equal to $\rho_w nS$. The parameters $n[-]$ and $S[-]$ are porosity and the degree of saturation respectively. According to the law of conservation of mass, the outflow of volume is equal to the change in mass concentration. Since the water outflow is equal to the divergence of the specific discharge, the continuity equation is presented as:

$$\underline{\nabla}^T\left(\rho_w \underline{q}\right) = -\frac{\partial}{\partial \mathrm{t}}\rho_w nS \tag{9}$$

By neglecting deformations of solid particles and gradients of water density (Boussinesq's approximation), the equation can be simplified to:

$$\underline{\nabla}^T\left(\rho_w \underline{q}\right) + S\underline{m}^T\frac{\partial \underline{\varepsilon}}{\partial \mathrm{t}} - n\left(\frac{S}{K_w} - \frac{\partial \mathrm{S}}{\partial p_w}\right)\frac{\partial p_w}{\partial \mathrm{t}} = 0 \tag{10}$$

Where:

$\underline{m}^T$	load factor $(= [1 \quad 1 \quad 1 \quad 0 \quad 0 \quad 0])$	$[-]$
$\underline{\varepsilon}$	strain vector	$[-]$
K_w	compression modulus of water	$[\mathrm{N/m^2}]$
p_w	pore water pressure	$[\mathrm{m/s^2}]$

For transient flow, the displacements of solid particles are neglected which leads to:

$$\underline{\nabla}^T \cdot \left(\rho_w \underline{q}\right) - n\left(\frac{S}{K_w} - \frac{\partial \mathrm{S}}{\partial p_w}\right)\frac{\partial p_w}{\partial \mathrm{t}} = 0 \tag{11}$$

For steady-state flow $\left(\frac{\partial p_w}{\partial \mathrm{t}} = 0\right)$, the continuity condition applies:

$$\underline{\nabla}^T \cdot \left(\rho_w \underline{q}\right) = 0 \tag{12}$$

The steady-state discharge vector can be expressed as:

$$\underline{q} = \begin{bmatrix} -k\,\partial h/\partial x \\ -k\,\partial h/\partial y \\ -k\,\partial h/\partial z \end{bmatrix} \tag{13}$$

Substitution of the discharge vector into the continuity condition leads to the Laplace equation:

$$\underline{\nabla}^T \cdot h = 0 \tag{14}$$

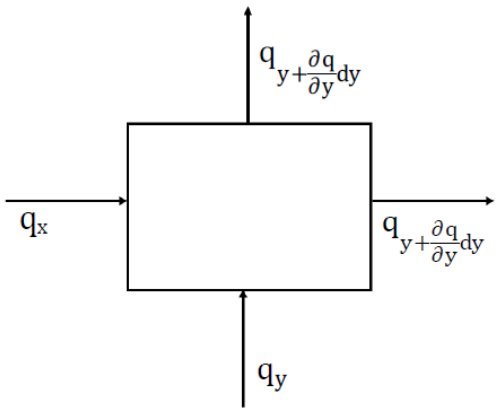

Figure 14: Continuity condition for an elementary area. No net inflow or outflow is present for this area as expressed in equation 15 (Bentley Systems, 2020)

From equation 15 can be concluded that the hydraulic head does not change over time when it is in steady-state conditions. This definition will be used in this study to indicate when the model reaches its steady-state condition, which is the moment the head or phreatic surface does not change anymore over time. This is an important condition since in this condition the maximum values will be reached and it is expected that these conditions will stay at this limit state for long periods of time.

2.2.3 Unsaturated models

Soil water storage in the unsaturated zone can be studied based on the soil-water characteristic curve (SWCC). The SWCC describes the relationship between soil suction and volumetric water content of the soil. The volumetric (or gravimetric) water content θ is the ratio between the volume of water to the total volume of soil. The SWCC depends on various factors such as type of soil, grain size distribution, plasticity and initial void ratio. (Hong, Jung, Kang, & Lee, 2016)
An overview of the typical features of the SWCC are presented in Figure 15. For the drying curve, three zones can be observed which are separated by the air-entry value (AEV) and residual conditions. The AEV is the suction value at which air starts to enter the soil and marks the beginning of desaturation. At the residual conditions, a residual suction value (RSV) is present which is defined as the suction corresponding to the residual moisture content. From this point onwards, no significant change of water content is present with increasing suction. (Eyo, Ng'ambi, & Abbey, 2022)

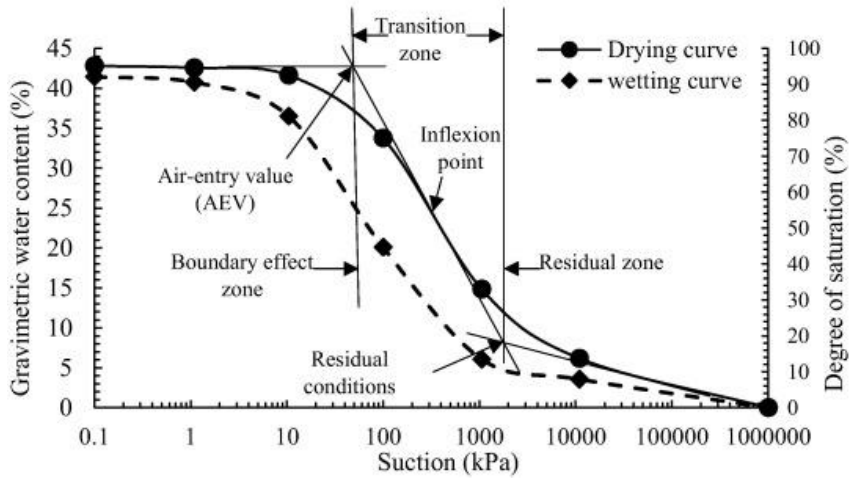

Figure 15: Overview of the soil–water characteristic curve (Eyo, Ng'ambi, & Abbey, 2022)

The measurements for the construction of the SWCC can be obtained in the laboratory for different test set-ups, where the soil suction is measured for varying water content. Mathematical equations have been developed which can fit these measurements to describe the unsaturated conditions of a soil, which are mainly water storage and permeability.
A study conducted by Rahimi, Rahardjo & Leong (2015) evaluated the performance of different SWCC models to fit certain laboratory measurements. Out of all these models, the formulations Van Genuchten (1980) and Fredlund & Xing (1994) had the overall lowest values of the RMSE and are therefore formulated and further discussed below.

Van Genuchten (1980):

$$\theta_w = \theta_r + \frac{\theta_s - \theta_r}{[1 + (\alpha\psi)^n]^{1-1/n}} \tag{15}$$

Where:

θ_w	actual volumetric water content	[−]
θ_r	residual volumetric water content	[−]
θ_s	saturated volumetric water content	[−]
ψ	soil suction	[kPa]
α	fitting parameter related to AEV	[…]
n	fitting parameter related to pore size distribution	[…]

Fredlund & Xing (1994):

$$\theta_w = C(\psi)\frac{\theta_s}{\left[\ln\left(\mathrm{e} + \left({}^{\psi}/_{a}\right)^n\right)\right]^m} \tag{16}$$

Where:

$$C(\psi) = 1 - \frac{\ln\left(1 + (\psi/\psi_r)\right)}{\ln\left(1 + (10^6/\psi_r)\right)}$$

$C(\psi)$	correction factor	[−]
ψ_r	suction corresponding to residual water content	[kPa]
e	Euler's number (=2.71828…)	[−]

a	fitting parameter related to AEV	[...]
n	fitting parameter related to the slope of the SWCC	[...]
m	fitting parameter related to the residual water content	[...]

The main difference between these equations is the behavior of the curve at high suctions. The Van Genuchten equation tends towards horizontal at high suctions, since the second term in this equation approaches zero at high suctions which leads to $\theta_w = \theta_r$. The Fredlund & Xing equation uses correction factor $C(\psi)$ instead, where the suction is set at 10^6 kPa at zero water content ($\theta_w = 0$). An overview of the behavior of both fits is presented in Figure 16.
The volumetric water content changes typically for suctions between 10^0-10^3 kPa for sandy soils and between 10^2-10^6 kPa for clayey soils (Fredlund & Xing, 1994). In this study, a wide range of soil types can be expected which are assumed to be unknown beforehand. For this reason, the Fredlund and Xing equation is chosen for this study to fit SWCC data and describe the unsaturated conditions for the numerical modelling.

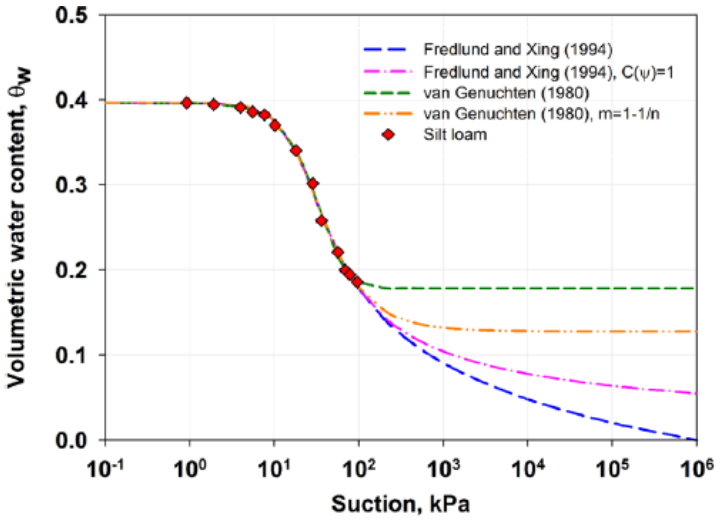

Figure 16: SWCC fits for different equations (Rahimi, Rahardjo, & Leong, 2015)

The SWCC can thus describe water storage for soils under unsaturated conditions, but it can also provide insight in permeability for the unsaturated soils. Based on the SWCC relationship from Fredlund & Xing (1994), the authors have proposed also a relationship for the permeability in unsaturated soils in Fredlund, Xing & Huang (1994). The relative permeability depends on the saturation of the soil, which is described as follows:

$$k_r^S(\psi) = \frac{\int_{\ln(\psi)}^{b} \frac{S(e^y) - S(\psi)}{e^y} S'(e^y) dy}{\int_{\ln(\psi_{aev})}^{b} \frac{S(e^y) - S(\psi_{aev})}{e^y} S'(e^y) dy} \tag{17}$$

Where:

k_r^S	relative coefficient of permeability	[−]
b	upper limit of integration (is normally 10^6)	[kPa]
S	Degree of saturation	[−]
y	dummy variable of integration representing the logarithm of suction	[−]
S'	derivative of the degree of saturation	[−]
ψ_{aev}	suction at air-entry value	[kPa]

The relationship for the relative permeability is presented in Figure 17. It can be seen that for low suctions the relative permeability is around $k_r = 1$, which is due to the high saturation of the soil. For increasing suction, k_r decreases due to a decrease of saturation and for $\lim_{\psi \to \infty} k_r(\psi) = 0$.

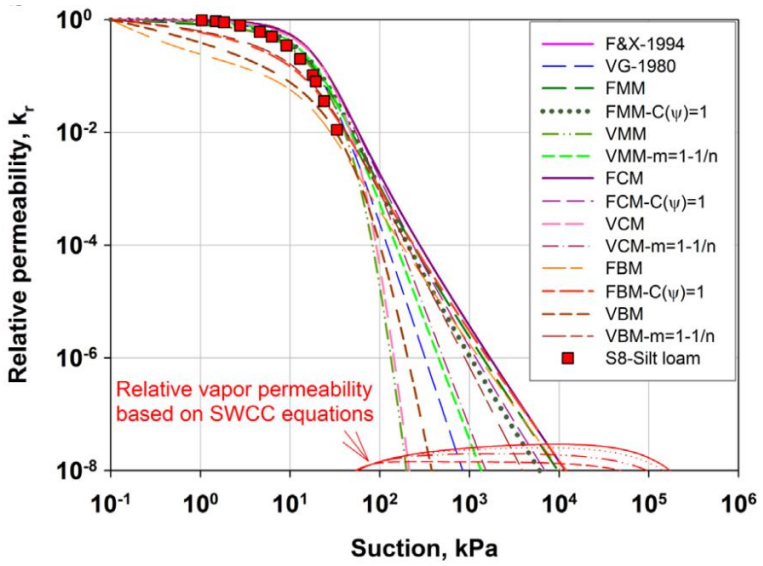

Figure 17: Relative permeability fits for different equations (Rahimi, Rahardjo, & Leong, 2015)

2.2.4 Solutions for groundwater flow

According to *Technisch rapport Waterspanningen bij Dijken* (TAW, 2004), four approaches can be distinguished to solve groundwater flow problems: analytical, analogical, graphical, and numerical. The strength of an analytical approach is the connection of the model to the theory. Differential equations are used to describe groundwater flow at given boundary conditions. A sensitivity analysis is relatively easy to perform and the input of soil parameters is simple. Simplifications and schematizations of the geometry are necessary however to find an analytical solution, which will therefore represent the real case less accurately. Therefore, these models will work best for two-dimensional homogeneous cases

The analogical and graphical approaches were popular in the era before the computer and are nowadays replaced by numerical approaches.

Numerical calculation models are increasingly used; they are becoming more and more user-friendly due to the menu-driven input and the powerful graphical postprocessing. A limitation of these models is that the calculation process is less transparent. Many parameters are required while it is not immediately clear how these parameters influence the outcome of the calculations. The extent to which the outcome of a calculation corresponds to reality is highly dependent on the applied calculation model, the schematization and the accuracy of the parameters involved in the calculation. Most numerical models are suitable for two-dimensional heterogeneous cases and can be categorized into:

- Analytical function method
- Boundary integral method
- Finite difference method, explicit or implicit (FDM)
- Finite element method (FEM)

The first two methods are not commonly used nowadays. Most of the models nowadays are FEM based due to the large freedom in the model to account for complex geometry.

Computer models can be used to approximate the Laplace equation in complex flow problems. This can be used in 1D, 2D or 3D modelling. Two methods are used primarily:

- Finite Difference Method (FDM): this method solves the Laplace equations by using linear algebraic equations. The flow region is divided into discrete rectangular grids with nodal

points. These points are assigned with different values for heads, which are either known or estimated. Using Darcy's law, a set of linear algebraic equations can be acquired. In these methods the number of nodal points is quite large and iterations of the solutions are often applied.

- Finite Element Method (FEM): this method divides the flow region into discrete elements by using an irregular shaped grid pattern and their corresponding equations. Material properties are taken into account for each element and boundary conditions are specified. The set of equations is solved to estimate the heads at each node and the flow for each element.

The FEM has a couple advantages over the FDM: (1) The complex geometry and irregular soil layers can be more easily modelled, (2) irregular sizes of the elements aid in modelling irregular seepage gradients.

2.2.5 Numerical models for groundwater flow

Seepage analysis of dikes is too complex to rely on geometrical and analytical methods to determine pore water pressures. Therefore, numerical models must be applied for this study. Several models and software programs may be suitable for this study, which are described extensively in Appendix A.1 and a short summary of the (dis)advantages is provided below.

Model	Advantages	Disadvantages
D-Geo Flow	✓ Software developed for flood defences ✓ Part of software series used for stability analyses	× Limited experience × Only uses Van Genuchten formulation × Cannot be used with scripting tool
COMSOL	✓ Contains two unsaturated flow models ✓ Can be used with MATLAB	× Quite complex software for multiple fields of engineering
Hydrus (2D/3D)	✓ Multiple unsaturated flow models	× Limited experience × Cannot be used with scripting tool
MODFLOW	✓ Open source ✓ Can be used with Python	× Only uses Brook-Corey formulation
PLAXIS (2D/3D)	✓ Multiple unsaturated flow models ✓ Predefined datasets	× Cannot be used with scripting tool

After careful consideration, PLAXIS has been selected as numerical software program for this study. This program satisfies the needs of a numerical model and has the following benefits for my study specifically:

- Extensive development of the numerical model/software for groundwater flow
- Multiple models are incorporated for flow in the unsaturated zone
- Easy-of-access and knowledge at TU Delft
- Availability of detailed reference manual (theoretical background information, program information, tutorials, etc.)

2.3 Phreatic surface in dikes

The location of the phreatic surface for dikes depends mainly on the (1) flood duration and (2) permeability of the dike body. In Figure 18b, the typical steady-state phreatic lines are given for a

homogeneous dike body. The permeability will not have an effect on the position of the phreatic surface in this homogeneous, steady-state case. In Figure 18a, the development of the phreatic surface for flood durations with a short period are shown. For stability assessments of the dike the worst-case scenarios regarding the factor of safety have to be considered, which can be more complicated to assess for transient conditions compared to steady-state conditions. (Ciria, 2013)
For real flood events, the transient flow conditions are more applicable. However, in dike stability design, the permanent flow conditions are considered. This is done by taking a design water level that is constant over time. This makes the design approach more straightforward and even safer because a higher internal phreatic line is considered.

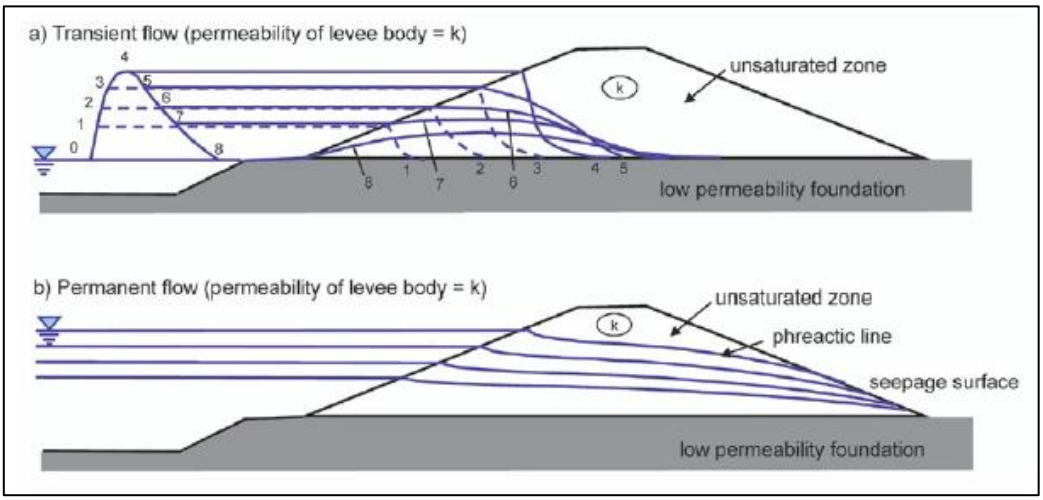

Figure 18: Comparison of the position of the phreatic surface for (a) transient states during a flood wave and (b) steady-state for the same water levels (Ciria, 2013)

The effect of permeability on the position of the phreatic line can be seen in Figure 19. The position of the phreatic surface is shown for two dikes with a different permeability. It shows that for a dike consisting of a higher permeability material the response of the phreatic surface is larger during a flood wave. This indicates that both permeability of the dike and the flood duration should be known to model the phreatic surface accurately.
Notice that for both figures the dike body is initially considered to be fully unsaturated. However, before the flood wave arrives, the dike can be significantly saturated. For low-permeability material the pore water pressure should be considered that is already present before the flood wave arrives. Also, precipitation that has infiltrated the dike body should be considered.

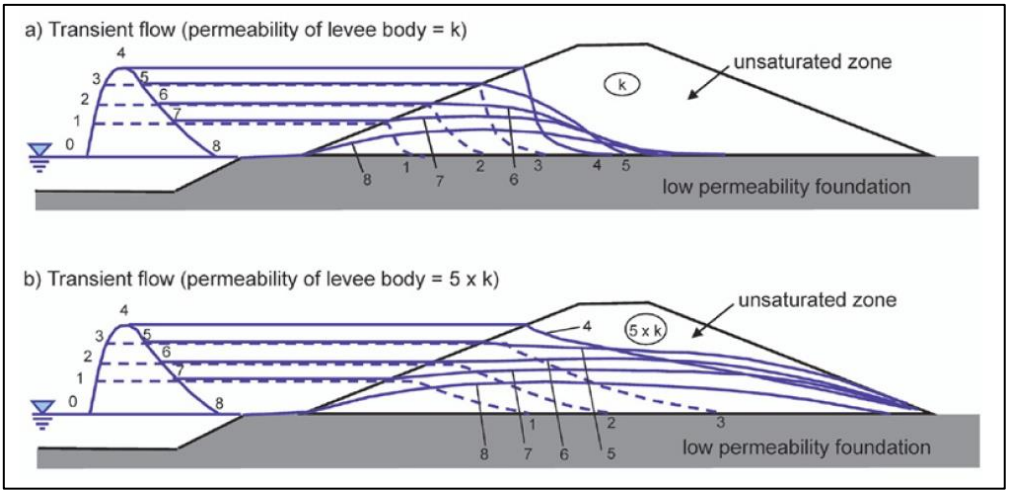

Figure 19: Effect of permeability on the position of the phreatic surface for different water levels (Ciria, 2013)

3 Numerical Modelling

This chapter discusses the steps that are taken in the numerical modelling process. The modelling process is described in section 3.1. Section 3.2 discusses the determination of soil parameters in the Geoscience & Engineering Laboratory. Section 3.3 describes the model, method and results of the numerical modelling of the WaterLab dike. Section 3.4 follows a similar structure for the numerical modelling of the Flood Proof Holland dike.

3.1 Modelling process

In order to create a proper numerical model, the modelling process should have small steps in-between leading to an accurate final model. The general order for the numerical modelling is to work from simple to complex. It starts off with creating a basic model to which new elements can be added. This will make it easier to validate the accuracy of the numerical model in describing the underlying physical phenomena.

The numerical model will be developed for two scales: (1) a small-scale dike in the WaterLab (TU Delft) and (2) an intermediate-scale dike at Flood Proof Holland. The modelling process is presented in Figure 20.
As mentioned earlier, the experiments at the WaterLab have already been carried out and the data has been processed as well. The dike is tested at a small-scale that comprises of homogeneous (permeable) material. The experiments for this dike have been measured under idealistic conditions. The dike profile is constant and measured precisely. The slopes are even, which makes the connection between the stiff plate and outer slope as good as can be. The water levels can be regulated accurately. The sensors are placed on the same level and distances are accurately measured. This dataset can therefore function well as a starting point for the numerical modelling. The WaterLab cases in which no interventions are made (Reference case) and in which the entire slope has been covered (Sealing case) are of interest. This will give insight in the bounds of the effect that the sealing will have on the development of the phreatic surface. Furthermore, is it important to check if the numerical model is in line with the measured values.

Once lessons are learned from the WaterLab cases, the numerical model can be scaled up to a model that characterizes the test dike at Flood Proof Holland. This dike is heterogeneous: a permeable core that is covered by a low-permeability layer. Following the cases from WaterLab, the dike can be modelled without interventions (Reference case) and with a plate (Sealing case). For both cases, the effect of a locally damaged area in the cover layer will be investigated as well. These cases can be compared with each other to point out the effect of the plate on the phreatic surface.

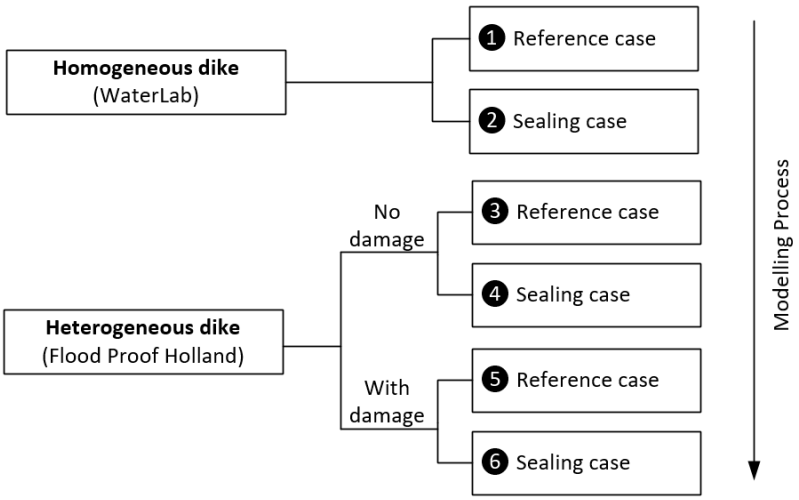

Figure 20: Numerical modelling process

3.2 Soil parameters

3.2.1 Method

Before an accurate model can be made, the input parameters of the different soil materials must be quantified. Samples of the soil material from the dike at the WaterLab and the dike at Flood Proof Holland have been investigated at the Geoscience & Engineering Laboratory (GSE Lab) at the TU Delft. The samples are created by taking a specimen of each material, drying the material in the oven, filling the sample holders with dried material and (fully) saturating each sample prior to testing. As opposed to in-situ sample collection, this method was necessary for the WaterLab dike, because only loose material was still available from the demolished dike. For samples from the Flood Proof Holland dike, this method is used because the samples can be more evenly distributed and compacted, which is important for the sensitive measurement equipment that is used.

The three soil parameters that the numerical model requires as input are investigated and are listed below.

- Saturated Volumetric Water Content (Saturated VWC)
  The saturated VWC, which is equal to the porosity of the soil n, is the volumetric water content at saturation. This parameter is needed for the fitting methods of the SWCC and hydraulic conductivity curve estimation methods.

- Saturated Hydraulic Conductivity (k_s)
  The hydraulic conductivity is a measure that describes the ability of water to pass through a saturated medium.

- Soil-Water Characteristic Curve (SWCC)
  The SWCC describes the relationship between soil suction and water content which is used to estimate the soil water storage and permeability of unsaturated soils.

The saturated VWC is simply determined by comparing the difference in weight (and thus volume) per sample between dry and saturated conditions. The saturated hydraulic conductivity is measured for each sample by a KSAT device, which measures the hydraulic conductivity based on the falling head test (based on Darcy's Law) as shown in Figure 21. The SWCC of the samples are measured with a HYPROP device, which measures the soil suction with tensio meters and changes in water content by changes in weight of the sample, which is shown in Figure 22. The wetting curve of the SWCC is measured, since the initially saturated samples dried during the experiments. These different experiments are described in detail in Appendix B.

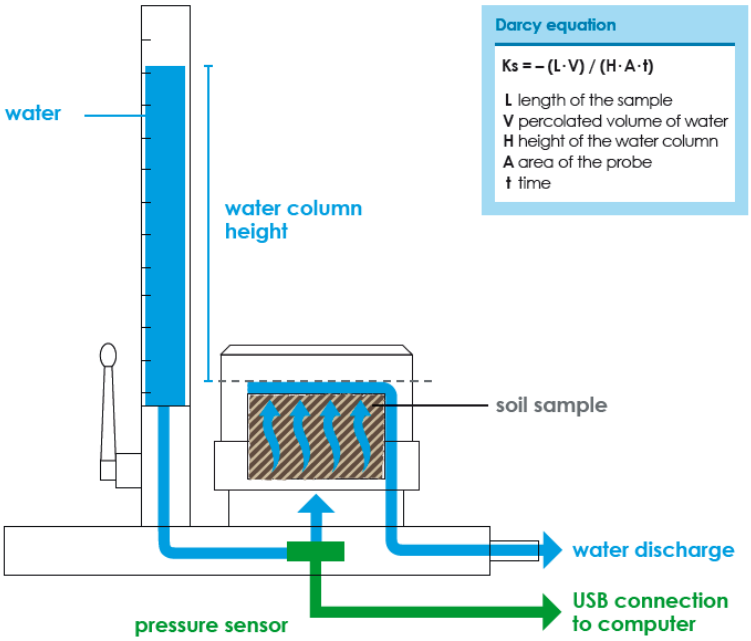

Figure 21: Description of KSAT device (Meter Group AG, 2020)

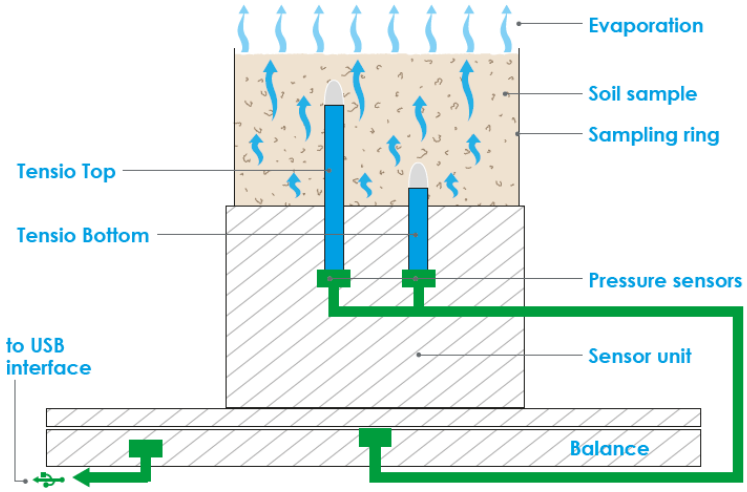

Figure 22: Description of Hyprop device (METER Group AG, 2018)

3.2.2 Results and remarks

The outcome of the soil experiments for the different soils are presented in Table 1 and Figure 23. Based on the results from the soil experiments, a few things can be pointed out:

- Small difference in Ks values between FPH dike cover and FPH dike core: the difference in order of magnitude is just O(1) which indicates that the performance of the cover as low-permeability layer is quite small. When the cover of the dike is damaged, the effect of this damaged location on the phreatic surface development of the core will be relatively small.
- Soil parameters for FPH dike core and WaterLab are similar: Permeability, saturated VWC and SWCC are close to each other. The material in the WaterLab was fine sand, which indicates that the FPH dike core also consists of sand.
- Soil parameters for FPH cover indicate a different material. The permeability is slightly lower, but the saturated VWC and SWCC are different compared to the other two materials. The

higher saturated VWC indicates a silt or clay material and the SWCC represents either of those as well.

The SWCC from the Hyprop measurements are consistent but show some irregularities. During the experiments, pore water evaporates and soil suction increases. The evaporation of water inside the sample is not evenly distributed along the sample, which lead to some small irregularities in the measurements. After most water is evaporated, the measurements show an indent at higher suctions due to the partial filling of the tension meters with air. Generally, the measurements in this region are not considered and SWCC models neglect the measurements in this region.

Table 1: Soil parameter values from KSAT tests

Material	Mean normalized Ks value [in m/s]	Saturated VWC [-]
FPH Cover	$2.06 * 10^{-06}$	0.515
FPH Core	$4.73 * 10^{-05}$	0.378
WaterLab	$8.54 * 10^{-05}$	0.347

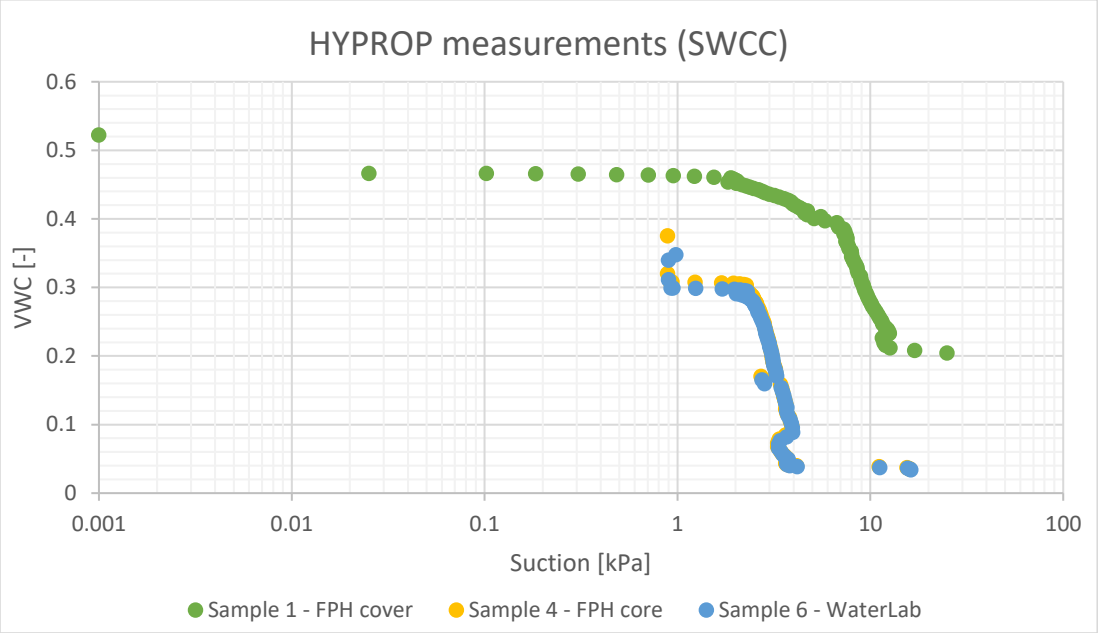

Figure 23: Measurements of the HYPROP experiments

In addition to the determination of the hydraulic conductivity of the FPH cover in the GSE laboratory, this value has been validated by an in-situ infiltrometer test. This simplistic test showed a hydraulic conductivity of $k_s = 8 \cdot 10^{-7}\mathrm{m/s}$, which is in the same order of magnitude as the value that is measured in the laboratory and indicates thus that this laboratory value is quite accurate. The infiltrometer test is described fully in Appendix C.3.

3.3 WaterLab experiments

3.3.1 Background

The main conclusion from the WaterLab experiments is that sealing of the outside dike slope results in a reduction of water level increase over time in case of an increasing outside water level. The steady-state condition is reached later in time for the case in which sealing is applied. The steady-state level for the case with sealing is however at the same level as the case without sealing. The

sealing has thus a solely delaying effect on the phreatic surface and not a decreasing effect on the maximum level of the phreatic surface in steady-state. This effect can be seen in Figure 24 for a (typical) measurement point at the dike crest.

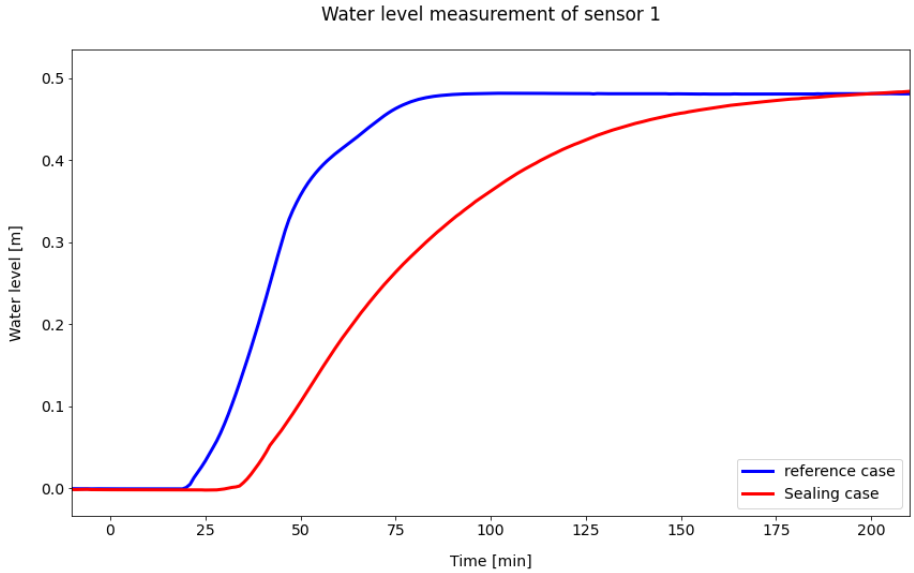

Figure 24: Effect of sealing on water level development over time

At the start of the measurement the sealing case had a delay in the moment it started to observe a water level change. During the experiment the rise of phreatic surface slowed down for the sealing case. The maximum water level for both cases in steady-state was similar.

3.3.2 Model

The WaterLab experiments can function as a good starting point for the build-up of a numerical model. The aim is to compare the phreatic surface development of the numerical model with the phreatic surface development of the physical model. Lessons can be learned from the similarities and differences between these two types of models that can be used for the field experiments at Flood Proof Holland.

The WaterLab dike is a small-scale homogeneous dike. The entire dike consists of permeable material that have the soil parameters as presented in section 3.2.2 (WaterLab material). The dike has been constructed in a flume in the WaterLab of the TU Delft. The flume has been used to model situations where the dike is subjected to time-varying water levels. The dimensions can be seen in Figure 25. A sieve analysis of the soil material, overview of the test set-up and sensor locations of the WaterLab dike are presented in Appendix B.4, which is part of the previous study conducted by Bart van der Wilt.

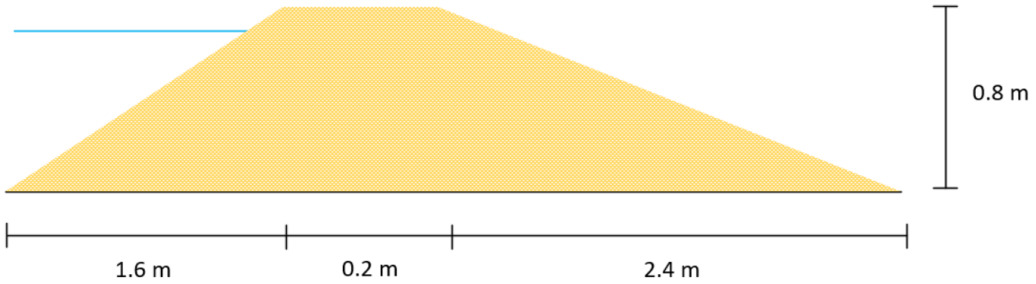

Figure 25: Dimensions of WaterLab dike (Not to scale)

On the outer slope (left slope in Figure 25), the varying water level can be created. On the inner slope, water pressure sensors are present that measure the pore water pressure at certain

locations. The measurements of the WaterLab experiments can be distinguished in two consecutive stages:

- Filling stage: The measurements started with an empty basin. The water level on the outer slope was increased until a high-water level and kept at this level. The phreatic surface of the dike increased over time. The measurements continued until the head in the standpipes were in steady-state.
- Emptying stage: The basin with a high-water level was emptied. The phreatic surface of the dike decreased over time. The measurements continued until the head in the standpipes were in steady-state.

For the proposed application of the BresDefender, only the filling stage is relevant since the BresDefender will be used to limit the water infiltration of the dike, which is occurring during the filling stage. The emptying stage is therefore not further analyzed in this thesis.

In these WaterLab experiments, numerous cases have been investigated with various degrees of sealing. The two most relevant cases for this study are as follows:

- Reference case: No measures are considered
- Sealing case: A plate has been placed which covers the entire left slope

These two cases will give insight in the comparison between numerical modelling and physical modelling for this test set-up.

3.3.3 Method

The goal for this part of the numerical modelling is to assess how well a numerical model can assess a physical model. In this study, the development of the phreatic surface over time should be captured for cases with and without plate for the WaterLab experiments. When the phreatic surface of the numerical model is similar to the one from the physical measurements, the numerical model is considered adequate.

Two important elements in both models are the steady-state time and steady-state level of the phreatic surface, which can be easily quantified and compared between both cases. The steady-state condition, which has a corresponding time and corresponding phreatic level, is assessed by observing the moment in time when the phreatic level does not change anymore. This specific moment is estimated by evaluating time intervals of 10 minutes. For the numerical model, this evaluation of the steady-state conditions is more accurate, since the numerical model shows a perfectly constant phreatic level from steady-state and a lot of datapoints are considered over the entire dike profile. For the physical model, this evaluation is slightly more difficult since sensors do not give a perfectly constant phreatic level at the steady-state condition and the number of sensors (datapoints) is limited over the dike profile. Therefore, an error range of 1 cm is assumed for the physical model to determine the steady-state condition.

The next sections will discuss the differences between the numerical model and physical model for the WaterLab experiments, which is done for the reference case and sealing case

3.3.4 Reference case

3.3.4.1 Numerical model

The numerical model, which is made in PLAXIS, is presented in Figure 25. The outer slope (the left slope in the figure) is subjected to a varying water level over time, which is the *head boundary*. On the inner slope is a *review boundary* because the exit point of the water at this location is unknown. The base of the dike has a *no flux boundary*, since the bottom of the flume is impermeable.

Figure 26: Boundary conditions for numerical model of WaterLab reference case

For this case, the experiments start with no phreatic surface inside the dike (sensors give zero head) and the flume is empty. When the measurements start, the flume is filled with water leading to a transient head at the outer slope of the dike, where filling of the flume is assumed to be linear. Once the flume is filled to 0.7m after 50 minutes, the water level is kept at this level until the end time of the numerical simulations (t_{end}).

Table 2: Head boundary for reference case

t [min]	h [m]
0	0
50	0.7
t_{end}	0.7

3.3.4.2 Results

In Figure 27 and Figure 28Figure 28, the results of the numerical and physical model are presented. Both models reach their steady-state condition at 110 minutes. Overall, it can be observed that the phreatic surface of the numerical model falls a bit behind on the one from the physical model initially, but it manages to rise above the physical model later. On top of that the numerical model has a more gradual development of the phreatic surface over time, while the physical model develops more abruptly. It can also be seen that the phreatic surface of the numerical model in steady-state condition is higher than the one measured in the experiments.

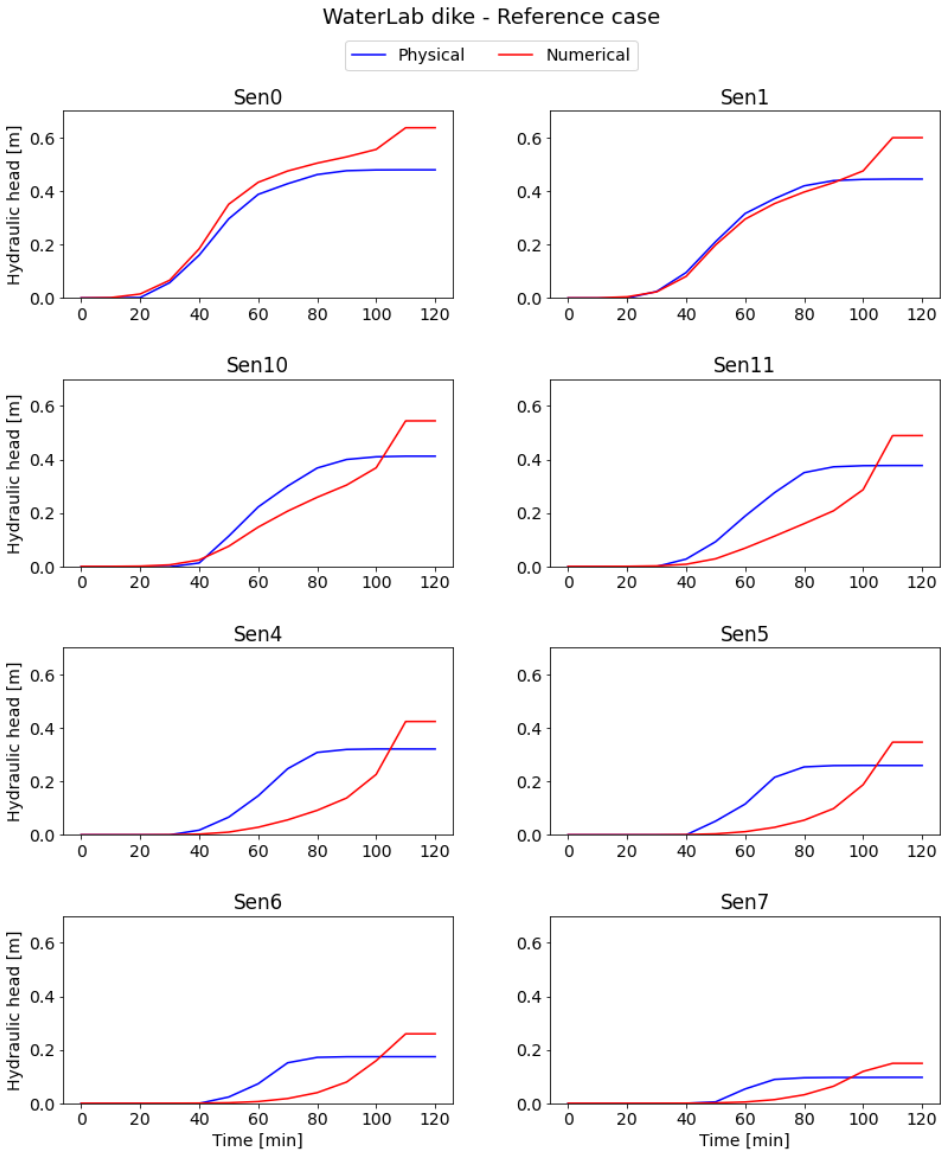

Figure 27: Overview of comparison between numerical model and physical model phreatic levels for the different sensor locations for the reference case of the WaterLab dike

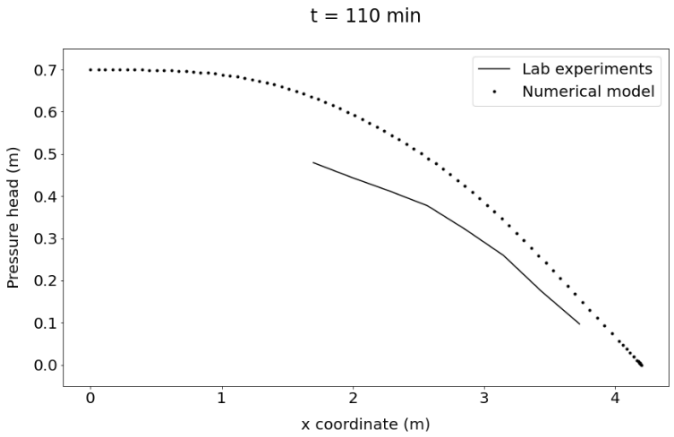

Figure 28: Cross section of the steady-state phreatic level for the reference case of the WaterLab dike

3.3.5 Sealing case

The sealing case describes the case in which a seal covers the entire outer slope of the dike. The sealing is a steel plate that models the steel BresDefender. The plate is stiff and covers the entire outer slope of the WaterLab dike. Extra attention has been paid to the connection between the edge of the plate and the side of the flume. This improved connection limits water flow around the edges of the plate, which models the plate as being infinitely wide and thus can this model be seen as two-dimensional.
As described in the conceptual model in section 1.2, the physical understanding of the connection between the plate and surface of the outer slope is quite complex. The texture of the grass cover, the compression of the grass cover due to the weight of the plate and the varying water pressure distribution along the edges of the plate are some of the many effects that should be considered. This is a complicated 3D problem with unknown variables and calculation methods to solve.

The options to model this connection in PLAXIS are limited to the use of soil layers. The connection can be modelled as an arbitrary soil layer in-between plate and outer slope where water must flow through. The two most viable variants of this additional layer are listed below.

- In-between layer: a transmissive layer in-between plate and outer slope where water must flow around the impermeable plate. No water can flow through the top and all water has to flow from the lower side of the plate through the layer.
- Interface layer: a transmissive layer on the cover where water can flow through the entire surface of the layer. The flow around the plate has been modelled as a flow through a transmissive layer.

In short, from preliminary modelling for both cases, the variant with the interface layer is used for this study. The in-between layer variant did not approach the results of the physical measurements at all. The reasoning is that the in-between layer assumes a two-dimensional case, where the plate has an infinite width and no flow is present at the sides. The test set-up at the WaterLab did not have a watertight connection at the sides of the plate. For the real-scale BresDefender it is not likely that flow at the sides of the plate can be minimized, which makes this a 3D problem essentially. The drawback from this interface layer model is that it does not explain the physical process well. The interface layer model is presented below.

3.3.5.1 Interface layer model

The sealing has been modelled in PLAXIS by an additional soil layer on the outer slope. This layer has a certain thickness (D), which is proportional to the flow resistance, and a certain hydraulic conductivity (k), which is inversely proportional to the flow resistance.

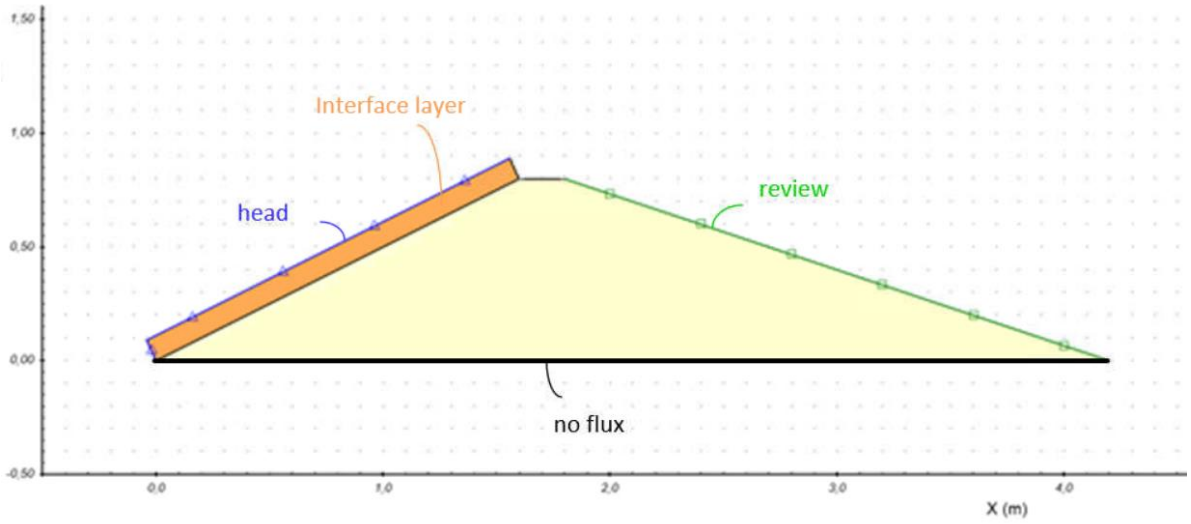

Figure 29: Numerical model of WaterLab sealing case (D = 0.1m)

The thickness of the layer of the interface is kept constant $(\mathrm{D} = 0.1\ \mathrm{m})$. The hydraulic conductivity of the interface layer is based on the hydraulic conductivity of the dike $(k_{int} = 8.54 \cdot 10^{-5}\ \mathrm{m/s})$. By increasing or decreasing the k_{int} by a certain factor, the numerical model can be calibrated based on the measurements of the physical model.

The sealing case is similar to the reference case as described in section 3.3.4, however the basin reached its maximum water level after 40 minutes.

Table 3: Head boundary for sealing case

t [min]	h [m]
0	0
40	0.7
t_{end}	0.7

3.3.5.2 Results

Two options of the numerical model with different values for the interface (with permeability k_{int} and $0.1k_{int}$) have been evaluated and are presented in Figure 30 and Figure 31. The time until the water level reaches the steady-state condition are similar between the numerical model (240 minutes) and physical model (300 minutes) with these parameters. The two numerical cases with different values for the interface represent the physical model quite good overall. In the beginning, the physical model exceeds the numerical model somewhat. In steady-state, both numerical models exceed the value of the physical model which is similar to the results of the reference case.

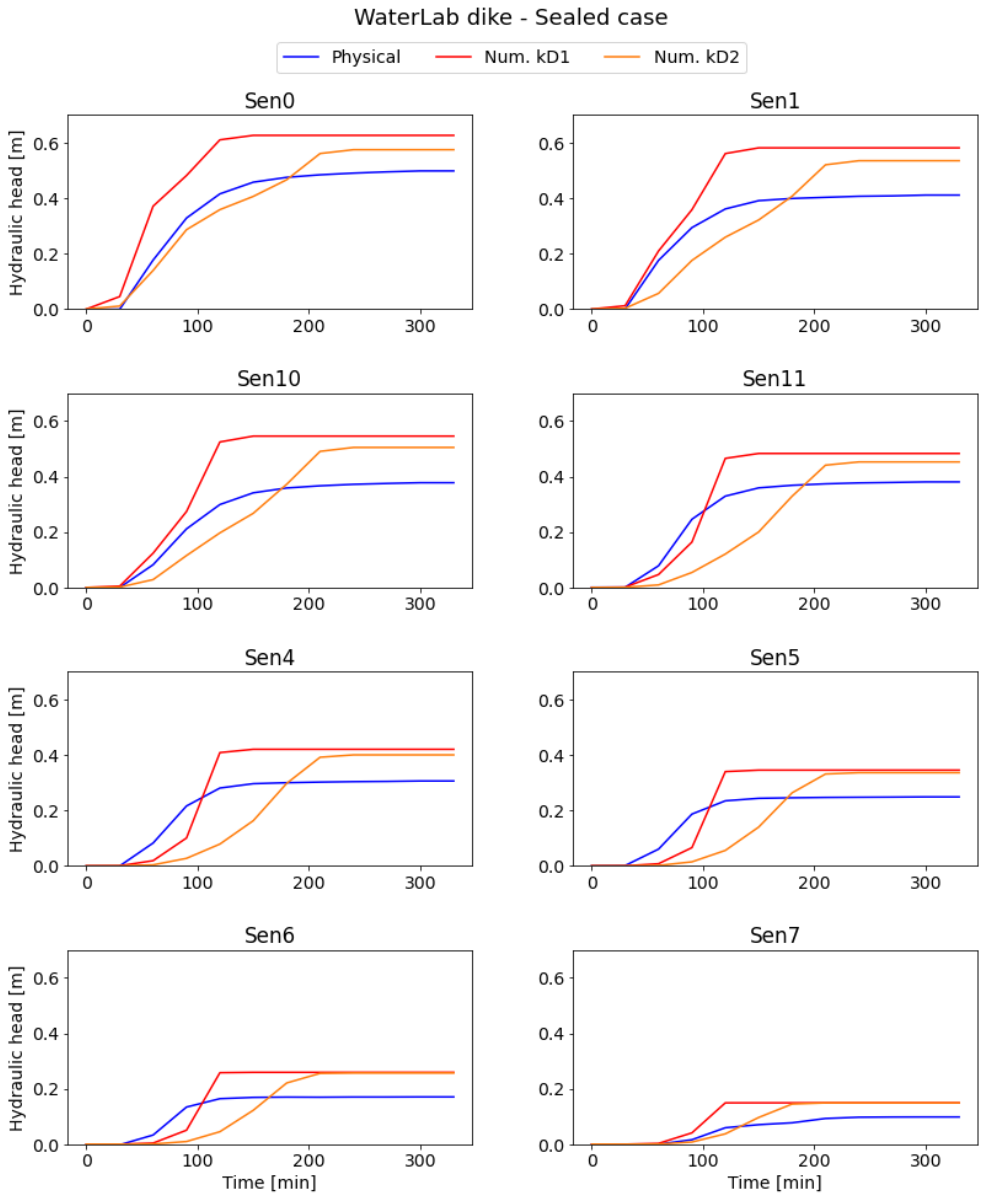

Figure 30: Overview of comparison between numerical model and physical model phreatic levels for the different sensor locations for the sealing case of the WaterLab dike

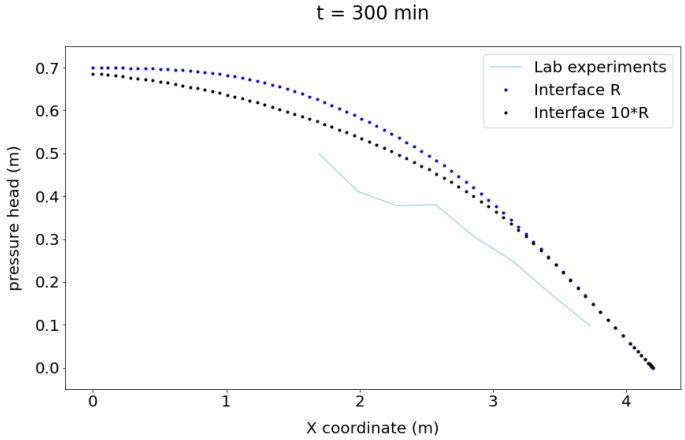

Figure 31: Cross section of the steady-state phreatic level for the sealing case of the WaterLab dike

3.3.6 Takeaways

Looking back at the numerical model of the WaterLab dike, the phreatic surface development of the physical model can be captured quite well in the proposed numerical model. With all parameters and calculation methods considered, the overall performance of the numerical model in describing the physical problem of this study is quite good.
It is still important however to find commonalities and irregularities in both models to learn lessons for the modelling yet to come. These remarks are listed below.

- Model offset: The phreatic levels for both models stay within a certain range from each other, even though a certain head difference between these two models can be observed. The phreatic level of the numerical model exceeds the level of the physical model. This should be taken into account for future model cases, where phreatic surface prediction from the numerical model may overestimate the measurements of the physical model.

- Interface modelling: The modelling of the plate-slope connection with a transmissive interface layer works quite well. The results point out that this model, which does not describe the physical process behind this interface layer, approaches the phreatic surface level of the physical measurements over time rather closely. By applying a constant thickness (D) and a variable permeability (k) this simplified model can be easily adopted for future cases.

- Model smoothness: The numerical model has a smoother progression of the phreatic surface compared to the physical model. The physical model follows an irregular pattern over the dike profile, where the numerical model has a smooth and regular (predictable) pattern. This difference is related to the large number of points, the theoretical (idealistic) equations, estimation of soil parameters, etc. It is therefore expected that this model smoothness will also be found in future numerical and physical models.

3.4 FPH experiments

Since the first lessons are learned from the WaterLab experiments, the numerical model can be scaled up to the dike of Flood Proof Holland. The aim of this numerical model of the FPH dike is to gain insight for the behavior of the phreatic surface for a larger scale dike that consists of heterogeneous material. This insight can be used to form a hypothesis prior to the physical model tests.

3.4.1 Model

The test dike at Flood Proof Hollands consists of two parts, which consist of the FPH cover and FPH core material. The corresponding soil parameters of both materials were presented in section 3.2.2.

On the outer slope of the dike is a time-dependent water level present, which models the filling of the outer basin over time. On the base of the dike is a no flux boundary implemented since the dike is built on concrete slabs where the effect of seepage is assumed to be insignificant. The inner slope of the dike has a review boundary similarly to the WaterLab dike. This numerical model is presented in Figure 32.

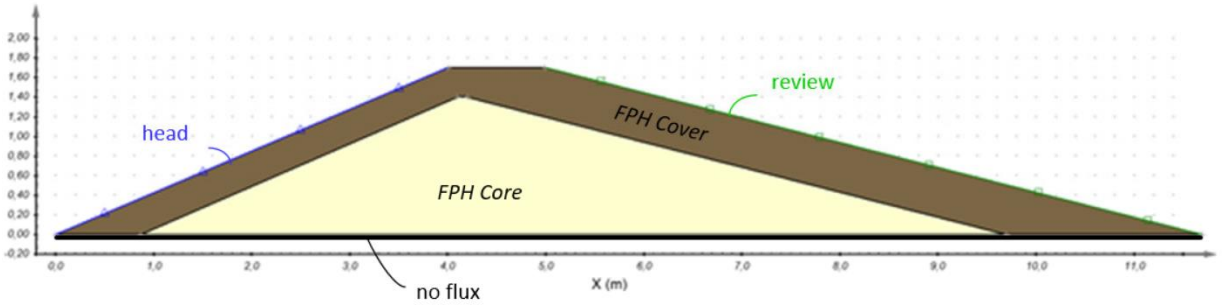

Figure 32: Numerical model of FPH dike

3.4.2 Method

As mentioned earlier, the numerical model process should be structured from simple to complex. The modelling starts with scaling up the WaterLab dike to the dimensions of the FPH dike, where both core and cover layer of the dike consist solely of soil material of the WaterLab dike (Case 1). This first case will give insight how a difference in scale affects the response of the phreatic surface. Thereafter the soil material of the entire dike is changed to the material of the core material of the FPH dike (Case 2) to give insight in the difference of effects for both materials. Thereafter all dike material is replaced by FPH cover material (Case 3) to check the same effect as measured in the previous case.

Once the homogeneous cases are modelled, the dike can be modeled in its heterogeneous composition. The case where the dike is unaltered (Case 4) and the case where the dike is locally damaged (Case 5) are examined. It should be kept in mind that this damage will be modelled in a two-dimensional numerical model, which will assume that the hole in the cover is over the entire width of the dike. This will not be the case in real practice and in the physical model. The results from these heterogeneous cases will therefore provide insight in the upper and lower bound of the phreatic surface level height and time until a steady-state condition is reached. The effect of the sealing for the damaged case is expected to lie between these bounds.

The sealing is not implemented any further in the numerical modelling of the FPH dike however, because no physical measurements are done so far and therefore the input parameters for the interface are unknown. The takeaways from the WaterLab model should therefore be considered as discussed in section 3.3.6.

3.4.3 Results

The time until reaching a steady-state condition of the phreatic surface for the different cases is presented in Table 4. A few remarks can be made on these time durations.

First, the steady-state time for Case 2 is larger than Case 1. This increase in time is caused by the lower permeability of the FPH core material ($k_s = 4.7\dot{3} \cdot 10^{-5}$ m/s) compared to the WaterLab material ($k_s = 8.54 \cdot 10^{-5}$ m/s). The same reasoning can be applied for Case 3, where the FPH cover material ($k_s = 2.06 \cdot 10^{-6}$ m/s) is used for the entire dike.

Second, when comparing Case 2 and Case 5, the model with the low-permeability cover (FPH cover material) needs a larger time to reach a steady-state condition than the model with the permeable cover ($k_s = 4.7\dot{3} \cdot 10^{-5}$ m/s).

Last, the presence of damage at the outer slope of the dike decreases the time until steady-state as can be seen from comparing Case 4 and Case 5.

Table 4: Steady-state time of the phreatic surface for different cases of the FPH dike

	Dike profile	Case	Steady-state time $\mathbf{t}[\mathbf{hr}]$
Case 1	Homogeneous	consists of WaterLab material	$\mathbf{20}$
Case 2	Homogeneous	consists of FPH core material	$\mathbf{35}$
Case 3	Homogeneous	consists of FPH cover material	$\mathbf{320}$
Case 4	Heterogeneous	Reference case with damage	$\mathbf{50}$
Case 5	Heterogeneous	Reference case without damage	$\mathbf{80}$

Besides the time until reaching a steady-state condition, the position of the phreatic surface in steady-state is also examined for the different cases, which is presented in Figure 33.
It can be observed that the differences between the cases are overall relatively small. Some differences can however be pointed out. First, the cases with homogeneous dike profiles (Case 1, Case 2 & Case 3) have an equal phreatic surface in steady-state. This means that permeability of the material itself does not affect the phreatic surface in steady-state.
Second, the introduction of the low-permeability cover layer (Case 5) affects the position of the phreatic surface. It can be seen that for Case 5, compared to the three homogeneous cases, the phreatic level for the interval $0.9 \leq x \leq 5.5$ smaller is and for interval $5.5 \leq x \leq 9.7$ larger is. For the former interval, the phreatic level is lower due to the presence of the low-permeability cover layer. This layer prevents the seepage such that the phreatic surface is even lower in steady-state. For the latter interval, the phreatic surface is also higher due to the low-permeability cover layer. This layer decreases the water outflow from inside the core leading to a higher phreatic surface.
Last, the presence of a damaged cover layer leads to a higher phreatic surface in steady-state. It can be seen for Case 4 that the phreatic surface is equal to the homogeneous cases for $3.0 \leq x \leq 4.0$ and follows a similar profile to Case 5 for the remainder of the dike profile with a lower phreatic level.

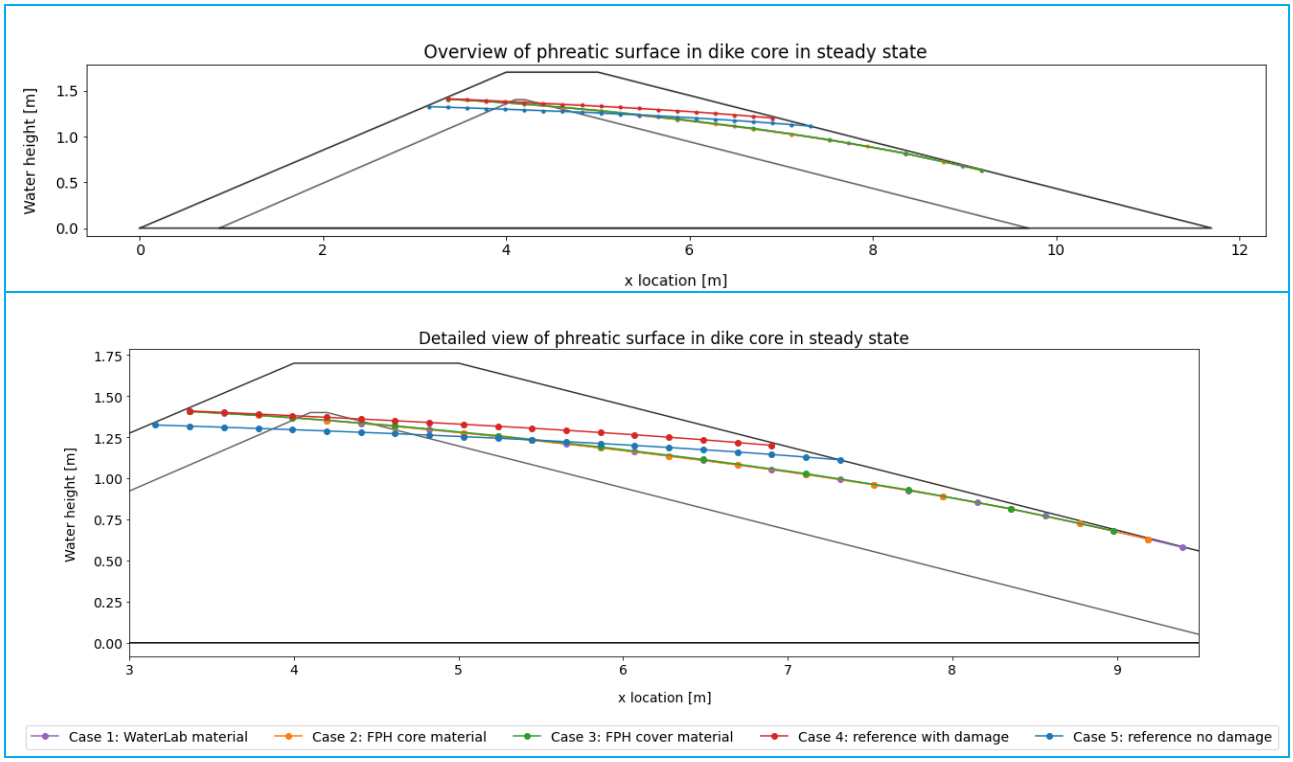

Figure 33: Phreatic surface level in steady-state for different cases of the FPH dike (to scale)

4 Physical Modelling

This chapter discusses the physical model experiments carried out at Flood Proof Holland. Section 4.1 explains the physical model with its dimensions and characteristics. Section 4.2 discusses the different materials that are used for the tests, which contain primarily the standpipes, sensors and data logger. Section 4.3 discusses the method of conducting the measurements. Section 4.4 proposes a hypothesis of the results of this field test.

4.1 Model

The physical model tests will be conducted at Flood Proof Holland (FPH). This is a test and demonstration facility that is used for innovative temporary embankments and dike stability research. The facility consists of multiple open-air basins that can be either filled or emptied at will to simulate flood events. This gives entrepreneurs, companies, governments and knowledge institutions the opportunity to test innovative flood protection measures in natural conditions.

4.1.1 Dimensions of dike

The test dike is an intermediate scale model that resembles a typical Dutch riverine dike: a permeable dike core covered by a low-permeability layer.

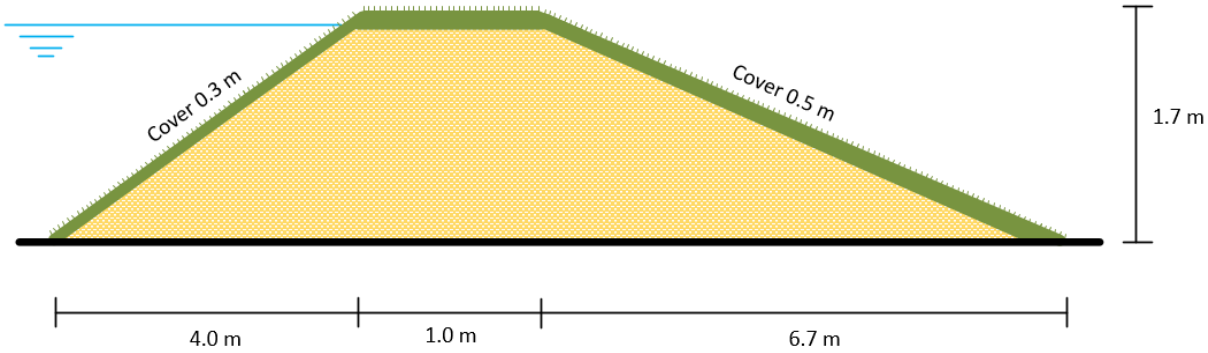

Figure 34: Dimensions of test dike. (Not to scale)

Figure 35: State of dike before physical tests

This dike is originally built in a large basin that separates it into a basin at the outer slope of the dike (outer basin) and a basin at the inner slope of the dike (inner basin). The inflow of water in the outer

basin can be regulated by a valve connected to a large adjacent basin. The outflow of water in the inner basin is regulated by a pump. Both basins are connected by means of a tube with a sliding door. A schematic overview of the test facility is given in Figure 36.

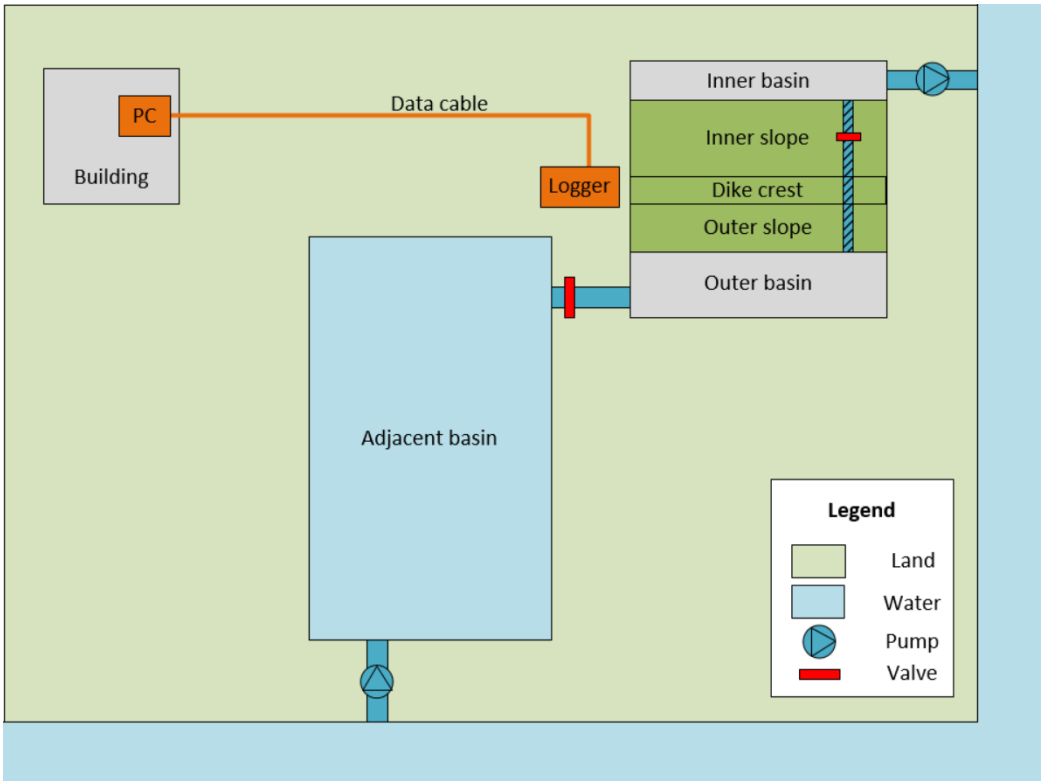

Figure 36: Schematic overview of the test set-up at Flood Proof Holland

4.1.2 Characteristics of dike

From the previous experiments in the WaterLab as described in section 3.3, it is concluded that sealing of the outside dike slope results in a reduction of water level increase over time. This effect was measured for a small-scale homogeneous dike. The question arises if this result can also be seen on a larger scale heterogeneous dike. A comparison between the dike in the WaterLab dike and in FPH dike are listed below.

Table 5: Comparison of dike characteristics

WaterLab dike	FPH dike
Homogeneous: Consists solely of permeable material	Heterogeneous: Consists of a permeable core covered by a low-permeability layer
Small scale dike: L = 3.8 m; W = 0.77 m; H = 0.8 m	Intermediate scale dike: L = 11.7 m; W = 20 m; H = 1.7 m
Regular geometry: dike profile is even and can be adjusted otherwise	Irregular geometry: dike profile is uneven and is fixed
2D model: the width of the dike is small and sensor placement is narrow	3D model: the width of the dike is large and sensors are disturbed over the width of the dike
Controlled environment: constant water levels, constant temperature, no wind, no rainfall	Uncontrolled environment: Variations in water levels, temperature, wind and rainfall

4.2 Materials

For these experiments, the phreatic surface within the dike has to be measured in space and time. The most precise and extensive option is to measure this phreatic surface with water pressure sensors. These sensors will be placed into standpipes to measure the phreatic surface at specific locations in the dike. The output signal of the sensors will be collected in the data logger at the dike. The data logger will transfer the data to the computer, where it can be stored and monitored. A schematic overview of this set-up is already be presented in Figure 36.

4.2.1 Standpipes

Standpipes are implemented to measure the phreatic surface at specific locations. The reason for using standpipes is to ensure that the measured value of the pressure at the bottom of the dike corresponds to the position of the phreatic line at that location. As can be seen in Figure 37, the equipotential lines in a dike body are perpendicular to the phreatic line. When the water level is high at one side of the dike and low on the other side, the phreatic line will be uneven over the dike profile. This will lead to curved equipotential lines, which causes the value of the pressure at the bottom of the dike to not correspond to the position of the phreatic line at the same location. The standpipes will make sure that both of them connect again due to the filter of the pipe, which will lead to a standing water column that can be more easily measured with pressure sensors.

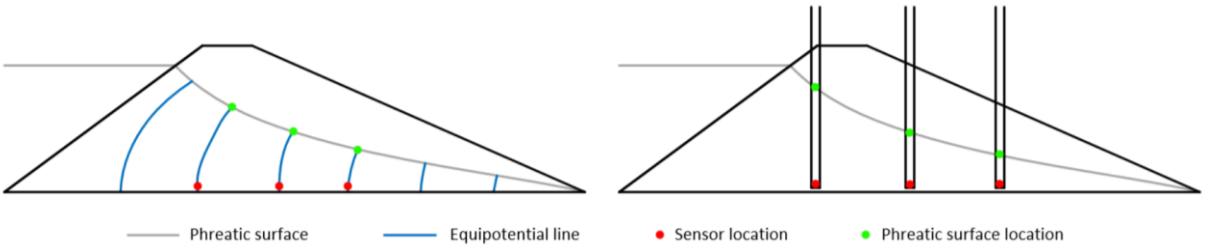

Figure 37: Effect of standpipes on measured phreatic surface location

Before the pipes can be placed in the dike, holes must first be drilled at the desired locations. These holes are drilled in the existing dike with a hand auger. The depth of these holes is dependent on the low-permeability layer at the bottom of the dike. These holes are drilled until this layer has been reached. It can be expected that this low-permeability layer is distributed unevenly over the dike profile, therefore the depth of the standpipes is expected to be uneven as well.

The pipes have a filter over the entire length that it has in the dike core. The purpose of this filter design is to make sure that the water surface in the standpipe represents the phreatic surface of the dike at that specific location. The pipes are fitted with filter sleeves to prevent clogging of the filter and the ingress of soil material into the pipe.

From a theoretical standpoint, standpipes will simplify the determination of location of the phreatic surface. The benefits from a practical standpoint are simple placement and removal of sensors, protection of sensor during placement and removal, and simple determination of the location of the sensors in the dike profile. The main drawback from the use of standpipes is that the dike profile is disturbed by vertical leakage paths. These leakage paths may increase the vertical seepage at the standpipe more than at larger distances from the standpipes and may influence the phreatic surface development due to water infiltration in the pipes.
Nevertheless, sensors will have to be placed on the bottom of the existing dike in some way. By not using standpipes at all, the hole has still to be backfilled which may also lead to variations in soil profile compared to the original state.

4.2.2 Sensors
Pressure sensors are used to determine the water height in the standpipes and in the basins. The sensors will be placed at the bottom of each standpipe where they will measure the pressure of the standing water column within the standpipe.
The sensors are of the submersible hydrostatic liquid level type. The sensor measures the pressure in a certain medium and compensates this value for the air pressure. The output signal of the sensor is in electric current and the specifications can be found in Appendix C

4.2.3 Data logger and software
The pressure sensors cannot be used standalone: the sensors need an external power source, the measurements need to be stored, and the sensors have to monitored in real-time. A data logger is placed at the dike location to power the sensors and to collect the measurements. A data cable is used to transfer the data from the logger to the computer in the local building at Flood Proof Holland. The computer contains software that can monitor the sensors in real-time and stores the measurements in data files (.dat files).
Detailed information of the data logger and software can be found in Appendix C.2.

4.3 Method
4.3.1 Identification of variables
The aim of this physical model is to give insight in the effect of a sealing on the phreatic surface in space and time for a heterogeneous intermediate scale dike. The tests are structured similarly to the cases of the numerical modelling as discussed in Chapter 3.4.

4.3.1.1 Independent variables
The independent variable is the variable that the experimenter purposely changes or manipulates generally.
In this case, the independent variables are (1) the type of emergency measure that is used on the dike and (2) the presence of a local damaged location on the outer slope of the dike. These emergency measure scenarios and damage conditions are discussed below.

Reference scenario
In this scenario, no additional emergency measures are implemented. This will model the development of the phreatic surface of the dike to a high-water condition under normal conditions. These measurements will therefore form a baseline that can be used to compare other emergency measures to.

Plate scenario
A stiff plate is placed on the outer slope of the dike for this scenario. The plate itself is made of glued-laminated timber and is weighted with sandbags. This will model implementation of the real-scale BresDefender pontoon for a dike under high-water conditions.

Figure 38: Plate scenario on FPH dike

Textile scenario

A textile (tarpaulin) is placed on the outer slope of the dike similarly to the previous scenario, which is made of polyethylene (PE) and is able to retain soil and water. Sandbags are placed on the edges of the textile to prevent it from washing away and water from flowing underneath it.

Figure 39: Textile scenario on FPH dike

Damage conditions

Each scenario is tested for two conditions: (1) with a damaged spot and (2) without a damaged spot in the outer slope of the dike. This damaged spot models the case in which the cover layer, consisting of low-permeability material, is locally eroded. This hole in the dike cover will amongst other things increase the seepage into the core of the dike, which effects the response of the phreatic surface.

Test cases

Combining the three emergency measure scenarios with the two conditions leads to six test cases in total. These cases are carried out in the following order.

Table 6: Measurement cases of FPH experiments

Case number	Emergency measure	Condition
Case 1	No measures	No damage
Case 2	Plate	No damage
Case 3	Plate	With damage
Case 4	No measures	With damage
Case 5	Textile	With damage
Case 6	Textile	No damage

4.3.1.2 Dependent variables

Since the independent variable has been identified leading to six test cases, the dependent variable can be identified as well. The dependent variable is the variable that changes in response to the changes in the independent variable. The dependent variable is thus the parameter that should be measured, which is in this case the phreatic surface development over time.

4.3.1.3 Control variables

The physical model is used to simulate the development of the phreatic surface under extreme conditions for different cases as mentioned earlier. In order to compare these different cases, it is important to carry out these experiments in the same way. Three important control variables, variables that should be kept constant, can be distinguished.

First, an experiment starts when the dike is in a drained condition. This is a good starting condition because it allows for a wide margin for changes in the phreatic surface and this condition is simple to replicate for consecutive experiments.

Second, an experiment ended when the phreatic surface reached a steady-state condition. This condition can be determined when the sensors measure a constant water level in the dike. This steady-state level is important to compare the effects of the different emergency measures.

Last, the water level in the outer basin and inner basin were kept as constant as possible. The water level in the outer basin represents a body of water that the dike must resist. This outer basin is filled to the highest possible water level and kept at this level over time to simulate a high-water condition. A visual marking is made in the basin so that this water level can be kept constant during filling and refilling. The water level in the inner basin represents the low-lying hinterland, which the dike has to protect against flooding. The water level in the inner basin should thus be kept as close to zero as possible. For every test scenario, the outer basin was (re)filled and the inner basin was emptied at specific time intervals.

4.3.2 Measurement conditions

The following boundary conditions and measurement conditions can be applied.

- **The measurement frequency is set at 4 times per hour.** This value is chosen because the expected duration of each experiment is a few days, which results for this frequency in 96 measurements per sensor per day. A larger measurement frequency could also be used, but this seems unnecessary for these experiments and will only lead to larger datasets.
- **The maximum water level in the outer basin is kept at 1.45 m at the location in the middle of the seal.** This water level in the outer basin is the maximum level until overtopping/overflow occurs (with a 10 cm margin for wind set-up and waves). This level may not be exceeded because this study only looks at high-water levels and this is also not taken into account for the numerical model. The bottom of the outer basin is sloped, where a measured water level of 1.40 m at sensor location 9 corresponds to a water level of 1.45 m at the location in the middle of the seal. At sensor location 9 is a visual marking present which aids in manual filling the basin to this specific water level.
- **Hourly refilling of outer basin and emptying of inner basin to keep the water levels as constant as possible**. The water level in the outer basin decreases over time due to seepage into the dike, the surrounding area and through the tube with sliding door. The water level in the inner basin increases due to leakage of dike and through tube with sliding door. It is therefore necessary to keep refilling the outer basin and emptying the inner basin hourly to keep the water levels in the basins as constant as possible.
- **The weather conditions were constant**. During the measurements at FPH, no precipitation occurred and the temperatures did not differ to much between the cases. Throughout the day the temperatures varied, which results in higher temperatures during the day and lower temperatures during the night.

4.3.3 Measurement procedure

For every measurement, a similar procedure has been followed to obtain reliable and consistent measurements and is described below. (Note: it is useful to use the overview of the FPH facility in mind, which is presented in Figure 36)

Stage	Description
Preparation	▪ Fully drain both basins and dike by pumping water out inner basin ▪ Filling of the adjacent basin at a maximum level ▪ Close the valve of the pipe which connects both basins
Filling stage	*Filling of outer basin* ▪ Open valve of pipe in outer basin ▪ Close valve of pipe in outer basin once the water level reaches 1.40 m at the visual marking *Keep basins at desired water levels* ▪ Every hour refill the outer basin to 1.40 m by opening and closing the valve of the pipe in the outer basin ▪ Every hour empty the inner basin by using the pump (Repeat both steps until the sensors reach a steady-state condition)
Emptying stage	*Emptying of outer basin* ▪ Open valve of pipe which connects both basins ▪ Turn on pump in inner basin (Wait until both basins are drained) ▪ Turn off pump in inner basin *Keep basins drained* ▪ Empty inner basin twice a day (morning and afternoon) (Repeat until the sensors reach zero water height)

4.3.4 Sensor locations

An overview of the sensor locations is presented in Figure 40. The sensors are located in rows over the dike profile: in the middle of the seal (sensor 11, 1, 3, 6), at the edge of the seal (sensor 8, 2, 4, 7) and at a distance of 1 width of the seal (sensor 10, 5). Their coordinates are given in Table 7.

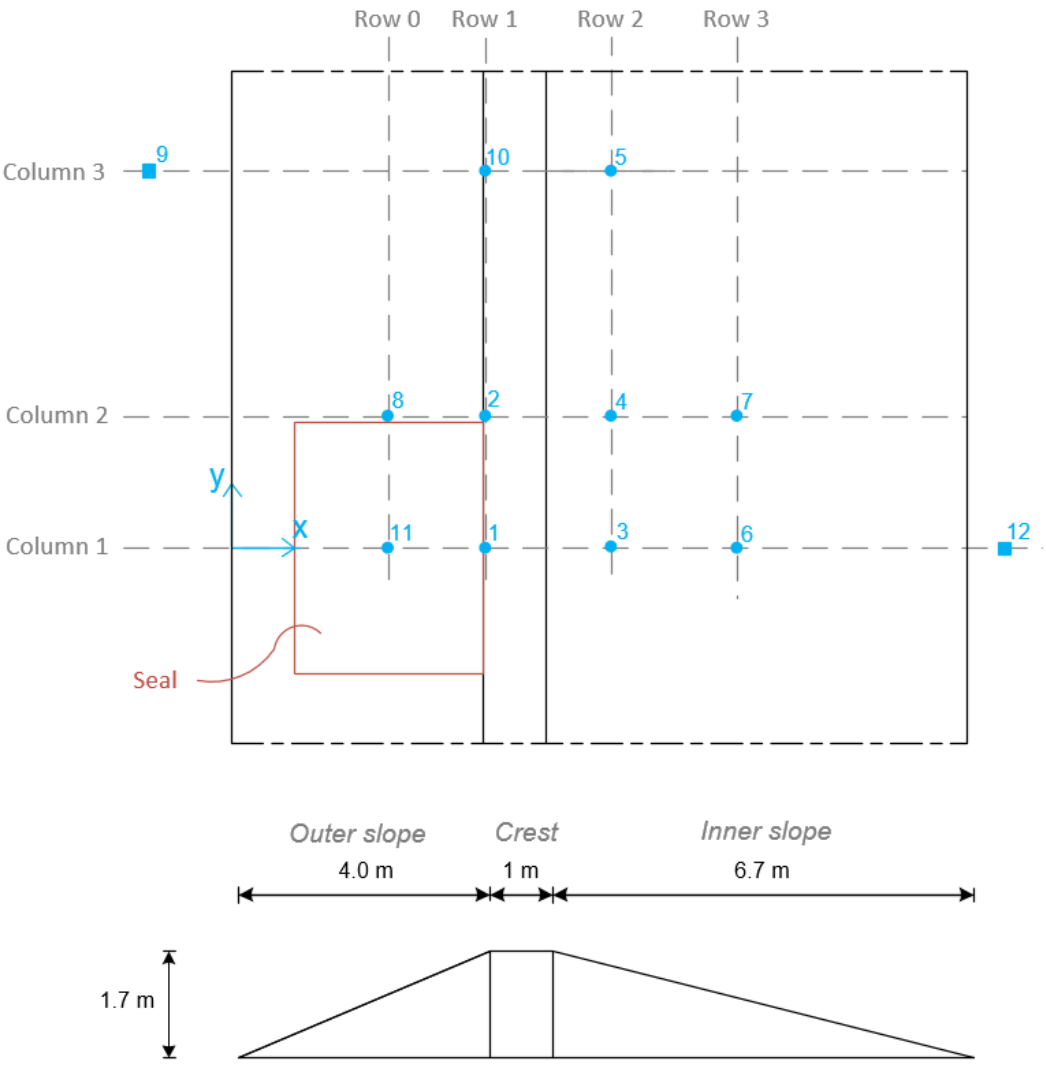

Figure 40: Overview of sensor locations of FPH dike

Table 7: Coordinates of sensors

	X-coordinate [m]	Y-coordinate [m]	Pipe depth [m]	Filter length [m]
Sensor 1	4.05	0.00	1.42	1.20
Sensor 2	4.05	2.00	1.55	1.20
Sensor 3	6.05	0.05	1.36	1.20
Sensor 4	6.10	2.05	1.36	1.20
Sensor 5	6.10	6.00	1.22	1.20
Sensor 6	7.95	0.05	0.76	0.60
Sensor 7	8.05	2.00	0.75	0.60
Sensor 8	2.50	2.50	0.85	0.70
Sensor 9	-	6.00	-	-
Sensor 10	4.05	6.05	1.50	0.40
Sensor 11	2.50	0.00	- *	- *
Sensor 12	-	0.00	-	-

* Note that sensor 11 is placed directly into the hole in the dike, so without the use of a standpipe

4.4 Hypothesis

Based on outcomes from the previous study and the numerical modelling of the WaterLab dike, the hypothesis for the experiments is that the seal will have a delaying effect on the phreatic surface of a dike. This delaying effect is expected to only occur for the damaged dike condition, because flow underneath the seal is only expected towards the hole due to pressure differences.
The delaying effect is expected to be found for locations near the seal, since seepage around the seal is expected. No decreasing effect is expected to be found for the phreatic surface level in steady-state, because the permeability of the dike will not be affected by the seal. The measured effect for cases with a flexible textile might be slightly higher compared to the cases with a stiff plate, because the connection between seal and dike slope is assumed to be better.

5 Results

This chapter discusses the results from the physical modelling. Section 5.1 describes the output of datasets from the physical measurements. Section 5.2 discusses the effect of both seals on the phreatic surface. Section 5.3 discusses the 3D effects of the textile.

5.1 Data output

Before the results can properly analyzed, it is first important to discuss the data output from the measurements. A typical overview of the measurements of experiment 6 are presented in Figure 41.
During the daytime of the filling stage of the dike of day 1, the water height for all sensors increased. During this period, the outer basin is refilled and inner basin is emptied every hour. During the evening and night, this is refilling and emptying is halted which leads to a large drop in outer basin water level and large rise in inner basin water level.
During the daytime of day 2, the basins are once again refilled and emptied respectively until their steady-state phreatic level. When this condition is reached, both basins are emptied which is the beginning of the emptying stage of the dike. During this stage, the basins are emptied every day twice (in the morning and afternoon) until the sensors read a water height of zero.
The steady-state condition was reached for all sensor locations on the first day of measurements. On the following days of measuring during the filling stage, none of the sensors reached a higher level at any time. This can for example be seen for sensor 8 in the figure, which reached a steady-state condition after measuring for 9 hours.

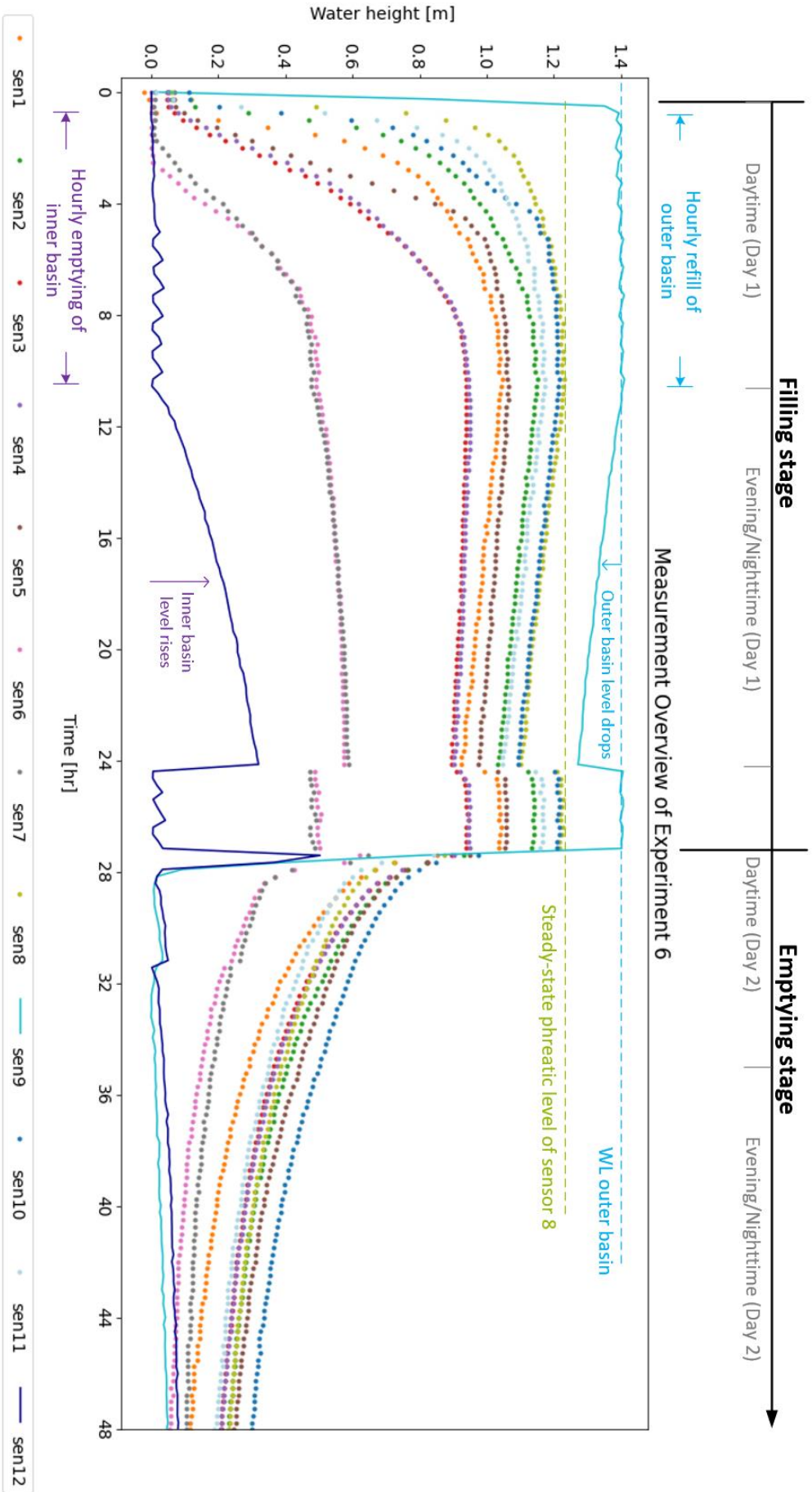

Figure 41: Typical measurement output during the filling stage and part of the emptying stage

5.2 Analysis of effects

5.2.1 Steady-state values

The time until reaching a steady-state is an important parameter in comparing the effect of emergency measures on the phreatic surface. These durations for the different test cases can be seen in Table 8.
The steady-state times for these cases are similar. The effect of damage is very small for the reference case and for cases with sealing.

Table 8: Time until reaching steady-state phreatic surface for physical model tests

Description	Case nr	Steady-state time t[hr]
Reference case: Undamaged	Case 1	8
Reference case: Damaged	Case 4	7.5
Plate case: Undamaged	Case 2	9
Plate case: Damaged	Case 3	9
Textile case: Undamaged	Case 6	10
Textile case: Damaged	Case 5	9.5

The phreatic level in steady-state is also important to discuss because it is the maximum level that the phreatic surface can become over time. These maximum levels can be seen in Table 9.
In general, the values of the phreatic surface differ slightly for the different cases. The plate case has almost no effect on the phreatic surface for both the undamaged and damaged scenario when compared to the reference case. The textile case shows only a slight decrease for the damaged scenario in respect to the corresponding reference case.

Table 9: Phreatic surface level in steady-state for physical model tests

Sensor locations		Steady-state phreatic level h[m]					
		Reference case		Plate case		Textile case	
		Undam*	Dam**	Undam	Dam	Undam	Dam
		Case 1	Case 4	Case 2	Case 3	Case 6	Case 5
Column 1	Sensor 11	–	1.26	–	1.27	1.17	1.20
	Sensor 8	1.21	1.28	1.22	1.27	1.23	1.24
Column 2	Sensor 1	1.05	1.12	1.05	1.11	1.04	1.07
	Sensor 2	1.14	1.21	1.14	1.19	1.14	1.16
	Sensor 10	–	1.24	1.21	1.23	1.22	1.22
Column 3	Sensor 3	0.93	1.00	0.94	0.99	0.94	0.96
	Sensor 4	0.94	1.01	0.95	1.00	0.95	0.96
	Sensor 5	1.03	1.10	1.04	1.08	1.06	1.07
Column 4	Sensor 6	0.48	0.54	0.50	0.53	0.49	0.51
	Sensor 7	0.48	0.53	0.49	0.52	0.48	0.49

* Undamaged conditions of dike (no hole in cover)
** Damaged conditions of dike (hole in cover)

5.2.2 Effects for an undamaged dike

The dike has been tested under undamaged conditions of the outer slope for 3 cases: the reference case, the case with a (stiff) plate, and case with a (flexible) textile. The behavior of the phreatic surface is examined for each case from a zero value to a steady-state value. Each sensor represents a location in the dike, where the position of the phreatic surface is measured. The sensors have been divided into rows and columns similarly to the sensor locations in Figure 40. For

every sensor location a plot is made of the measurements for the reference case and one of the cases with an emergency measure (plate or textile).

5.2.2.1 Plate on an undamaged dike

The reference case (experiment 1) and the case with a plate (experiment 2) for a dike without damage on the outer slope have been compared in Figure 42.
It can be noticed that for both cases the measurements of the phreatic surface are close to each other. This can be seen for all sensors during filling and in steady-state.

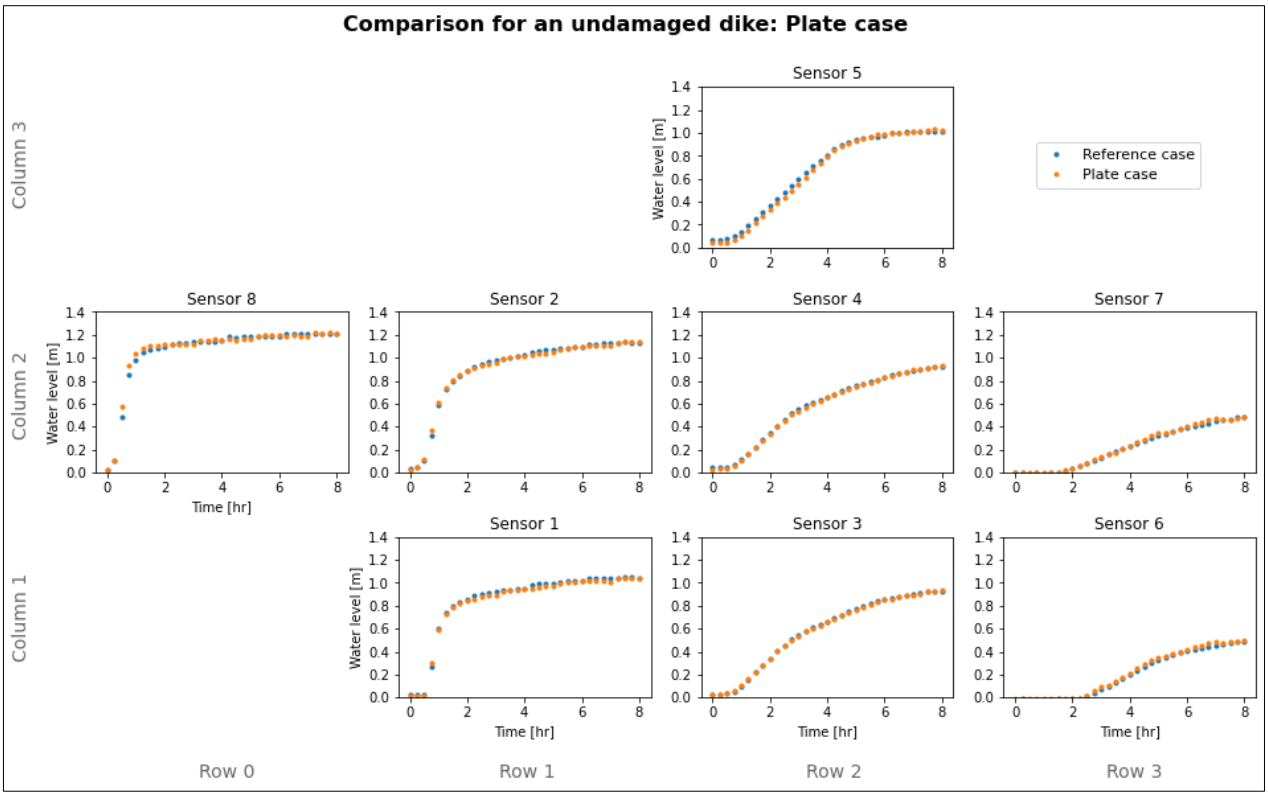

Figure 42: Comparison for an undamaged dike: Plate case

5.2.2.2 Textile on an undamaged dike

The reference case (experiment 1) and the case with a textile (experiment 6) for a dike without damage on the outer slope have been compared in Figure 43.
It can be observed that for sensor 1 the water level for the textile case during filling is lower compared to the reference case. Over time the difference between these two cases gets smaller and they lie close to each other in steady-state. The other sensor measurements however show no significant change.

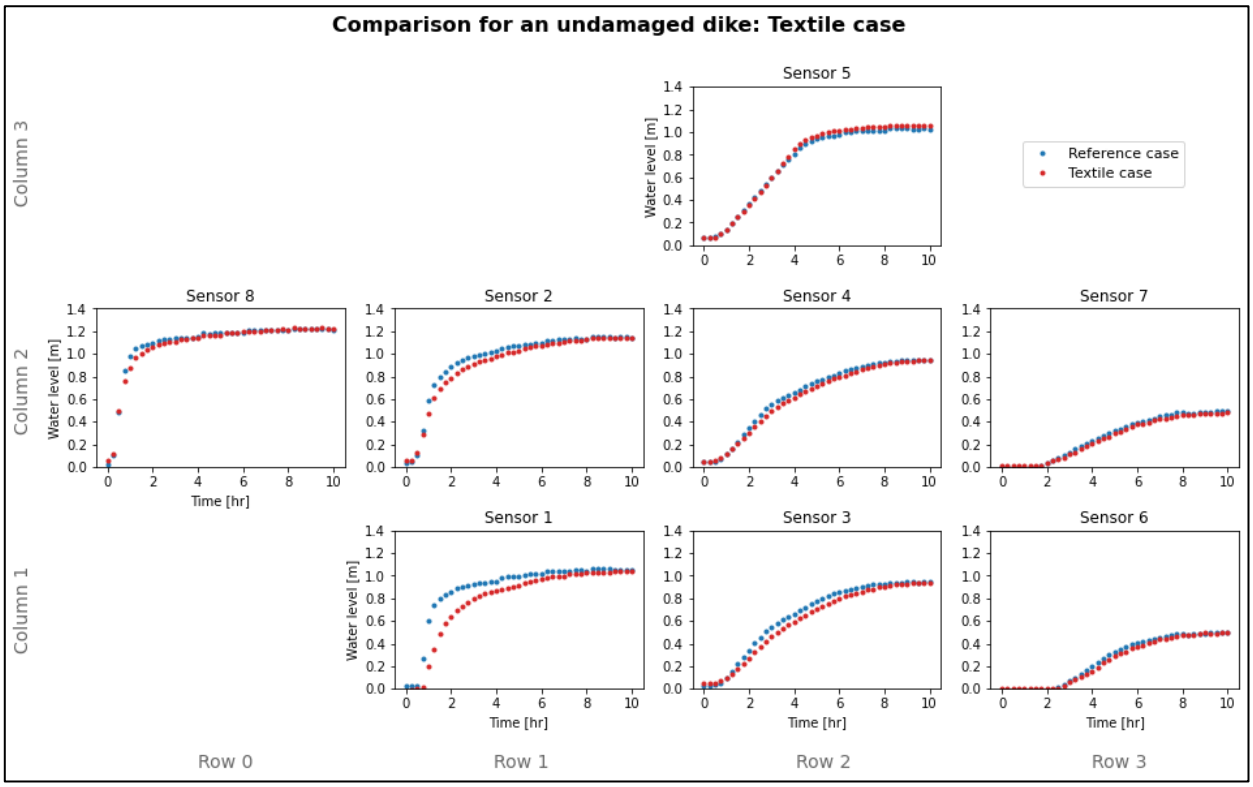

Figure 43: Comparison for an undamaged dike: Textile case

5.2.3 Effects for damaged dike

Similar to the undamaged conditions of the dike in the previous section, the dike had also been tested under damaged conditions of the outer slope. A local hole had been made in the outer slope of the dike with part of the low-permeability cover layer being removed. The same three cases where measured: the case in which no emergency measures are taken (reference case), the case where the hole is covered by a stiff plate (plate case) and the case where the hole is covered by a flexible textile (textile case). The same test procedure and sensor locations are used as in the previous section.

5.2.3.1 Damage on a dike

The reference case for an undamaged dike (experiment 1) and reference case for a damaged dike (experiment 4) have been compared in Figure 44.

It can be noticed that the measurements of the damaged dike are overall lower than the measurements of the undamaged dike. For row 0 and row 1 the difference between these two remains constant over time. For row 2 and row 3 the difference increases over time and decreases around steady-state. The measurements in steady-state for the damaged case are higher than for the undamaged case.

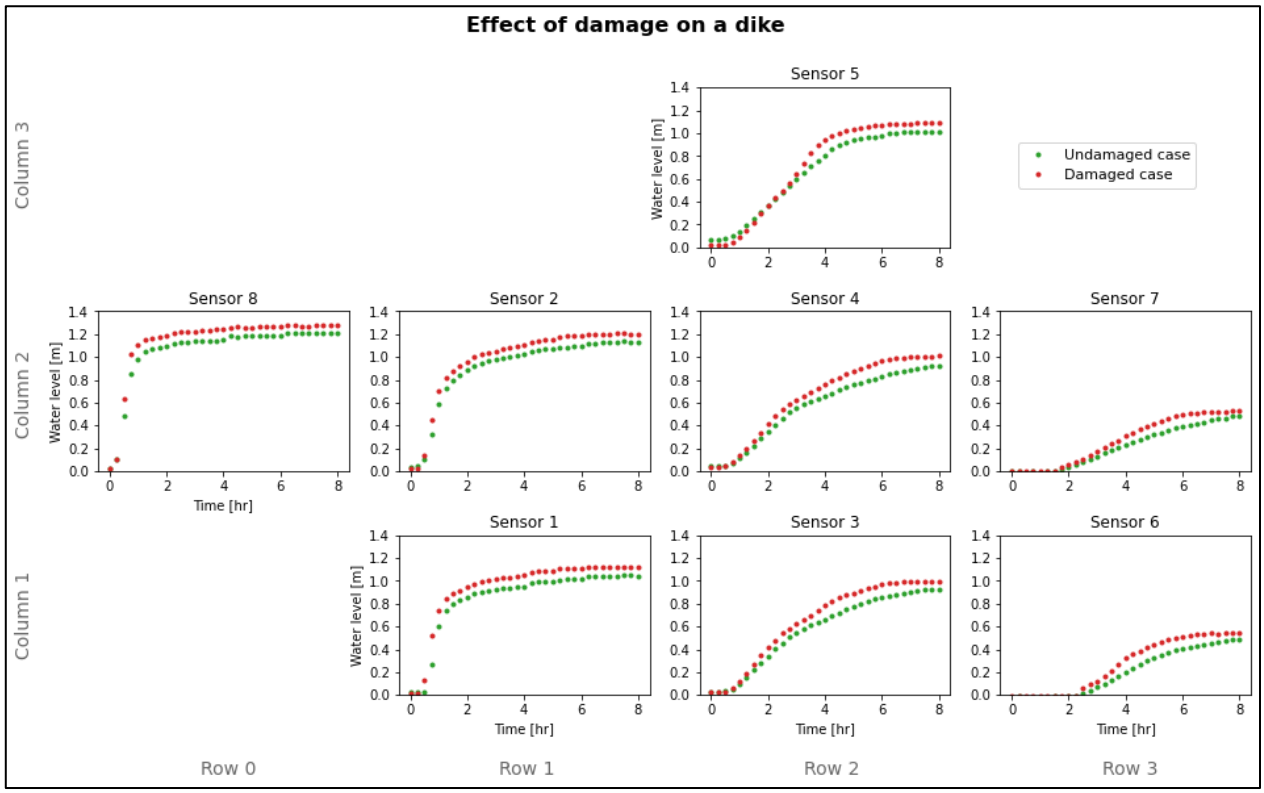

Figure 44: Effect of damage on a dike

5.2.3.2 Plate on a damaged dike

The reference case (experiment 4) and the case with a plate (experiment 3) for a dike with damage on the outer slope have been compared in Figure 45.

It can be noticed that, similarly to the undamaged condition, both cases the measurements of the phreatic surface are close to each other for row 0 and row 1. The case with the plate has a marginal reduction for row 2 and row 3 during filling but reaches the same steady-state level as the reference case.

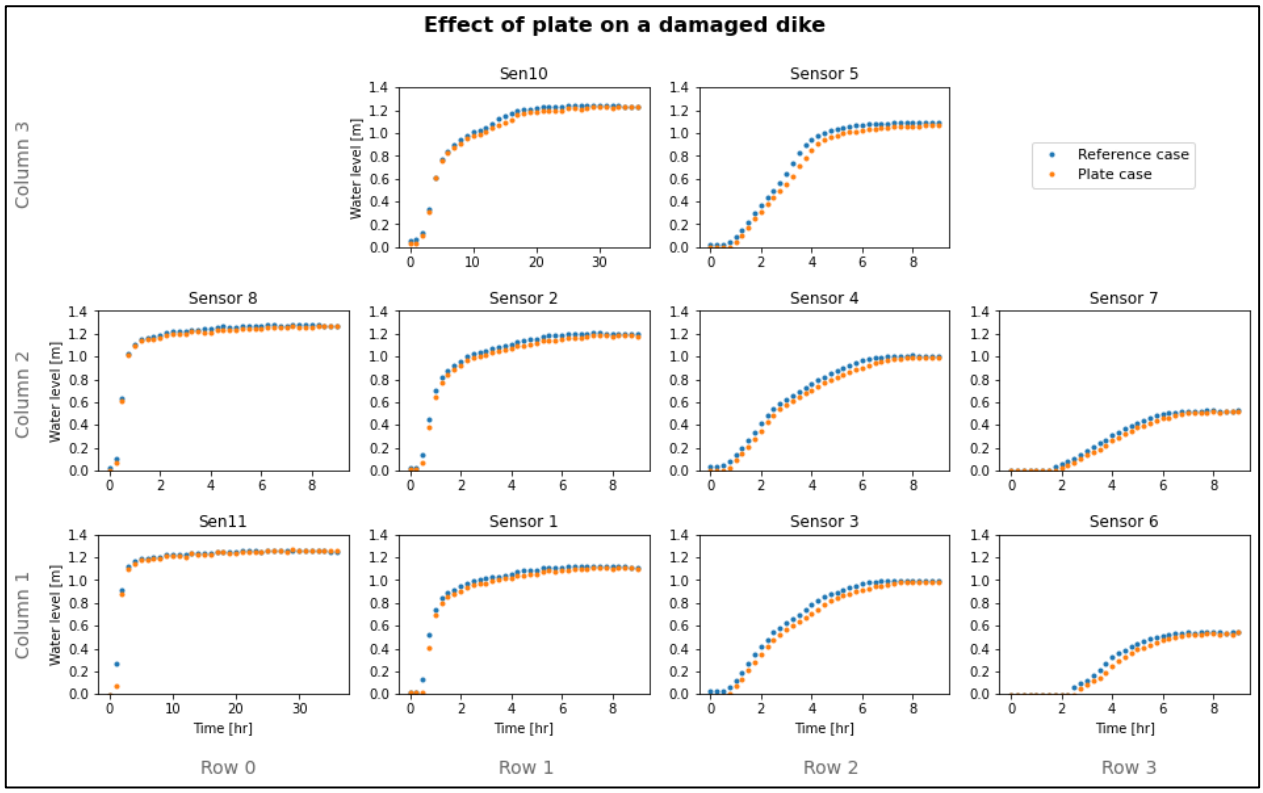

Figure 45: Comparison for a damaged dike: Plate case

5.2.3.3 Textile on a damaged dike

The reference case (experiment 4) and the case with a textile (experiment 5) for a dike with damage on the outer slope have been compared in Figure 46.

The delaying effect, that was noticed with the textile for the undamaged case in section 5.2.2.2, is now even more visible. Especially sensor 1, which is located close to the textile, shows a large difference between the cases. Sensor 2, sensor 3 and sensor 4 show this effect as well with a smaller difference. The other sensors have a difference which is small to none.

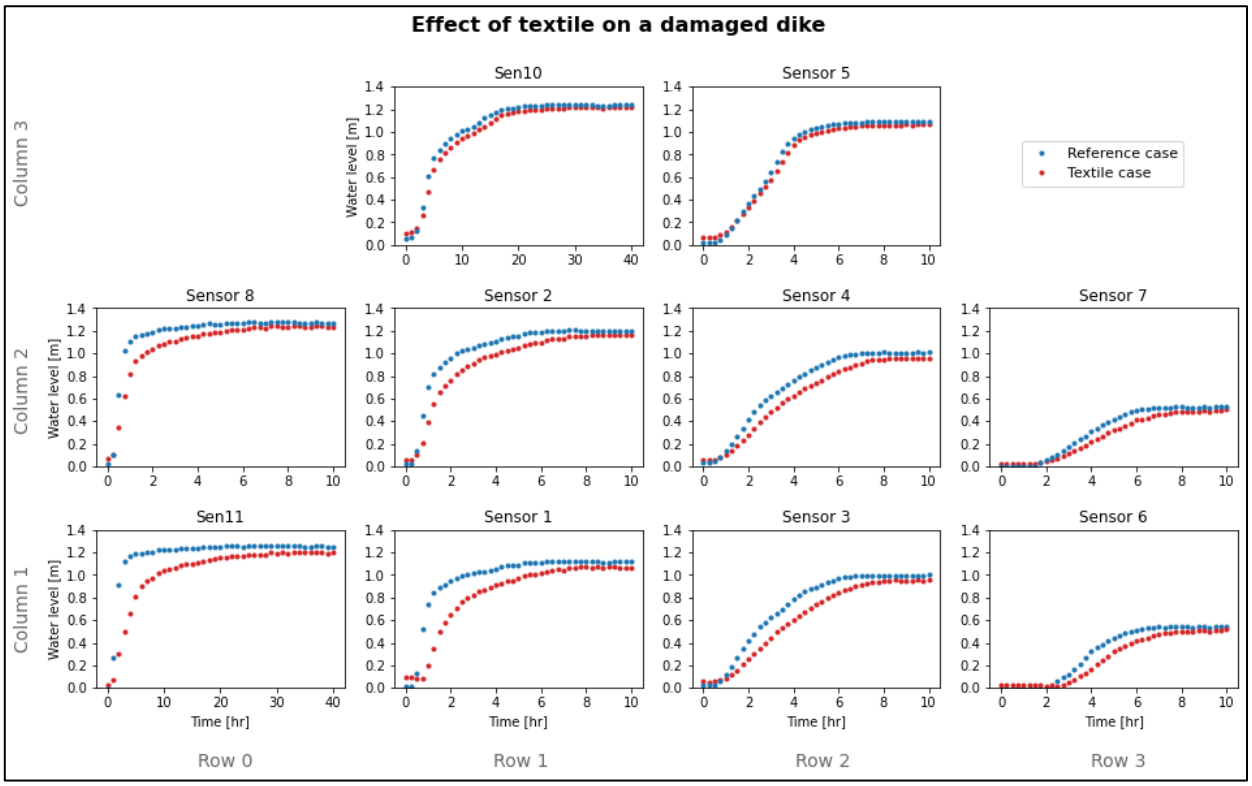

Figure 46: Comparison for a damaged dike: Textile case

5.2.4 Selection emergency measure

As can be seen from the previous sections, the delaying effect for the cases with a textile is more clearly visible than for the cases with the plate. Both plate and textile can be compared for a damaged dike condition in Figure 47.

Due to the relative large effect for the textile case and the relative small effect for the plate case, it is decided to further elaborate on the measurements from the textile case in the following sections.

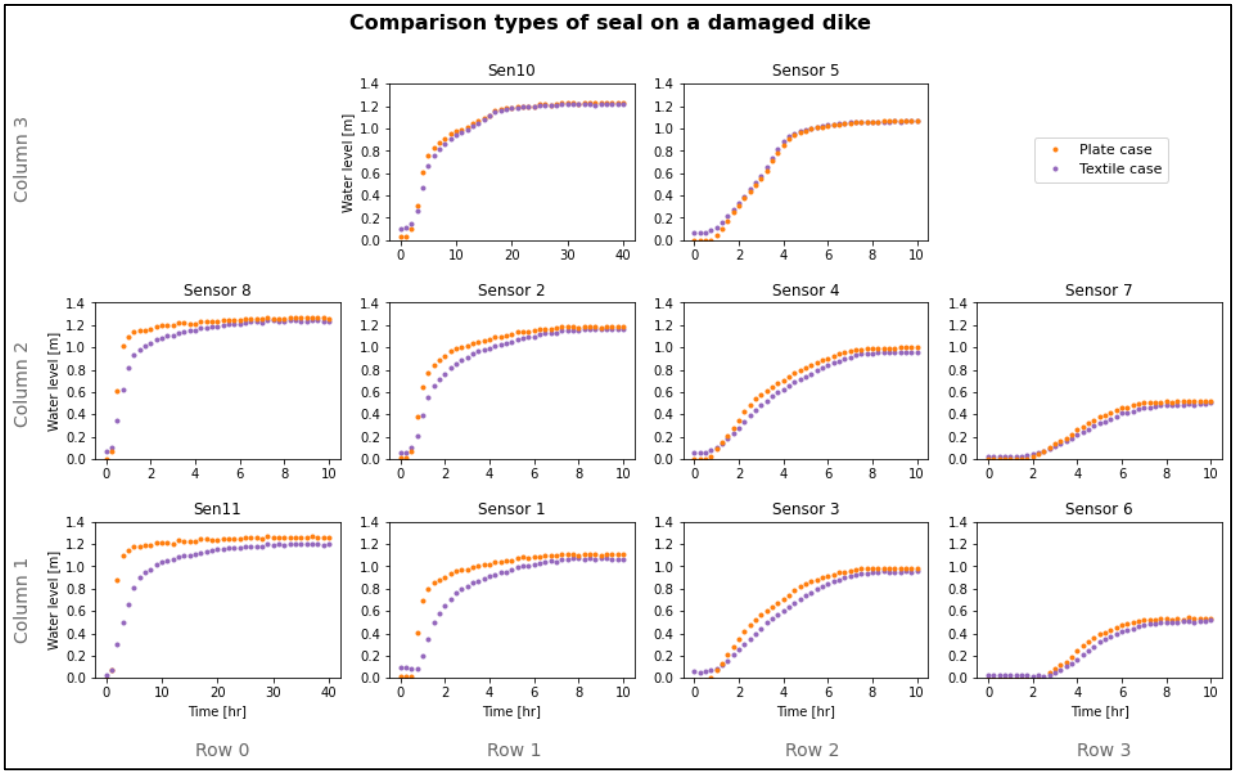

Figure 47: Comparison of plate and textile for a damaged dike

5.3 3D approach

5.3.1 Height map

From the results of the textile cases (section 5.2) can be seen that the delaying effect of the textile is strongly reflected at some locations in the dike. At other locations however this effect seems small or even non-existent. It is therefore convenient to approach the change of the phreatic surface over time as a 3D problem. This involves looking at the difference in phreatic level between the case where a textile is placed on the outer slope and the associated reference case (depending on the damage condition of the dike). This difference in elevation can be plotted over the length and width of the crest and inner slope of the dike, where sensors make measurements over time. An overview of the test set-up that is used for the construction of the 2D height maps is presented in Figure 48. The obtained measurements at the specific sensor locations will analyzed with a multivariate function to obtain insight in the phreatic surface differences over the entire crest and inner slope of the dike. The specific multivariate function that is used in this analysis is the *multiquadric radial basis function*, which performs well for unsteady groundwater flow problems in general (Zheng, Li, & Wang, 2019). The input for the model is the locations of the sensors in (x,y)-coordinates and height difference in phreatic surface between the textile case and reference case at the sensor locations. The function will return the height difference between the cases for a large number of grid points in the (x,y)-plane, which contains the crest and inner slope of the dike as presented in Figure 48.

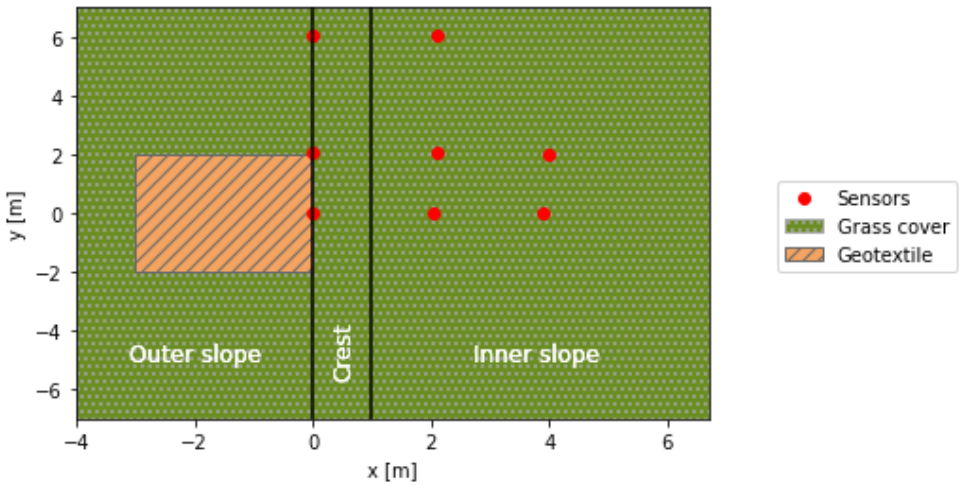

Figure 48: Overview of test set-up for the 2D height maps (Not to scale)

5.3.2 Scenario 1: Undamaged dike

The textile case for an undamaged dike is compared to the corresponding reference case in Figure 49.

The phreatic level directly behind the textile is decreased initially. Over time this difference in phreatic level evens out over space and time. In steady-state no difference in phreatic level can be observed between textile case and reference case.

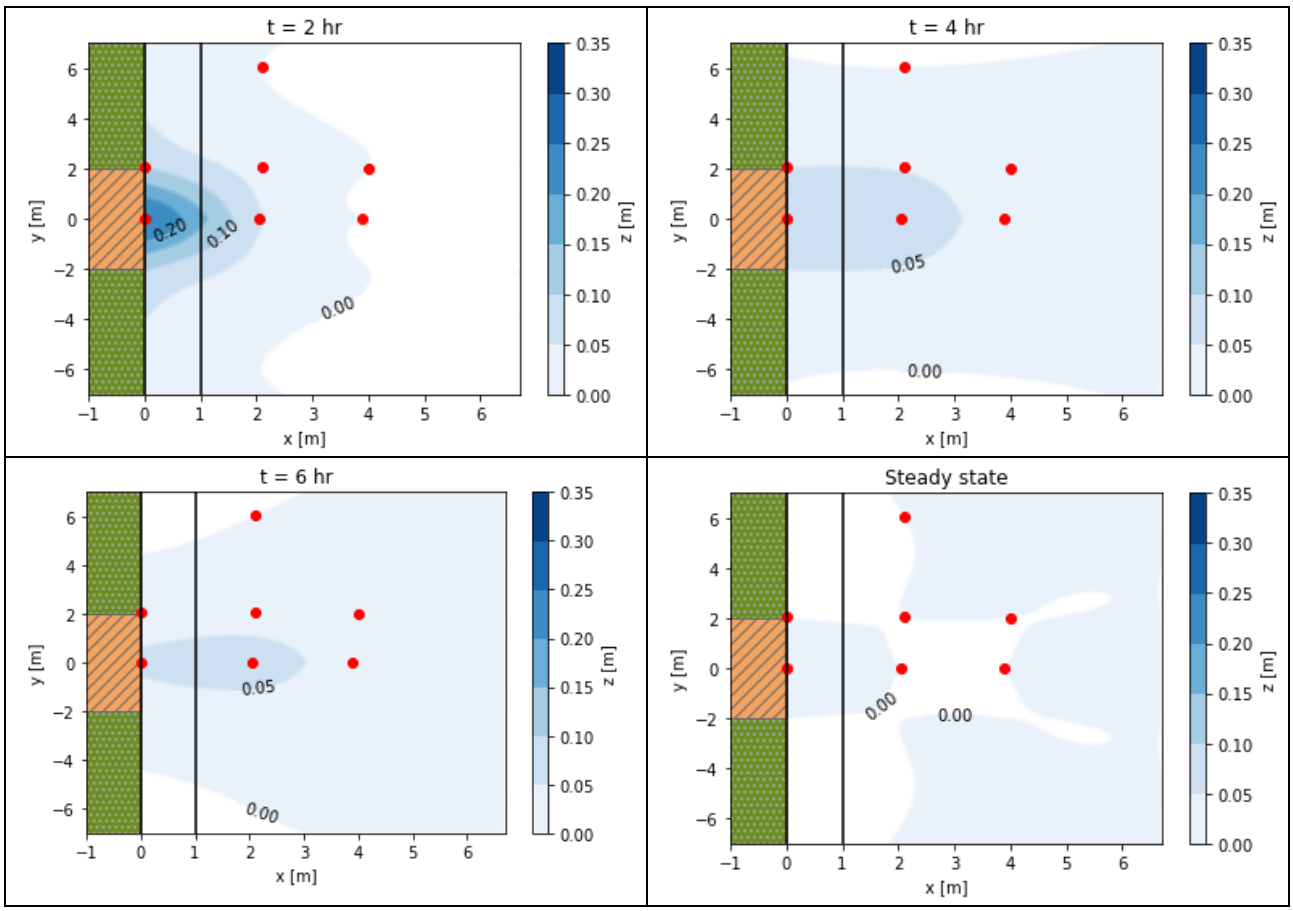

Figure 49: 2D Height maps for the phreatic level difference between the textile case and reference case for an undamaged dike. The z-value is defined as the phreatic surface level of the reference case minus the phreatic surface level of the textile case.

5.3.3 Scenario 2: Damaged dike

The textile case for a damaged dike is compared to the corresponding reference case in Figure 50.

The differences in phreatic level follow a similar development as for the undamaged dike scenario. The differences in phreatic level between the textile case and reference case are even larger.

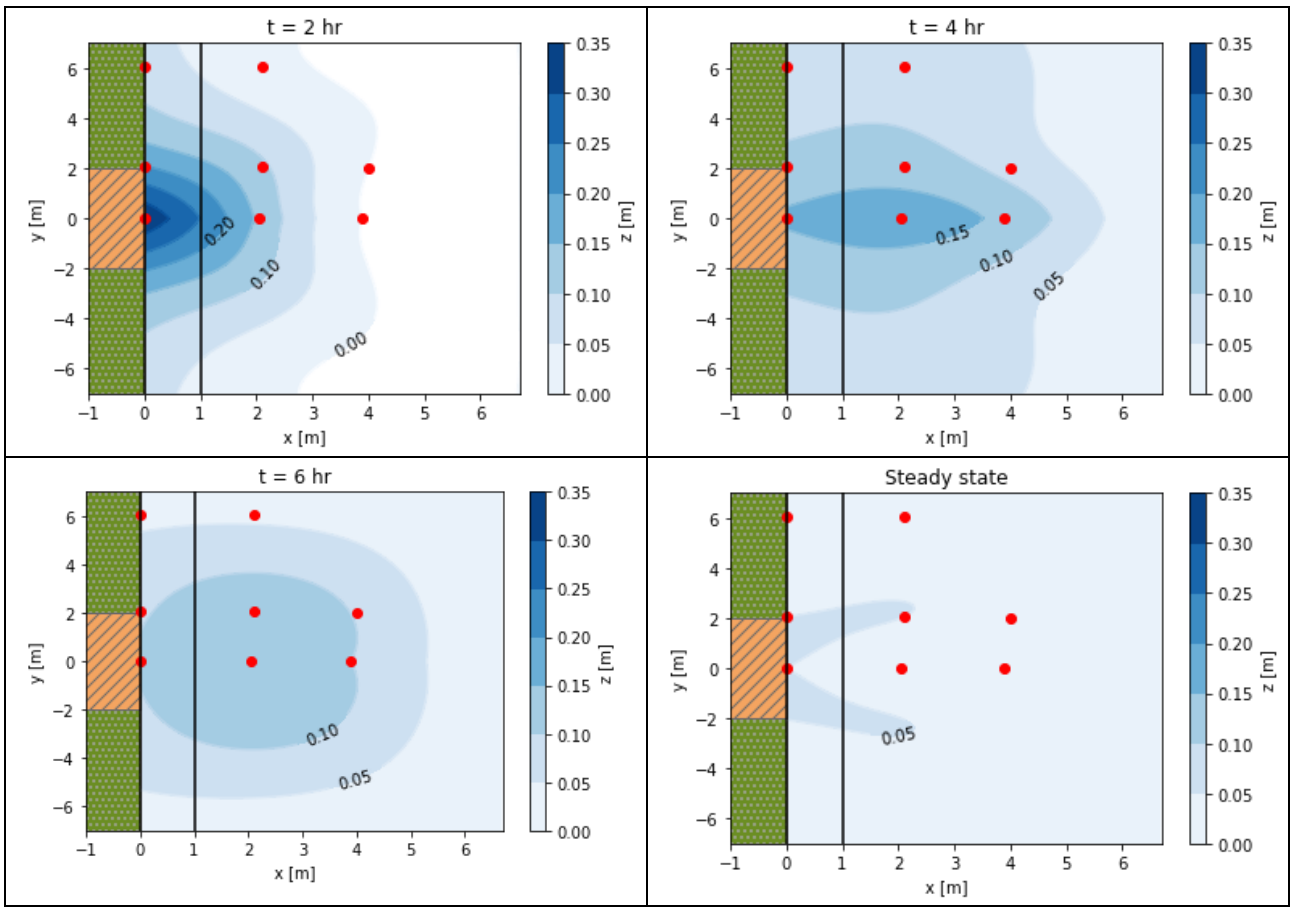

Figure 50: 2D Height maps for the phreatic level difference between the textile case and reference case for a damaged dike. The z-value is defined as the phreatic surface level of the reference case minus the phreatic surface level of the textile case.

6 Calibration and dike safety

Section 6.1 shows the calibration of the numerical model based on the results of the physical model at Flood Proof Holland. Additionally, section 6.2 shows the results for the macro stability and micro stability analyses.

6.1 Calibration of numerical model

6.1.1 Comparison of models

The results of the physical measurements in Flood Proof Holland can be used to calibrate the initially constructed numerical model as presented in section 3.4. Before a calibration can be made, the initial numerical model should be compared to the physical model. The comparison between both models can most easily performed by considering two factors: position of the phreatic surface in steady-state or time until reaching the steady-state condition. Both reference cases (with and without damage) are taken into account and dike cross-section directly behind the hole in the cover is considered (Column 1 in Figure 40). For both models, the position of the phreatic surface in steady-state is thus determined on the locations of sensor 1, 3 and 6. The time until reaching a steady-state condition is for the physical model determined when the overall model shows no changes in the phreatic surface over time.

The results of this comparison are presented in Table 10 and Table 11. In Table 10 can be observed that phreatic level in steady-state is significantly higher for the numerical model at all sensor locations for both reference cases. In Table 11 can be seen that for both reference cases the time until reaching a steady-state condition is much larger for the numerical model.

Table 10: Comparison of steady-state phreatic levels

	Steady-state phreatic level $\mathbf{h}[\mathbf{m}]$					
	Reference case: Undamaged			Reference case: Damaged		
	Sensor 1	Sensor 3	Sensor 6	Sensor 1	Sensor 3	Sensor 6
Physical model	1.12	1.00	0.54	1.05	0.92	0.48
Numerical model	1.32	1.20	0.89*	1.38	1.27	0.89*

Table 11: Comparison of steady-state times

	Steady-state time $\mathbf{t}[\mathbf{hr}]$	
	Reference case: Undamaged	Reference case: Damaged
Physical model	8	7.5
Numerical model	80	50

* Note that the phreatic surface at sensor location 6 is limited to 0.89 m, since this is the height of the dike at this location and the phreatic surface can only exist within the dike.

6.1.2 Approach for calibration

6.1.2.1 Parameter to calibrate

Based on the results of the physical model, the numerical model should be calibrated to capture the development of the phreatic surface and the effect of the textile on that phreatic surface more

realistically. For the approach of the calibration, it is assumed that only soil parameters should be changed. Parameters related to boundary conditions, geometry of the dike and calculation methods are assumed to be accurate and remain unchanged. Within the parameters for the soil material, the permeability (k_s) of the cover material and core material of the FPH dike is adjusted for the calibration of the numerical model. The choice for this soil parameter is based on the fact that the permeability that is assumed in the numerical model is expected to be lower in reality when compared to the permeability that is used in the physical model. Two contributions to this difference in permeability can be explained by the initial moisture content and compaction of the soil, which are described below.

Initial moisture content

The initial conditions in the unsaturated zone cannot be described properly in the numerical model. The initial conditions in PLAXIS are limited to initial phreatic levels inside the dike. The effect of climate conditions, such as temperature, precipitation, and evaporation, have been considered but these had no significant effect on steady-state times of the numerical model. Therefore, the numerical model assumes that no water is present in the dike before testing and the initial moisture content is thus zero.

In the physical model tests, the initial moisture content is expected to not be zero before starting each test. The FPH dike was drained in-between tests for multiple days, where was waited until the phreatic level in the dike reached zero. The presence of water, which remained in the pores of the unsaturated zone, may increase the saturation of pores and could be seen, from a numerical point of view, as an increase of permeability of the soil material. A calibrated numerical model should therefore use a higher permeability to account for this effect.

Compaction

The input parameters of the soil have tested in the laboratory. Soil material is taken from both the dike cover and dike core of the FPH dike. The material is dried and put into sample holders. The compaction of the soil for these samples is assumed to be higher than the compaction inside the dike. Especially, the obtained measurements of the saturated hydraulic conductivity are expected to have a lower value (less permeable) compared to the values inside the dike. A calibrated numerical model should therefore use a higher permeability to account for this effect as well.

Besides both these contributions, the choice for changing the permeability of the soil is also based on easy of understanding of the parameter. Soil parameters related to the soil water storage (SWCC) could in theory also be used in the calibration, however the understanding of the underlying parameters is quite complex and changes in these cannot be carried out easily.

6.1.2.2 Condition to calibrate

Ideally, the numerical model should be calibrated in such manner that the phreatic level in steady-state and steady-state time are similar to the physical model.

During calibration of the numerical model, it is found that decrease of the phreatic level in steady-state based on changing the permeability is very limited. The phreatic level in steady-state for the numerical model can be lowered by increasing the ratio between the permeability between core and cover layer, which results in a lower k-value for the cover layer and higher k-value for the core. The effect of increasing the ratio, however, proved to have a relatively small effect on the position of the phreatic surface in steady-state. Even for extreme ratios (order of magnitude above 5), the lowering of the position of the phreatic surface is limited. For example, for the undamaged reference case, at location of sensor 1 only a decrease of 0.05 m compared to the original situation could be realized, which is not near the intended decrease of 0.2 m which is measured in the physical model. The decrease of steady-state phreatic level is therefore limited.

A similar offset between steady-state phreatic level of the numerical and physical model was also observed for the WaterLab dike as discussed in section 3.3. The steady-state phreatic level of the numerical model shows also a higher location for the reference case when compared to the measurements of the physical model. The effects of initial moisture content and compaction are expected to play a smaller role on the numerical model of the WaterLab dike, because the measurements are conducted inside (no precipitation, constant humidity), the dike is small-scale (more constant compaction) and consists of homogeneous sand material (good drainage and similar compaction to laboratory tests of soil).
It is assumed that this offset between steady-state phreatic level for the WaterLab dike and FPH dike is related to some unknown cause. Therefore, calibration of the numerical model of the FPH dike based on the steady-state phreatic level is not advised and it is opted to calibrate based on the time until reaching a steady-state condition of the phreatic surface.

6.1.3 Method of calibration

As mentioned earlier, the goal of this calibrated numerical model is to capture the development of the phreatic surface and the effect of the textile on that phreatic surface more realistically. In order to do so, the calibration is separated in two steps:

Step 1: Calibration of the dike material
The permeability of the cover and core material of the dike will be obtained by calibration on the reference cases (with an undamaged and damaged cover).

Step 2: Calibration of the interface material
The permeability of the interface material of the textile will be obtained by calibration on the textile cases (with an undamaged and damaged cover).

The numerical model will thus be calibrated based on the time until the phreatic surface reaches its steady-state condition by increasing the permeability of the soil material. For the first step, it is assumed that the effects of the initial moisture content and compaction influence the permeability of the material of the cover and core of the dike to the same degree and that, therefore, the ratio between the permeability of the core and the permeability of the cover should remain equal. This means that when the input parameter for the permeability of the core material is changed with a certain factor, the permeability of the cover material will also be changed with that factor. This method helps keeping the calibration straightforward and will not change the initial behavior of the phreatic surface severely (compared to changing the permeability of just one of the materials).

Once the reference cases are calibrated, the second step can be taken to calibrate the textile cases. Similar to the numerical model of the sealed case of the WaterLab dike as mentioned in section 3.3.5, the textile case can also be modelled with an interface layer for the FPH dike and is presented in Figure 51. The interface layer is placed on top of the dike cover and has a thickness equal to the thickness of the dike cover. The interface layer covers around 3/4 of the top part of the dike cover and is located in the middle of the hole in the dike cover, which is equal to the location of the textile in the physical modelling at FPH. This means that, similar to the WaterLab dike, the flow around the textile is modelled as a flow through the interface layer. For the calibration of the permeability of the interface layer is looked into both textile cases.

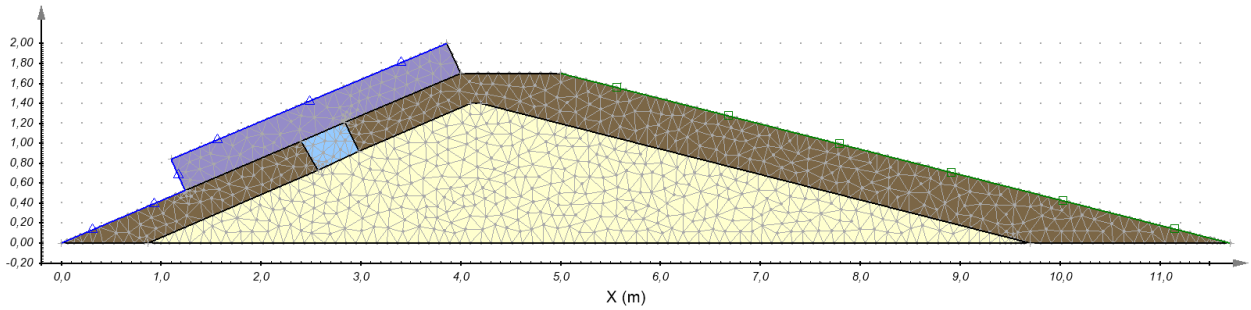

Figure 51: Numerical model of FPH dike for the textile case with damage.
Note that the hole in the outer cover is modelled by a high transmissive layer (in blue), since this is an empty hole that can be filled with water.

6.1.4 Results

Step 1: Calibration of the dike material

The calibration of the numerical model is done iteratively until both reference cases have steady-state time values that lie close to the values of the physical model. The initial permeability of the core and cover are
$k_{core} = 1.7 \cdot 10^{-1}$ m/hr and $k_{cover} = 7.42 \cdot 10^{-3}$ m/hr respectively. Ultimately, it follows from the calibration that both the permeability of the core and cover are increased by a factor of 10, which are now respectively $k_{core} = 1.7$ m/hr and $k_{cover} = 7.42 \cdot 10^{-2}$ m/hr. This calibration happens also to increase the steady-state time with a factor of 10. The results of the steady-state times are presented in Table 12 and the development over time of the phreatic surface is visualized in Figure 52.
In Table 12, it can be observed that the steady-state times for the undamaged reference case are equal for the physical model and numerical model. For the damaged case, however, still a difference between both models is present. This can probably be explained two-dimensional character of the numerical model, which assumes that the hole is present over the entire width of the dike. However, this is not the case, which will result in a slower rate of seepage and thus a larger steady-state time in reality as the physical model points out.
For the development of the phreatic surface in Figure 52, it can be seen that the calibrated numerical model has a significantly higher steady-state phreatic level than the physical model for both reference cases. It is already discussed in section 6.1.2.2 that the offset between both models is similar for the models of the WaterLab dike and this can also be seen for this calibrated reference case.

Table 12: Calibration of steady-state times for reference cases

	Steady-state time t[hr]	
	Reference case: Undamaged	Reference case: Damaged
Physical model	8	7.5
Calibrated numerical model	8	5

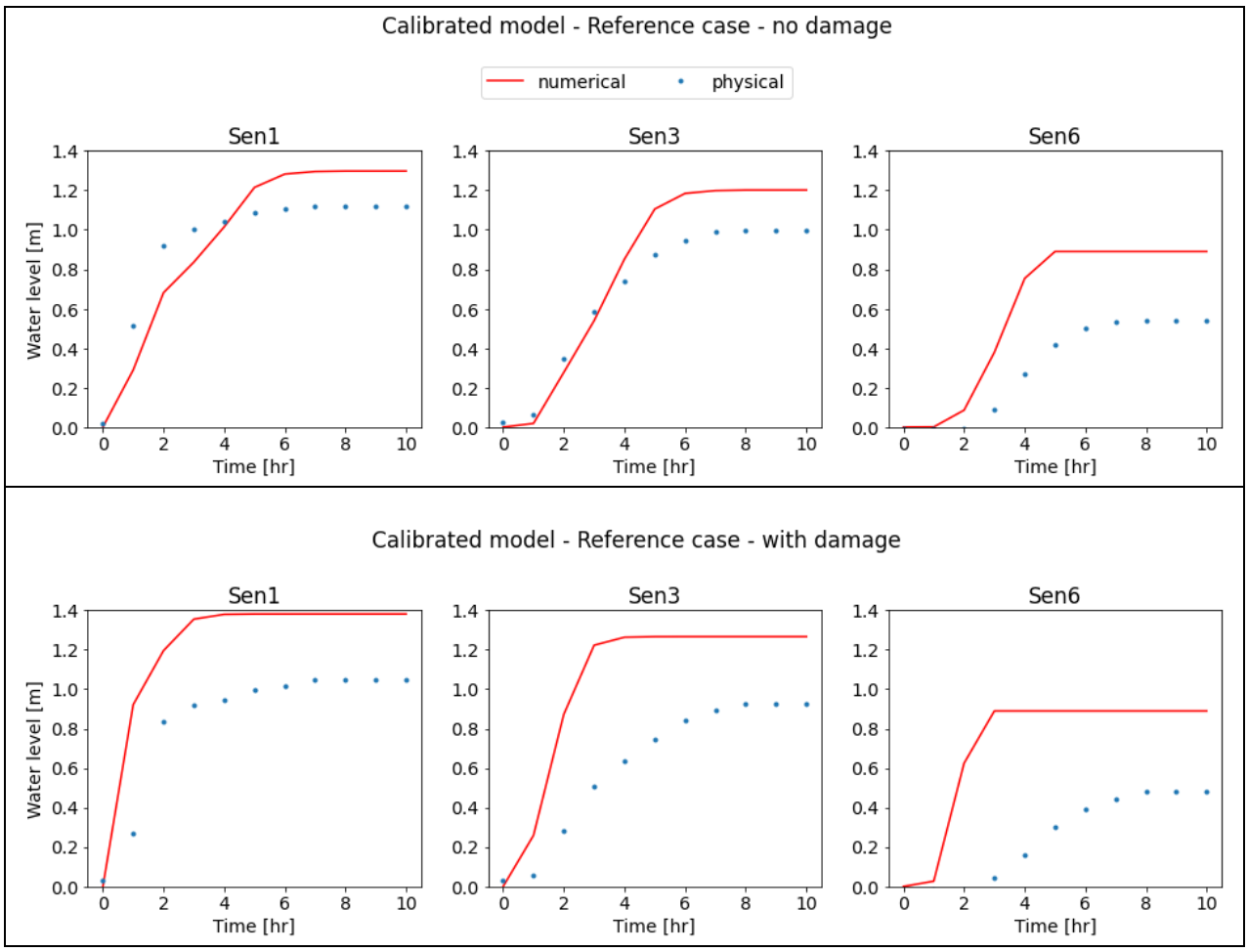

Figure 52: Comparison of the calibrated numerical model and physical model for the reference cases.

Step 2: Calibration of the interface material

With the parameters for the permeability from the calibrated numerical model, the calibration is performed for the material of the interface layer based on the textile cases. Ultimately, it follows that the interface layer material has a permeability equal to the permeability of the cover material of the calibrated numerical model, which is equal to $k_{inter} = k_{cover} = 7.42 \cdot 10^{-2}$ m/hr.

In Table 13, it can be seen that the steady-state times of the calibrated numerical model are close to the ones from the physical model for both textile cases. In Figure 53, a similar development of the phreatic surface can be seen as for the reference case from step 1, where the numerical model reaches a higher phreatic surface than the physical model.

Table 13: Calibration of steady-state times for textile cases

	Steady-state time $\mathbf{t}[\mathbf{hr}]$	
	Textile case: Undamaged	Textile case: Damaged
Physical model	10	9.5
Calibrated numerical model	10	9

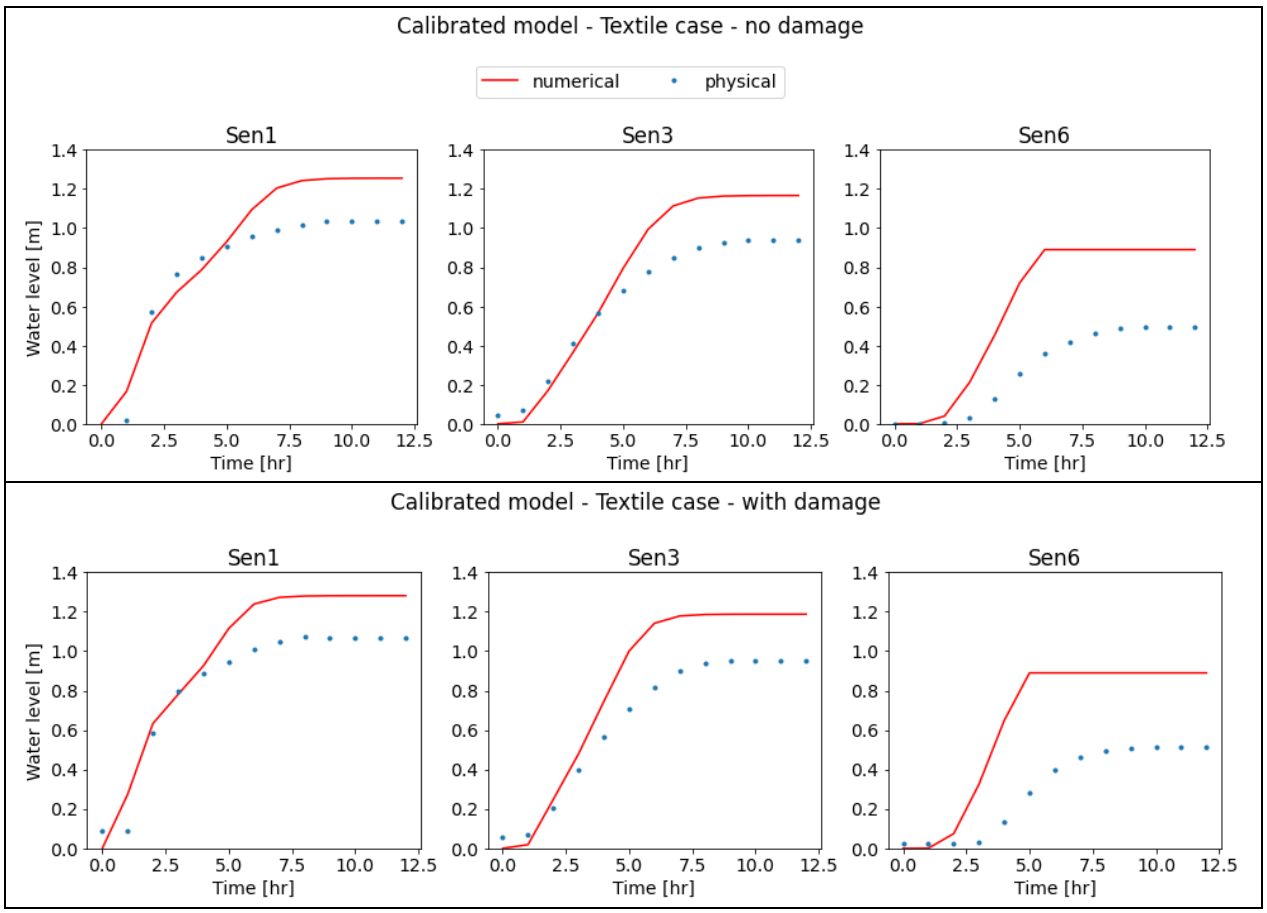

Figure 53: Comparison of the calibrated numerical model and physical model for the textile cases.

6.1.5 Performance of the textile

Besides the goal to calibrate the numerical model itself, the calibrated numerical model can also help understand the boundaries of the effect of the textile and the performance of the textile under current circumstances. The lower boundary of the effect of the textile occurs when the textile has no effect on the phreatic surface of the dike and can be numerically modelled with an extremely high permeability, which corresponds to the measured reference cases. The upper boundary of the effect of the textile occurs when the textile is impermeable (extremely low permeability) and can be numerically modelled with no seepage through the interface layer which can be modelled with a no flux boundary for this interface layer. Based on these two boundaries, the performance of the textile in the current state of the calibrated numerical model can be analyzed.

The results are presented in Table 14 and Table 15. Both the steady-state time and steady-state phreatic level of the textile case in its current state indicate that its effect is closer to the lower bound than the upper bound. Especially, the steady-state time could idealistically be more than doubled as the upper bound suggests for both damaged conditions. The phreatic levels should be taken with a grain of salt as the numerical model is not calibrated for the phreatic level, however, the upper bound implies that the steady-state phreatic level could potentially be lowered compared to the current state of the textile.

Table 14: Comparison of steady-state times with textile case boundaries

		Steady-state time $t[hr]$	
		Undamaged	Damaged
Lower bound	Reference case	8	5
Current state	Textile case	11	10
Upper bound	No flux case	24	24

Table 15: Comparison of steady-state phreatic levels with textile case boundaries

		Steady-state phreatic level $h[m]$					
		Undamaged			Damaged		
		Sensor 1	Sensor 3	Sensor 6	Sensor 1	Sensor 3	Sensor 6
Lower bound	Reference case	1.32	1.20	0.89*	1.38	1.27	0.89*
Current state	Textile case	1.26	1.17	0.89*	1.28	1.19	0.89*
Upper bound	No flux case	1.10	1.06	0.89*	1.10	1.06	0.89*

6.2 Dike safety analysis

The results of the physical measurements can also be used to check dike safety criteria. Two failure mechanisms are considered: macro stability and micro stability. The measurements of the phreatic surface in the dike profile directly behind the textile is considered over time. The background, methods and approaches are presented in Appendix D. In the paragraphs below, the results are presented and discussed.

6.2.1 Macro stability

The result of the macro stability analysis is shown in Figure 54. The overall differences in factor of safety between the cases is marginal over time, which can be seen on the plot on the left-hand side. On the right-hand side plot, some remarks can be made however when looking closely at the different cases:

- The cases with implementation of a textile lead to a higher FoS over time than the corresponding reference cases. At the start of the experiments, the phreatic level in the dike is zero which leads to the maximum value of 3.52 for the FoS. During the experiments, the phreatic surface for each case increases with a different rate which leads to a varying decrease of the FoS over time for each case. At the end of the experiments, the phreatic levels reach a constant level (steady-state condition) which leads to a constant FoS.
- The textile case with a damaged cover has a larger FoS than the undamaged reference case, which indicates that the implementation of a textile is beneficial in terms of macro stability

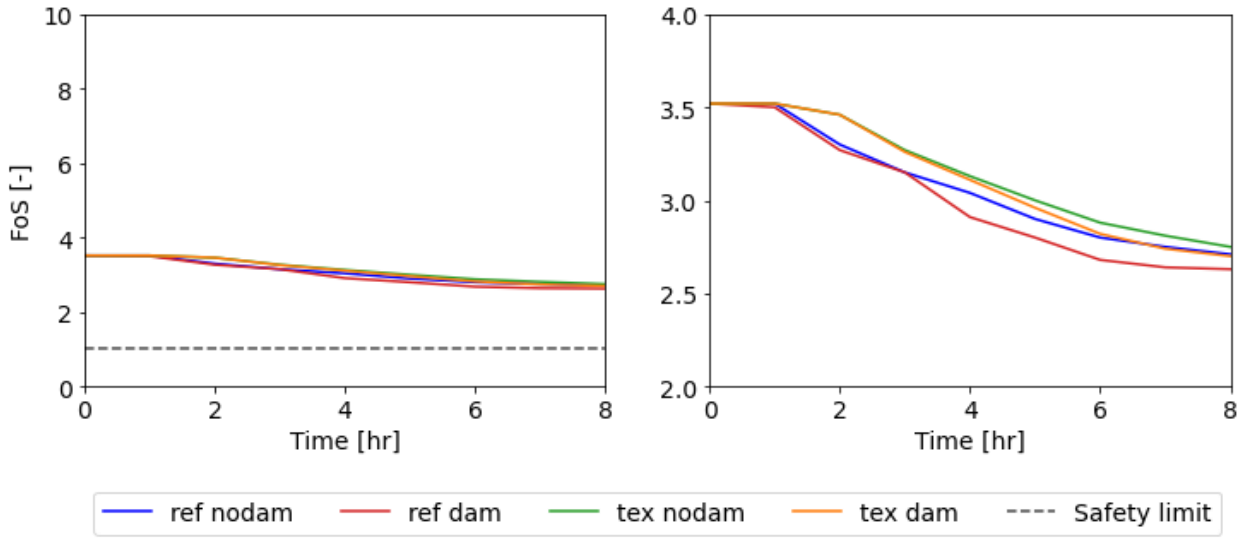

Figure 54: Macro stability analysis with time-varying factor of safety (FoS).

6.2.2 Micro stability

The development of the factor of safety for micro stability during filling for the different FPH experiment cases is presented in Figure 55. The safety factor is very high in the beginning due to the water height of zero. Over time the safety factor decreases due the increase of water height and stabilizes in the end at a minimum value because the water height reaches a steady-state condition.

All cases stay above the critical value for the safety factor of 1.0, so are considered safe against uplift of the clay cover. It can be seen that the reference case with damage has the lowest safety factor in transient condition, where the other three cases lie more closely to each other. This difference decreases over time and is in steady-state marginal.

Both textile cases show an increased safety factor over time compared to the corresponding reference cases. This increase is for undamaged conditions negligible small, but for the damaged conditions quite substantial.

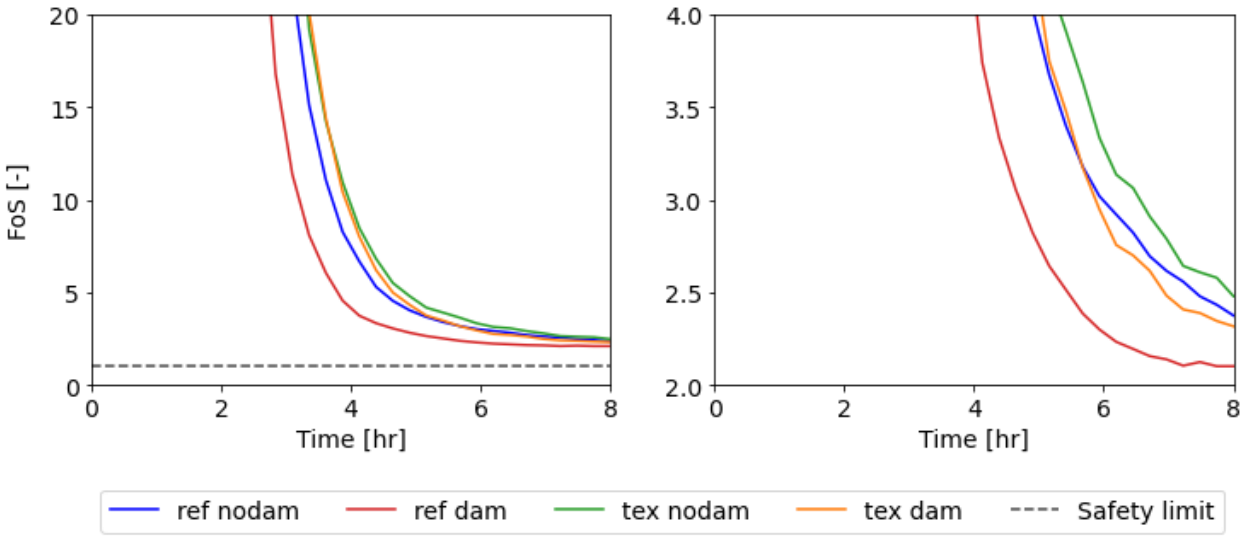

Figure 55: Micro stability safety criterium

7 Discussion

This study focused on the effects of covering part of the outer slope of a dike to influence the phreatic surface level. Results have been found with numerical and physical approaches to answer the research questions. The interpretations, assumptions and limitations of these results are discussed in this chapter.

7.1 Interpretation of effects

The interpretation of the outcomes of this study are important to improve the understanding of the underlying problems. To understand the effect that the sealing has on the phreatic surface, it is important to find similar patterns between the numerical and physical approaches.

Delaying effect

First, the textile sealing has a time-varying decreasing effect on the phreatic surface level inside a dike. The measurements of the physical model show that initially the phreatic surface level is decreased significantly close to the textile. The explanation is that the textile covers part of the dike and prevents seepage at this location. The application of this textile as sealing is quite good due to the connection between sealing and dike cover. The outer slope of the dike has an uneven profile, which is expected for real-scale scenarios where a sealing may be applied. The more flexible nature of the textile improves this sealing-cover connection. The textile is made of flexible impermeable material, which retains water and soil, and is weighted by sandbags. When using a stiff plate as sealing, the decreasing effect of the sealing on the phreatic surface is significantly smaller. The plate cannot shape itself to the outer slope, which makes the connection between plate and cover suboptimal. This poor connection increases water flow underneath the plate and makes the effect, that the plate has on the phreatic surface development, therefore small.

Decreasing effect

The phreatic level in steady-state is not significantly affected by the sealing. The phreatic surface level for the plate case reaches a similar maximum height with respect to the reference case. For the textile case, a lowering of the phreatic level in the range of $0 - 5\ \mathrm{cm}$ can be observed. This effect is small when compared to the height of the phreatic surface level that is still present in steady-state. The application of a textile on a real-scale dike will therefore be considered too small when for this intermediate test case, tested under beneficial conditions for the sealing, the effect is already estimated to be small.
The lack of a decreasing effect of the textile is in line with the conclusion from the previous study with the WaterLab experiments. This study concluded that for a homogeneous small-scale dike no change of phreatic level could be observed when the entire outer slope of a dike was sealed.
The reasoning for this lack of phreatic level decrease is that the permeability of dike material does not affect the phreatic surface level in steady-state. From the numerical model of the FPH dike is concluded that for different dike materials the phreatic level in steady-state is similar.

Steady-state time

The textile has a small effect on the time until the phreatic surface level reaches a steady-state. The textile cases with damaged and undamaged condition reach the steady-state level later than the corresponding reference cases. Especially, when comparing the damaged textile case with the undamaged reference case, the measured steady-state time is even larger for the damaged textile case. This is a promising result that suggests that a locally damaged dike can be covered with a textile and behave similar to its undamaged condition.

Influence length of textile

From the height maps can be seen that phreatic level directly behind the textile is decreased initially for the textile case of the FPH experiments. This decrease in phreatic level is strongest close to the textile and becomes weaker for larger distances. This textile affects the phreatic surface level with a certain influence length and influence width.
This reasoning behind this effect is very intuitive as seepage is blocked due to the textile. The distance that water must travel to reach the area behind the textile is therefore increased. Especially, for the damaged scenario of the outer slope, the free flow of water into the dike core is prevented leading to a substantial phreatic surface difference directly behind the textile initially. The seepage is locally hindered at the location of the textile but remains unaffected for the rest of the outer slope. The permeability of the dike cover is after all constant and will not be influenced by the textile. Over time, the phreatic surface increases over the whole dike profile and the phreatic surface evens out behind the textile.

Dike safety

The textile may have a beneficial effect on dike safety over time. For micro stability, the safety factor is higher for cases with a textile higher during high-water conditions due to the lower phreatic surface at the inner toe of the dike. The delaying effect of the phreatic surface is reflected in the safety factor, where the implementation of a textile delays the reduction of safety factor over time. Similar to the delaying effect of the phreatic surface is the effect on the phreatic surface higher for a dike with damaged conditions.
Due the dimensions of the test dike at FPH, the proposed effect in dike safety is only indicative since the FPH dike will not fail for the considered failure mechanisms in the steady-state condition. Therefore, the proposed increasing effect in dike safety is only hypothetical and not based on actual states of failure.

7.2 Assumptions and limitations

7.2.1 Numerical modelling

WaterLab dike

The data from the WaterLab experiments originates from a study that is carried out prior to this study. These measurements aid this study, since the experiments have been carried out and the data has already been processed. This saves a lot of time in this study.
The limitation is however that certain known unknowns and unknown unknowns cannot be easily identified for these experiments. Only information that is reported in the previous study can be used. For example, for the sealing case of the WaterLab experiments the entire outer slope is covered with an impermeable plate. The effects of leakages around the plate are assumed to be small due to the even slope and extra attention to minimize flow around the sides of the plate. The measured effect of the plate on the phreatic surface development is, with respect to the reference measurement, still relatively small. This indicates that there must still be leaks around the plate that have not been addressed. The unknown cause of these leaks can therefore not be included in the numerical model
Another limitation of the numerical modelling of the WaterLab dike is that it consists only of a homogeneous soil profile. The results show that the permeability of a homogeneous dike have no effect on the phreatic level in steady-state. For a heterogeneous dike, the phreatic surface in steady-state changes however. The step from small-scale homogeneous to intermediate-scale heterogeneous dike is therefore quite large. An additional step with a small-scale heterogeneous dike would be beneficial in the effect of the low-permeability cover layer on the phreatic level in the dike.

FPH dike

The results from the physical model show that the phreatic surface development is a three-dimensional problem. The numerical model is two-dimensional however, which does not account

for effects over its width. By implementing a hole in the cover of the outer slope and/or a sealing on the outer slope, the effect of these adjustments will be modelled over the entire dike width. This means that for the textile case the hole and the plate are modelled over the entire width of the dike. Effects of flow around the sides of the sealing cannot be modelled for example. The numerical model is therefore limited to its two dimensions while it is trying to describe a three-dimensional physical problem.

7.2.2 Physical modelling

Dike profile

The profile of the dike is not even over length and width. This is most probably caused by settlements and previous experiments. Also, in the FPH dike are still tubes present in the dike profile that may cause leakage paths, which are presented in Appendix E.1. From the reference measurements, no local effects on the phreatic surface could be observed due to these tubes, however, a global effect on the entire region of the measured dike cannot be disproved.
It should be noted that the dike had a more even profile when initially constructed, which is presented in Appendix E.2. No variations are assumed in the dimensions of the dike; however, it can be observed from the initial photograph of the FPH dike that some settlements may have occurred. In reality, it is even doubted that the construction of the FPH dike is carried out very precisely initially and, after many experiments and time, the dimensions of the dike are even further away from the initial dimensions.
On top of that, the soil profile, which is described in the previous experiment, is assumed to be accurate for the current state of the dike and the is assumed to consist of two types of soil materials: low-permeability cover material and permeable core material. It is also doubted that both materials consist of a homogeneous material since this material is used in bulk and the exact thickness of the FPH cover material (either 0.3 m for the outer slope and 0.5 m for the core and inner slope) may fluctuate over the entire dike width as well.

Sensor locations

The measured differences in phreatic surface should only be compared between the cases and cannot be used to determine the phreatic level at a certain level in the dike precisely. The differences in phreatic surface between the cases are relatively small. Therefore, the location of the sensors needs to be known precisely. To do so, the geometry of the dike and distances between the sensors are measured by hand. Measurement inaccuracies are inevitable in length and width. Furthermore, the sensors are not expected to be on the same level. The holes for the standpipes were drilled until the low-permeability layer at the foundation was reached. This layer is not expected to be at the same depth over the entire dike profile. The combination of this uneven layer and an uneven dike profile makes it difficult to get all sensors on the same depth.

Test duration

The certainty in determining steady-state time durations for the FPH experiments is limited by the test duration. Measurements were done during the day where the outer basin was refilled and the inner basin was emptied every hour. This laborious process was necessary since the tube with sliding leaked a significant amount of water from the outer basin into the inner basin. The measured steady-state times seem plausible in general, although a longer duration of the measurements on the first day would help to provide more certainty when the steady-state had been reached.

8 Conclusions and recommendations

This chapter describes the conclusions from this study. In Section 8.1, the research questions are answered to formulate to answer the main research question of this study. Section 8.2 presents recommendations for future research to help understand the implications of this study.

8.1 Conclusions

8.1.1 Research questions

The objective of this study was to provide more insight in the effect of a seal on the development of the phreatic surface. In order to fulfill this objective, research questions have been formulated which will be answered in this section.

1. "What type of effects of a seal on the phreatic surface can be distinguished?"

The two main effects that can be distinguished are the delaying effect and decreasing effect.
The seal has a delaying effect on the development of phreatic surface level of a dike in space and time. When a dike is subjected to a high-water at its outer slope, the rise of phreatic surface level over time is dampened by sealing part of that outer slope. When reviewing this effect over the dike profile, the phreatic surface level is affected more strongly for locations close to the seal. The delaying effect on the phreatic surface is also stronger for cases where the dike cover has been locally damaged. The placement of a seal on top of this damaged location indicates that the phreatic surface can be decreased severely over time close to that damaged location, especially when compared to the case where no measures are taken at all. For the FPH case where a textile is used as seal, a decrease of 30 cm is present directly behind the textile after measuring for 2 hours for the damaged dike scenario. This maximum value of 30 cm dissipates, however, over time and is in steady-state no longer present. This delaying effect of the seal results in a longer time period until the phreatic surface reaches its steady-state level. The time until reaching a steady-state condition was increased with 15% for the plate cases and 25% for the textile cases when compared to the corresponding reference cases.

The seal has however no significant decreasing effect on the phreatic surface in a dike in steady-state. The location of the phreatic surface in steady-state is similar for cases where a seal on the outer slope of the dike is placed and cases where no measures are taken. The effect of damage on the outer slope did not change the location of the phreatic surface in steady-state either. Therefore, the effect of a seal to decrease the phreatic level in a dike in steady-state is not useful.

The results of the FPH measurements are also in correspondence with the results of the WaterLab measurements, which show that only a delaying effect is present and no decreasing effect when applying a seal. When considering the delaying effect, the approach of protection on top of a damaged dike shows potential as a time-dependent emergency measure against dike failure.

2. "How can the effect of a seal on the phreatic surface be described by a numerical model?"

The effect of the seal on the phreatic surface is modelled by an interface layer. Two-dimensional numerical models are created in PLAXIS with the module PlaxFlow to describe the phreatic surface

development in the dike profile over time. The seal on the outer slope of the dike is modelled by an additional transmissive layer on top of the outer slope, which is known as the interface layer. This interface layer models the leakages around the impermeable seal by flow through a transmissive layer. A value for the permeability of this interface layer can be found which should have a similar value to the cover layer of the dike, as the calibrated numerical model of the FPH dike suggests. This numerical modelling approach for a seal does not describe the underlying physical process but can help illustrate the effect of the seal on the phreatic surface.

3. "What is the effect of leakages around a seal on the phreatic surface?

The effect of leakages around the seal can be observed in the development of the phreatic surface. These effects depend on (1) the connection between seal and dike cover and (2) the 3D effect of the seal.
The connection between seal and dike cover is important since presence of water flow is predicted underneath the sealing. Especially for a seal on a damaged dike condition, the high-water pressure at the bottom of the seal and the low-water pressure inside the hole are expected to result in water flow underneath the seal. The connection between seal and dike cover is therefore approached with two types of measures: a stiff plate and a flexible textile. The physical experiments with a plate showed a small effect on the phreatic surface over time. The experiments with a textile showed a larger effect on the phreatic surface. The main difference between these approaches is the connection between seal and cover, which is considered better for the flexible construction. The textile can form itself more easily to the uneven dike profile and the water pressure on top of the textile leads to a great connection.

Besides the importance of flow underneath the plate, leakages around the seal affect the phreatic surface in three dimensions. The effect of leakage has been considered in 2D dimensions (length and height of the dike), but it also affects the phreatic surface when considering the width of the seal and the width of the dike. Within this influence width, the delaying effect on the phreatic surface is stronger for locations near the seal and weaker at larger distances from the seal. For the textile cases, the influence of the textile is still visible for locations at a distance of one plate width (at 6 m from hole, and at 4 m from the edge of the textile).

4. "What effect does a seal have on the phreatic surface for real-scale dikes with heterogeneous soils?"

The effect for this type of dike has been examined primarily with a physical model. This physical model contained an intermediate scale dike which consisted of a low-permeability cover layer and a permeable core. The results indicate that for this larger scale dike similar effects of the sealing can be distinguished as for the small-scale dike. The delaying effect is present and the decreasing effect is absent.
The heterogeneous soil profile however affects the phreatic surface development. The low-permeability cover slows the rise of the phreatic surface down inside the permeable core. The phreatic level in steady-state is different than for homogeneous dike profiles. When the dike cover is damaged, the phreatic surface increases faster compared to its undamaged conditions. This damaged location undermines the integrity of the low-permeability cover, which exposes the dike core and increases therefore the phreatic surface inside the dike. The effect of the sealing is thus very relevant for this type of dike profile because it can improve the overall integrity of the dike cover.

5. “What is the effect of a seal on the safety of a dike for various failure mechanisms?”

The seal indicates a tiny improvement in dike safety. The assessment of macro stability and micro stability suggest that the seal may have a delaying effect, like the phreatic surface, on dike failure. The seal reduces the phreatic surface increase over time and this leads to a higher safety factor over time. For damaged dike conditions in particular, the effect of the seal on dike safety is demonstrated to be even stronger. The outcomes of this simplified dike safety analyses are promising, however the extent to which a seal can function as emergency measure to improve dike safety remains yet to be seen.

8.1.2 Main research question

The five research questions provide a basis to formulate an answer for the main research question. The main research question was formulated as:

> “What is the effect of a seal on the phreatic surface of a dike in space and time under extreme conditions?”

As described in the answers to the research questions, the effect of a seal on the phreatic surface is multi-layered in nature. Multiple approaches to the problem have led to uncovering different components relating to the seal and phreatic surface of a dike.

The main conclusion of this study however is the delaying effect of the seal on the phreatic surface. The implementation of a seal on the outer slope of a dike can dampen the rise of the phreatic surface over time when this dike is subjected to high-water conditions.
This effect is proven to be stronger for cases where the low-permeability cover of the outer slope is locally damaged. When the phreatic surface reaches a steady-state level, however, the seal shows no decreasing effect on the phreatic surface level. In terms of medical practice, the seal can be seen as a sort of bandage that can be used on this 'injured' dike, which is not intended to directly heal the wound but to support it over time.
An additional characteristic for this delaying effect is the three-dimensional dependency where the effect is stronger for areas that are located directly behind the seal. In general, the closer behind the seal, the greater the delaying effect.

Besides the effects of a seal, conclusions can also be made on the type of seal. Overall, the flexible textile performs better in delaying the rise of the phreatic surface compared to the stiff plate. The connection between seal and dike cover has shown to be of greater importance in the performance of a seal than weight of the seal. The approach of using a BresDefender pontoon (stiff plate) as emergency measure to limit seepage is therefore not preferred in its current state. The application of a textile, however, may result locally in stronger time-dependent effects on the phreatic surface.

8.2 Recommendations

8.2.1 Leakage of sealing

A point of interest throughout this study was the effect of leakage around the seal on the development of the phreatic surface. Especially for the case of a damaged location in the dike cover, the degree of leakage will ultimately determine the effectiveness of a certain seal in the prevention of seepage into the dike core.
Leakage is expected to occur (1) underneath the bottom of the seal and (2) around the sides of the seal when the core is exposed and high-water conditions are present at dike.
The connection between seal and dike slope is proven to influence the effectivity of a seal on the phreatic surface. This connection is not watertight and facilitates intrusion of water underneath the seal. The driving force for water flow in this case is the pressure difference between (1) the

submerged sides of the seal (high pressure) and inside the dike core (low pressure). Water is expected to flow from high-pressure locations towards low-pressure locations, which results in this case in flow underneath the seal towards the hole in the dike.

Future studies should focus on the amount of leakage at the seal and can be described with a conceptual model, which is schematized in Figure 56. The aim of this study should be to quantify the flow into the hole (marked with a red cross in the figure) over time and the following boundary conditions can be applied at this location. At the left-hand side of the hole, a water height of h_L is present due to the high-water level outside of the dike, which is assumed constant over time. At the right-hand side of the hole, a lower water height of h_R is present due to the water pressure at the hole caused by the rise of the phreatic surface over time. Initially, the value of h_R is equal to atmospheric pressure because the phreatic surface is located below the hole, which leads to a constant high flow velocity in the hole as shown in phase I of the flow velocity development in Figure 56. Over time, the phreatic surface increases and this leads to an increase of the water height h_R and increase in flow velocity as seen in phase 2. When the phreatic surface of the dike reaches its steady-state condition, the flow velocity also reaches a steady-state condition which is a constant value over time as shown in phase 3.

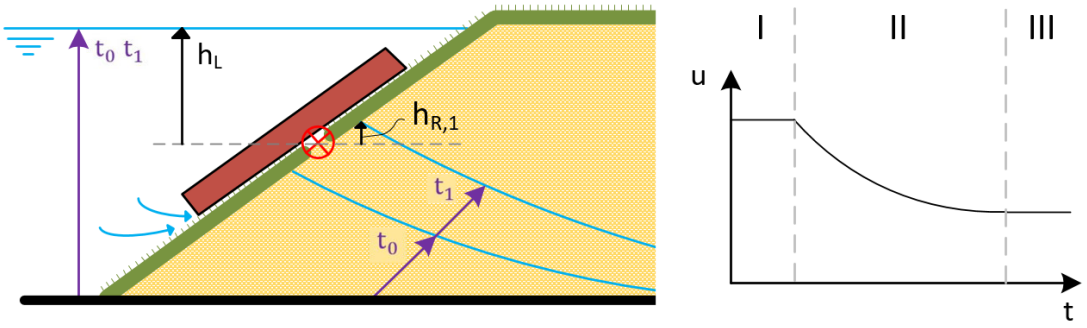

Figure 56: Schematization of conceptual model for leakage of seal (Left) and flow velocity development into the hole (Right)

8.2.2 Influence width of sealing

As concluded in this study, the effect of the seal on the phreatic surface is present in all three dimensions. The seal has a 3D effect with a certain influence range over the length and width of the dike, where the phreatic surface of the dike is delayed. The distance to the seal is important for this effect and this makes further investigation into the dimensions of the seal relevant.
The length of the seal, measured along dike length (dike profile), and width of the seal, measured along dike width, can be varied to find different responses in phreatic surface. The end product of such a study should give insight in the area and phreatic surface level differences depending on the dimensions of the seal. It is plausible that at least a physical model must be applied for such a study, since calculation methods and numerical models to model this behavior are lacking at this moment.
In Figure 57, the contours are drawn with a maximum influence width $W_{influence}$ and maximum influence length $L_{influence}$ of the phreatic surface for a certain moment in time, where the water height decreases are labelled (similar to the height maps in section 5.3.1. Based on varying dimensions of the seal W_{seal} and L_{seal}, a relationship can be found to seal dimensions and effects on the phreatic surface. This will aid in the understanding how large the dimensions of a seal have on a certain region of the phreatic surface of a dike.

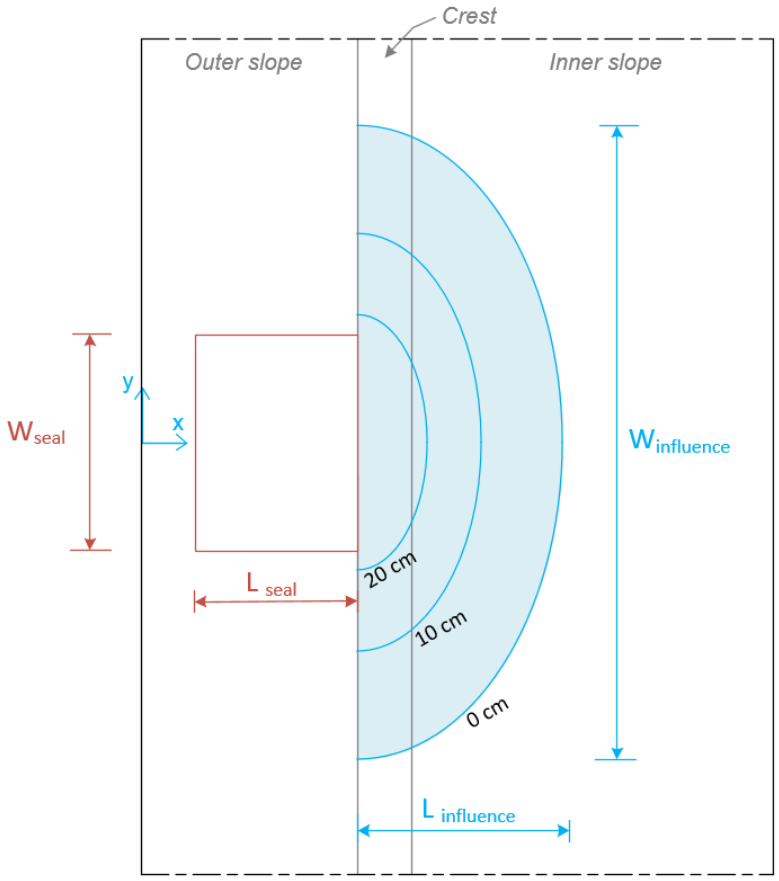

Figure 57: Conceptual approach to influence length and width of seal

8.2.3 Stiffness of sealing

As can be concluded from the results of the physical modelling, the performance of sealing the outer slope of a dike with a plate or textile shows to be different and is attributed to the difference in stiffness between the two. The reasoning is that the flexible textile can form itself better to the uneven dike slope than the stiff plate, which improves the seal-cover connection and thus prevents leakages underneath the seal.

Since the material of the seal influence the effect of the seal, research into the elastic modulus (E) of the material of the seal is considered to be quite interesting. The stiff plate of the physical modelling is made of glued-laminated timber, which is guessed to have an E-modulus of roughly 10 GPa. (Engineering Toolbox, 2011) The flexible textile consists of polyethylene, which has an E-modulus of only 0.2 GPa. (Designerdata, 2019) Future research should focus on finding a relationship between the effect of the seal and elasticity of the material. This could be achieved by looking at cases where the difference of the material is changed, where also a steel plate is used (E-modulus of steel is around 200 GPa) as this is expected to be closer to the stiffness of the real BresDefender pontoon.

References

Ashtiani, R. S. (2017, October 16). *Lecture 5 - Soil Water Characteristic Curves (SWCC).* From http://www.rezasalehi.com/: http://www.rezasalehi.com/uploads/1/3/8/0/13809333/lecture_5-swcc.pdf

Bentley Systems. (2020). *PLAXIS 2D Reference Manual.*

Bentley Systems. (2020). *PLAXIS 2D-Manual.*

CFBR. (2010). *Earthen dams and levees stability justification – Recommendations guideline.* France: French Committee for Dams and Reservoirs.

Ciria. (2013). *The International Levee Handbook.* London: CIRIA.

COMSOL. (2013). *Subsurface Flow Module User's Guide.*

De Bruijn, H., De Vries, G., & `t Hart, R. (2018). *Fenomenologische beschrijving - Faalmechanismen WBI.* Deltares.

De Raadt, W., Jaspers Focks, D., Van Hoven, A., & Regeling, E. (2015). How to Determine the Phreatic Surface in a Dike During Storm Conditions with Wave Overtopping: A Method Applied to the Afsluitdijk . *Geotechnical Safety and Risk* (pp. 509-515). IOS Press .

Deltares. (2018). *D-Geo Flow user manual.*

Deltares. (n.d.). *D-Stability*. From Deltares: https://www.deltares.nl/nl/software/d-stability-nl/

Deltares. (n.d.). *Wiki Noodmaatregelen Waterkeringen*. From Deltares.nl: https://v-web002.deltares.nl/sterktenoodmaatregelen/index.php

Designerdata. (2019). *LDPE*. From Designerdata.nl: https://designerdata.nl/materials/plastics/thermo-plastics/low-density-polyethylene

Eijkelkamp Soil & Water. (2019). *Dubbele ringinfiltrometer - Handleiding.* Giesbeek.

Engineering Toolbox. (2011). *Wood, Panel and Structural Timber Products - Mechanical Properties*. From engineeringtoolbox.com: https://www.engineeringtoolbox.com/timber-mechanical-properties-d_1789.html

Eyo, E., Ng'ambi, S., & Abbey, S. (2022). An overview of soil–water characteristic curves of stabilised soils and their influential factors. *Journal of King Saud University - Engineering Sciences*, 31-45.

Fokkens, B. (2006). THE DUTCH STRATEGY FOR SAFETY AND RIVER FLOOD PREVENTION. *Extreme Hydrological Events: New Concepts for Security* (pp. 337-352). Dordrecht: Springer.

Fredlund, D. G., Xing, A., & Huang, S. (1994). Predicting the Permeability Function for Unsaturated Soils Using the Soil-Water Characteristic Curve. *Canadian Geotechnical Journal 31*, 533-546.

Fredlund, D., & Xing, A. (1994). Equations for the soil-water characteristic curve. *Canadian Geotechnical Journal 31*, 521-532.

Han, Z., Han, S., Teak Oh, W., & Vanapalli, S. (2014). Modelling the Stress-Settlement Behavior of Shallow Foundation in Unsaturated Sand Using Sigma/W and Plaxis. *Geo Regina 2014.* Regina, Canada: Geo Regina.

Hong, W., Jung, Y., Kang, S., & Lee, J. (2016). Estimation of soil-water characteristic curves in multiple-cycles using membrane and TDR system. *Materials 9*, 1019.

Janssen, D., Schmets, A. J., Hofland, B., Dado, E., & Jonkman, S. N. (2021). BresDefender: A potential emergency measure to prevent or postpone a dike breach. *FLOODrisk 2020 - 4th European Conference on Flood Risk Management.*

Jonkman, S., Jorissen, R., Schweckendiek, T., & Van Den Bos, J. (2018). *Flood Defences - lecture notes.* Delft: TU Delft.

Jonkman, S., Jorissen, R., Schweckendiek, T., & Van den Bos, J. (2018). *Flood defences: Lecture notes CIE5314.* Delft.

Jonkman, S., Kok, M., & Vrijling, J. (2008). Flood Risk Assessment in the Netherlands: A Case Study. *Risk Analysis*, 1357-1373.

Kaliakin, V. N. (2017). Chapter 5 - Example Problems Involving In Situ Stresses Under Hydrostatic Conditions. In V. N. Kaliakin, *Soil Mechanics: Calculations, Principles, and Methods* (pp. 205-242). Oxford: Butterworth-Heinemann.

METER Group AG. (2018). *HYPROP 2 - Operation Manual.* Munich, Germany: METER Group AG.

Meter Group AG. (2020). *KSAT - Operation Manual.*

Miller, S. (1994). *Handbook for Agrohydrology.* Chatham, United Kingdom: NRI.

Novak, V., & Hlavacikova, H. (2019). *Applied Soil Hydrology: Theory and Applications of Transport in Porous.* Cham, Switzerland: Springer.

Pavlovsky, N. N. (1956). *Collected Works.* Leningrad: Nauk USSR.

Poldermans, J. (2020, November 4). *Hoe maak je dertig kilometer dijk onkruidvrij?* From stad en groen: https://www.stad-en-groen.nl/article/34501/hoe-maak-je-dertig-kilometer-dijk-onkruidvrij

Rahimi, A., Rahardjo, H., & Leong, E. (2015). Effects of soil–water characteristic curve and relative permeability equations on estimation of unsaturated permeability function. *Soils and Foundations 55*, 1400-1411.

Rijkswaterstaat. (2019). *Schematiseringshandleiding microstabiliteit.* Ministerie van Infrastructuur en Waterstaat.

Rijkswaterstaat. (2021). *Room for the River* . From Rijkswaterstaat: https://www.rijkswaterstaat.nl/en/about-us/gems-of-rijkswaterstaat/room-for-the-river#what-is-the-problem

Rijkswaterstaat. (2022). *Hoogwaterbeschermingsprogramma (HWBP)*. From Rijkswaterstaat: https://www.rijkswaterstaat.nl/water/waterbeheer/bescherming-tegen-het-water/maatregelen-om-overstromingen-te-voorkomen/hoogwaterbeschermingsprogramma

RTV Noord. (2022, Februari 27). *Quiz: Wat weet jij van hoogwater in Groningen?* From RTV Noord: https://www.rtvnoord.nl/nieuws/898898/quiz-wat-weet-jij-van-hoogwater-in-groningen

Schiereck, G. (1998). *Grondslagen voor waterkeren.* Rijkswaterstaat.

Šim nek, J., Van Genuchten, M. T., & Šejna, M. (2020). *HYDRUS Technical Manual (version 3).* Prague, Czech Republic: PC Progress.

Smith, I. (2014). *Smith's Elements of Soil Mechanics (9th edition).* Chichester: John Wiley & Sons, Ltd.

TAW. (2001). *Technisch rapport Waterkerende grondconstructies.* Delft.

TAW. (2004). *Technisch Rapport Waterspanningen bij dijken.* Den Haag: Rijkswaterstaat.

USACE. (1993). *Engineering and Design: Seepage Analysis and Control for Dams.* Washington, D.C.: Department of the Army.

USGS. (2021). *MODFLOW and Related Programs*. From USGS.gov: https://www.usgs.gov/mission-areas/water-resources/science/modflow-and-related-programs?qt-science_center_objects=0#qt-science_center_objects

Van Genuchten, M. T. (1980). Closed-form equation for predicting the hydraulic conductivity of unsaturated soils. *Soil Science Society of America Journal: Vol 44*, 892-898.

Verruijt, A. (2012). *Soil Mechanics.* Delft.

Wu, S., Han, L., Cheng, Z., Zhang, X., & Cheng, H. (2019). Study on the limit equilibrium slice method considering characteristics of inter-slice normal forces distribution: the improved Spencer method. *Environmental Earth Sciences*.

Zheng, K., Li, C., & Wang, F. (2019). Gaussian Radial Basis Function for Unsteady. *IOP Conference Series: Earth and Environmental Science.* IOP Publishing.

List of Figures

Figure 1: Overview of failure mechanisms of flood defences (Schiereck, 1998) 2
Figure 2: Pontoon used as temporary bridge element 3
Figure 3: Phases leading to implementation of BresDefender 3
Figure 4: Application scenarios for BresDefender 4
Figure 5: Physical model without plate (left) and with plate (right) 5
Figure 6: Conceptual model of the BresDefender (with a damaged location in the cover). 6
Figure 7: Assumed phreatic surface level decrease in steady-state due to sealing during high-water conditions 6
Figure 8: Expected phreatic surface development over time for increasing water level 6
Figure 9: Pore water pressure distribution with capillary rise above the phreatic surface. (Kaliakin, 2017) 10
Figure 10: Schematic illustration of inner and outer slope failure (Ciria, 2013) 11
Figure 11: Schematic illustration of a slip circle modelled using the method of slices (Verruijt, 2012) 12
Figure 12: Failure process due to micro-instability (De Bruijn, De Vries, & `t Hart, 2018) 12
Figure 13: Schematic representation of perpendicular equilibrium soil segment with various forces 13
Figure 14: Continuity condition for an elementary area. No net inflow or outflow is present for this area 16
Figure 15: Overview of the soil–water characteristic curve (Eyo, Ng'ambi, & Abbey, 2022)..... 17
Figure 16: SWCC fits for different equations (Rahimi, Rahardjo, & Leong, 2015)..... 18
Figure 17: Relative permeability fits for different equations (Rahimi, Rahardjo, & Leong, 2015).... 19
Figure 18: Comparison of the position of the phreatic surface for (a) transient states during a flood wave and (b) steady-state for the same water levels (Ciria, 2013) 21
Figure 19: Effect of permeability on the position of the phreatic surface for different water levels (Ciria, 2013) 21
Figure 20: Numerical modelling process 23
Figure 21: Description of KSAT device (Meter Group AG, 2020)..... 24
Figure 22: Description of Hyprop device (METER Group AG, 2018) 24
Figure 23: Measurements of the HYPROP experiments 25
Figure 24: Effect of sealing on water level development over time 26
Figure 25: Dimensions of WaterLab dike (Not to scale)..... 26
Figure 26: Boundary conditions for numerical model of WaterLab reference case 28
Figure 27: Overview of comparison between numerical model and physical model phreatic levels for the different sensor locations for the reference case of the WaterLab dike 29
Figure 28: Cross section of the steady-state phreatic level for the reference case of the WaterLab dike 29
Figure 29: Numerical model of WaterLab sealing case (D = 0.1m)..... 30
Figure 30: Overview of comparison between numerical model and physical model phreatic levels for the different sensor locations for the sealing case of the WaterLab dike 32
Figure 31: Cross section of the steady-state phreatic level for the sealing case of the WaterLab dike 32
Figure 32: Numerical model of FPH dike..... 34
Figure 33: Phreatic surface level in steady-state for different cases of the FPH dike (to scale) 35
Figure 34: Dimensions of test dike. (Not to scale) 36
Figure 35: State of dike before physical tests..... 36

Figure 36: Schematic overview of the test set-up at Flood Proof Holland 37
Figure 37: Effect of standpipes on measured phreatic surface location 38
Figure 38: Plate scenario on FPH dike 40
Figure 39: Textile scenario on FPH dike 40
Figure 40: Overview of sensor locations of FPH dike 43
Figure 41: Typical measurement output during the filling stage and part of the emptying stage 46
Figure 42: Comparison for an undamaged dike: Plate case 48
Figure 43: Comparison for an undamaged dike: Textile case 49
Figure 44: Effect of damage on a dike 50
Figure 45: Comparison for a damaged dike: Plate case 51
Figure 46: Comparison for a damaged dike: Textile case 52
Figure 47: Comparison of plate and textile for a damaged dike 52
Figure 48: Overview of test set-up for the 2D height maps (Not to scale) 53
Figure 49: 2D Height maps for the phreatic level difference between the textile case and reference case for an undamaged dike. The z-value is defined as the phreatic surface level of the reference case minus the phreatic surface level of the textile case. 54
Figure 50: 2D Height maps for the phreatic level difference between the textile case and reference case for a damaged dike. The z-value is defined as the phreatic surface level of the reference case minus the phreatic surface level of the textile case. 55
Figure 51: Numerical model of FPH dike for the textile case with damage. 59
Figure 52: Comparison of the calibrated numerical model and physical model for the reference cases. 60
Figure 53: Comparison of the calibrated numerical model and physical model for the textile cases. 61
Figure 54: Macro stability analysis with time-varying factor of safety (FoS). 63
Figure 55: Micro stability safety criterium 63
Figure 56: Schematization of conceptual model for leakage of seal (Left) and 70
Figure 57: Conceptual approach to influence length and width of seal 71
Figure 58: Schematic illustration of a slip circle modelled using the method of slices (Verruijt, 2012) 80
Figure 59: Schematic illustration of the Uplift-Van model (Jonkman, Jorissen, Schweckendiek, & Van Den Bos, 2018) 81
Figure 60: Schematic illustration of the Spencer method. (Wu, Han, Cheng, Zhang, & Cheng, 2019) 81
Figure 61: Classification of Ks values 81
Figure 62: Overview of KSAT device 81
Figure 63: Example of KSAT data logger interface 81
Figure 64: Overview of HYPROP device 81
Figure 65: Optimal measuring curve 81
Figure 66: Measurements of the HYPROP experiments 81
Figure 67: 3D view of set-up of WaterLab dike 81
Figure 68: Top view of set-up of WaterLab dike 81
Figure 69: Sieve analysis of WaterLab dike material 81
Figure 70: Pressure transducer 82
Figure 71: Dimensions of pressure transducer 83
Figure 72: Enclosure with data logger and other devices 83
Figure 73: Monitoring interface of LoggerNet 84
Figure 74: Functioning of double ring infiltrometer (Miller, 1994) 85
Figure 75: The placement and use of the double ring infiltrometer 86
Figure 76: Development of the permeability over time from the infiltrometer test 87
Figure 77: Phreatic line for D-Stability model (for Case 1 at t = 8 hours) 88

Figure 78: Slip plane boundary for D-Stability model (for Case 1 at t = 8 hours) 89
Figure 79: Sliding door of tube which goes through dike. The hydrostatic water pressure from..... 91
Figure 80: Inner slope of dike where water is present at the dike surface directly above the tube with sliding door 92
Figure 81: Schematization of previous experiment set-up 93
Figure 82: Excavated tube with infiltration box 93
Figure 83: Infiltration box and drain. 94
Figure 84: FPH dike right after construction (Picture by Joost Pol)..... 94

List of Tables

Table 1: Soil parameter values from KSAT tests 25
Table 2: Head boundary for reference case 28
Table 3: Head boundary for sealing case 31
Table 4: Steady-state time of the phreatic surface for different cases of the FPH dike 35
Table 5: Comparison of dike characteristics 37
Table 6: Measurement cases of FPH experiments 40
Table 7: Coordinates of sensors 43
Table 8: Time until reaching steady-state phreatic surface for physical model tests 47
Table 9: Phreatic surface level in steady-state for physical model tests 47
Table 10: Comparison of steady-state phreatic levels 56
Table 11: Comparison of steady-state times 56
Table 12: Calibration of steady-state times for reference cases 59
Table 13: Calibration of steady-state times for textile cases 60
Table 14: Comparison of steady-state times with textile case boundaries 62
Table 15: Comparison of steady-state phreatic levels with textile case boundaries 62
Table 16: Normalized Ks values at 20 C [in m/s] 81
Table 17: Overview of Ks values and soil characterization 81
Table 18: Coordinates of sensors of WaterLab dike 81
Table 19: Input parameters for micro stability assessment 90

A. Theory

A.1 Numerical model selection

Multiple numerical models have been considered for the development of a numerical model for this study. The considered models are discussed below.

D-Geo Flow

D-Geo Flow is a software model from Deltares that is used to calculate 2D groundwater flow problems. The software program runs the FEM-based model DgFlow and has a module for piping. Several types of boundary conditions that can be used for the model such as water levels, flux and no-flow boundaries. This program uses the Van Genuchten model to account for flow in the unsaturated zone. (Deltares, 2018)

The first version of D-Geo Flow has been released in 2018. This means that the software program has not been used extensively in dike design and analysis, which makes it difficult to use because this software model lacks experience. On top of that, the user manual is quite modest and may need to be extended to make it more user-friendly. These factors may complicate the numerical modelling process in this study.

COMSOL

COMSOL Multiphysics is a FEM analysis software for several fields of physics. These modules contain chemical, electrical, mechanical and hydraulic applications. COMSOL contains a subsurface flow module to simulate flow in a porous medium. This program uses the (1) Van Genuchten and (2) Brooks and Corey models to describe flow in the unsaturated zone and water retention. On top of that, the model can simulate flow in fractures and can be used in combination with MATLAB. (COMSOL, 2013)

Hydrus (2D/3D)

Hydrus is a software package to model movement of water, heat and solutions in saturated porous media in two- and three-dimensions. The software program is capable of implementing multiple types of time-varying boundary conditions. The unsaturated zone can be modelled using a variety of functions, such as Van Genuchten, Brooks and Corey, and Durner. The flow region itself may consist of nonuniform soils and flow can occur in a 2D-plane or in a fully 3D domain. On top of that, various add-on modules are present to model very specific cases. The SLOPE Cube module can, for example, simulate soil properties such as total stress, effective stress, soil suction and can depending on those determine a local factor of safety. (Šimůnek, Van Genuchten, & Šejna, 2020)

MODFLOW

MODFLOW is a finite-difference groundwater flow modelling program, which is developed by the United States Geological Survey (USGS). This program allows users to develop a numerical groundwater model of the hydrogeologic environment at a specific field site. The source code is public available, which means that the program is free to use. Therefore, different packages have been developed for a variety of purposes. A useful package seems the FLoPy package, which is a Python package to develop and run MODFLOW models. This makes data transfer from the model into python (and vice versa) more straightforward. MODFLOW can also model flow in the unsaturated zone when combined with a package. However, this package uses only the Brook and Corey model, which makes it suboptimal compared to other numerical software models that can also use the more commonly used Van Genuchten formulation. (USGS, 2021)

PLAXIS (2D/3D)

The finite element program PLAXIS has the add-on module PlaxFlow. PLAXIS runs in its standard model only groundwater flow in stationary conditions. The implementation of the PlaxFlow module makes modelling of transient groundwater flow problems also possible. Multiple options are present to model the unsaturated model, such as the Van Genuchten model, the Approximate Van Genuchten Model and user-defined soil water retention curves. (Bentley Systems, 2020)

A.2 Limit Equilibrium Methods

The most used limit equilibrium models (LEMs) in Dutch practice are described below.

Bishop/Fellenius

Two commonly applied methods are the (simplified) Bishop method and the method by Fellenius (also known as the Ordinary Method of Slices). The difference for both methods is in the calculation of the normal effective stress σ'_n. Both methods assess the moment equilibrium for a circular slip plane. Based on the the driving moment M_s and resisting moment M_r, the factor of safety can be defined as the ratio between these two parameters and is defined below.

$$FoS = \frac{M_r}{M_s} = \frac{\sum[(c + \sigma'_n \tan\phi)/\cos\alpha}{\sum \gamma h \sin\alpha} \tag{18}$$

Where:

c	cohesion	$[\mathrm{kPa}]$
σ'_n	normal effective stress	$[\mathrm{kN/m^2}]$
ϕ	friction angle	$[°]$
α	angle of rotation	$[°]$
γ	unit weight	$[\mathrm{kN/m^3}]$
h	height of a slice	$[\mathrm{m}]$

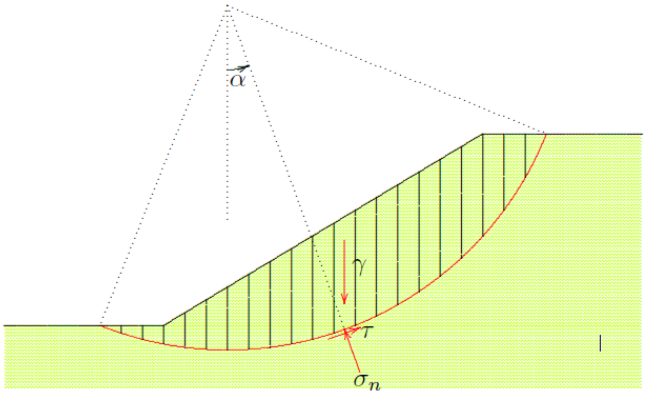

Figure 58: Schematic illustration of a slip circle modelled using the method of slices (Verruijt, 2012)

Uplift-Van

In certain conditions the critical slip circle does not have a circular shape as described in the methods of Bishop and Fellenius. This is typical for cases in uplift conditions. In this case, water can enter the aquifer beneath the dike, which results in an increase of pore water pressure. This can lead to a significant decrease of the effective stresses under the blanket. When the effective stresses are cut down to zero, we have an 'uplift' condition, where the blanket floats on the aquifer. The critical sliding surface is therefore typically more elongated horizontally. This is illustrated in Figure 59.

This Uplift-Van model models the sliding surface by using a circular shape at the active side and a combination of a horizontal plane and a circular shape at the passive side. The slices in the horizontal plane are modelled such that horizontal force equilibrium is present between the active and passive side.

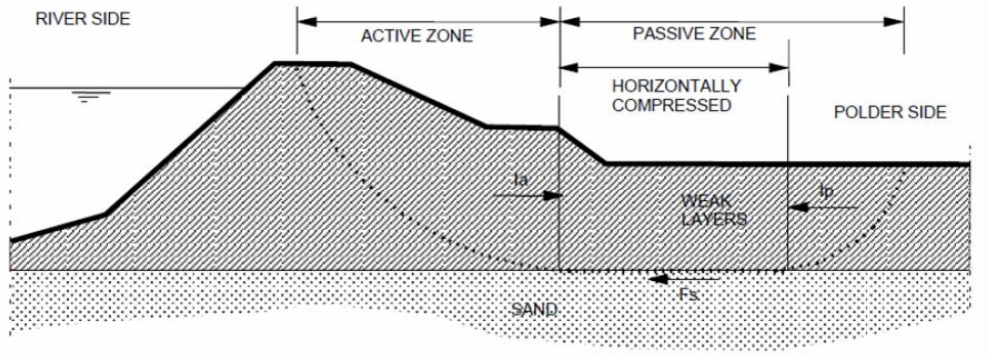

Figure 59: Schematic illustration of the Uplift-Van model (Jonkman, Jorissen, Schweckendiek, & Van Den Bos, 2018)

Spencer

The Spencer method uses piece-wise linear elements to construct the sliding surface. This method is therefore applicable for a wide range of potential sliding surfaces (circular, horizontal, etc.), but also shapes that cannot be represented well by the methods that are mentioned earlier. On top of that, the Spencer method considers all three equilibria (horizontal forces, vertical forces and moments).

Until now, the use of the Spencer method was quite uncommon due to the tedious manual work in finding the critical sliding surface. However, due to the development of computer algorithms, the search for sliding surface has been automated. Implementation of pre-defined search bounds (method Spencer-Van der Meij) make this method more time-efficient.

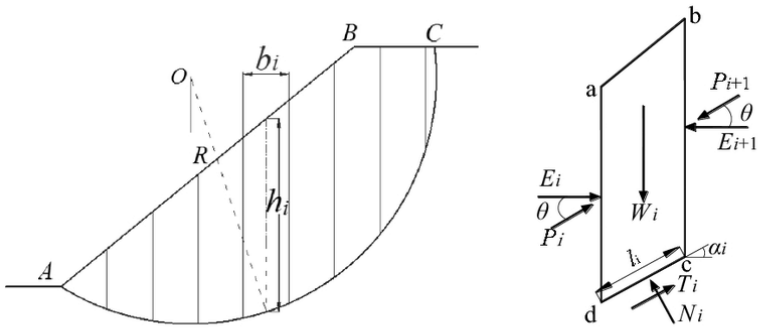

(a) Diagram of a slope slice (b) Stress of slice *i*

Figure 60: Schematic illustration of the Spencer method. (Wu, Han, Cheng, Zhang, & Cheng, 2019)

The different LEMs show different approaches to force and moment equilibria and they all have their advantages and disadvantages. The Bishop method is simplistic and commonly used, but is limited for uplift conditions since only circular slip circles are considered. The Uplift-Van method, on the contrary, can be used for uplift conditions and is suitable for more horizontal sliding planes, which makes this method also quite specific. The Spencer method is the most flexible option and can be applied for various shapes, but there is still limited experience with this method.

B. Soil Investigation

C. Physical modelling

C.1 Sensor specifications

The submersible pressure transducers are manufactured by First Sensor AG and are part of the hydrostatic liquid level sensors (KTE/KTW8000...CS series). The transducers have a plastic housing for continuous level measurement in storage tanks and basins. They can be supplied with a FKM seal for acids or an EPDM seal for base, which are not relevant for the pH neutral basin water. Each transducer is equipped with a piezo resistant ceramic pressure sensor and is housed in a chemically resistant PPS plastic housing. The specifications of the transducers are presented below.

Measuring range	: 0…6mH_20
Output signal	: 4…20mA
Supply voltage	: 9…32V
Sensor material	: Ceramic (Al_2O_3)
Housing	: Polyphenylene sulfide (PPS)
Connection	: 2-wire PE cable with built-in capillary and moisture-resistant filter
Process temperature	: Max. -10…+70°C
Protection Class	: IP68
Cable length	: 10m
Cable material	: Polythene (PE)
Sealing material	: Viton (FKM)

Figure 70: Pressure transducer

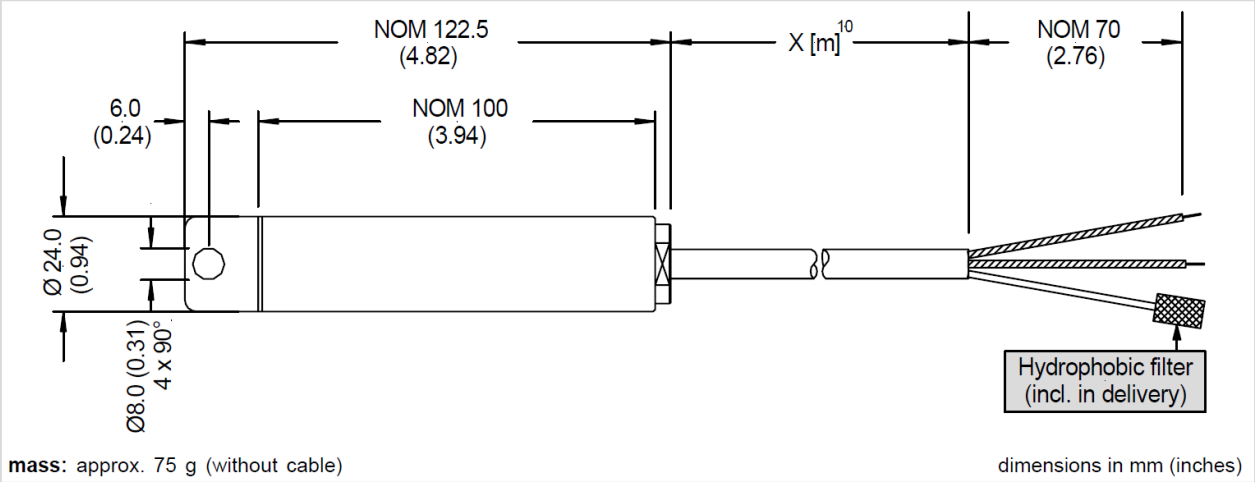

Figure 71: Dimensions of pressure transducer

C.2 Data logger

The data logger and software are produced by Campbell Scientific Inc. and are provided by Deltares. The data logger is located amongst other devices in an enclosure that can be transported easily and is suitable for use in all weather conditions.

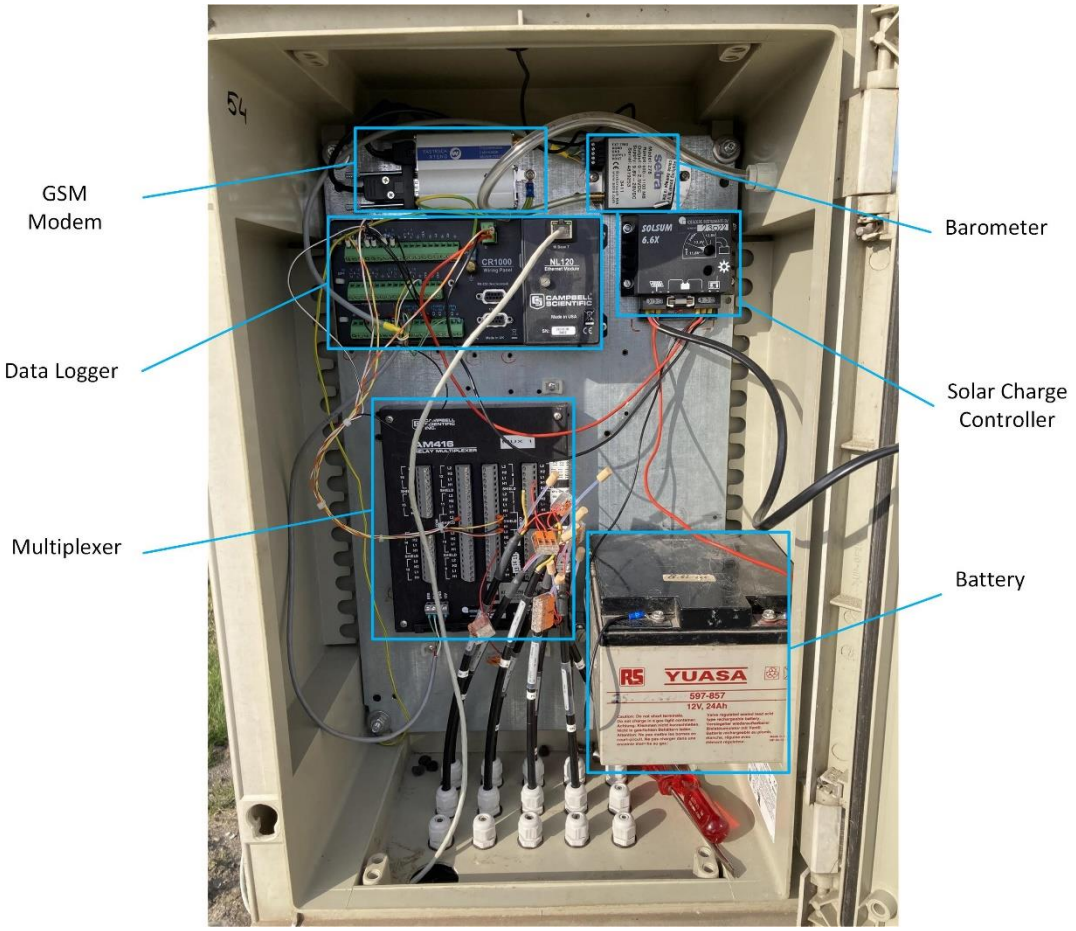

Figure 72: Enclosure with data logger and other devices

The signal processing occurs in the following order:

1. The battery provides power to the multiplex (AM416: relay multiplexer), which powers the sensors at set time intervals.
2. The sensors take a measurement and outputs a signal in electric current.

3. The multiplex relays this to the data logger (CR1000: wiring panel, NL120: ethernet module), which transforms the signal from a current into a voltage by a constant resistance and stores the measurements.
4. The data logger transfers the measurements through the 100 m UTP ethernet cable to the computer.

On the computer is datalogger support software LoggerNet installed. This program is used to set up and control the data logger, to monitor the sensors, and to collect the data files.

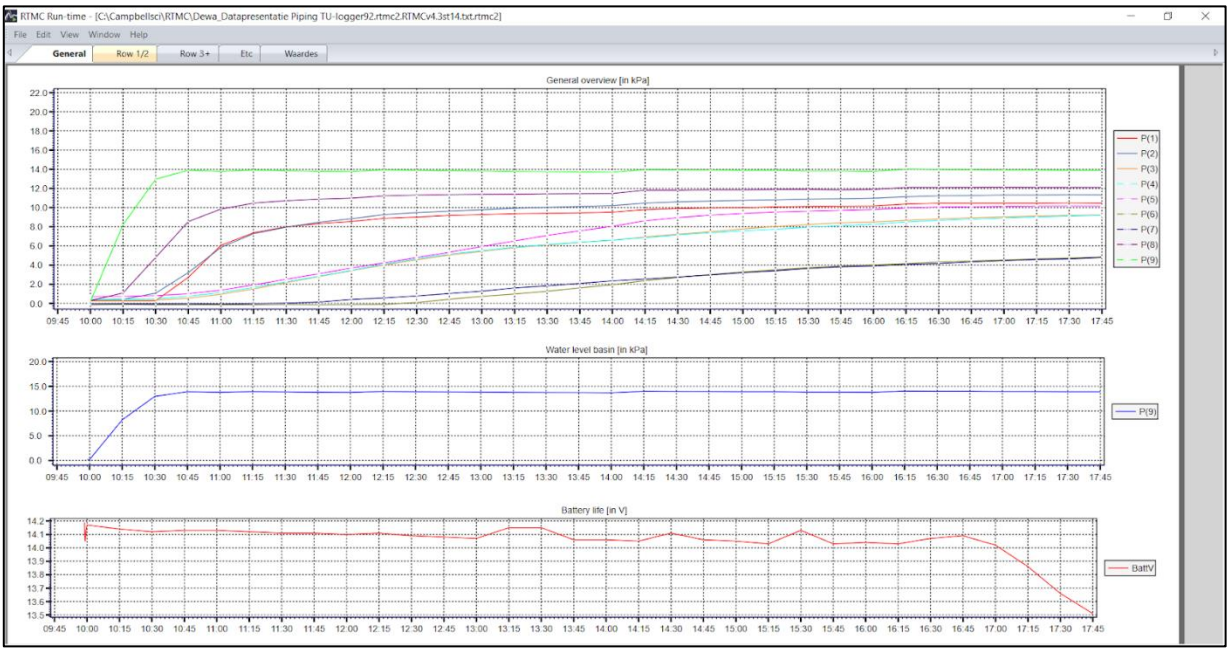

Figure 73: Monitoring interface of LoggerNet

C.3 Infiltrometer

Introduction

The permeability of the cover of the FPH dike has been measured with a KSAT device in the Geoscience and Engineering Laboratory at the TU Delft. This parameter has however been obtained from samples, where the originated soil has been dried, sample holders are filled and saturated before conducting the measurements of the saturated hydraulic conductivity. Differences between this value and the hydraulic conductivity in the field can therefore differ and validation of the value obtained in the laboratory is advised.

The hydraulic conductivity of the cover of the FPH dike is in-situ estimated with a double ring infiltrometer, which is simplistic variant that is self-made. This device consists of two rings:

1. The inner ring: this ring is used to measure the water height in the ring and thus to determine the water infiltration into the cover
2. The outer ring: within this ring the water height is kept constant to the inner ring to make sure that the water infiltration in the inner ring is only vertical, which is presented in Figure 74 .

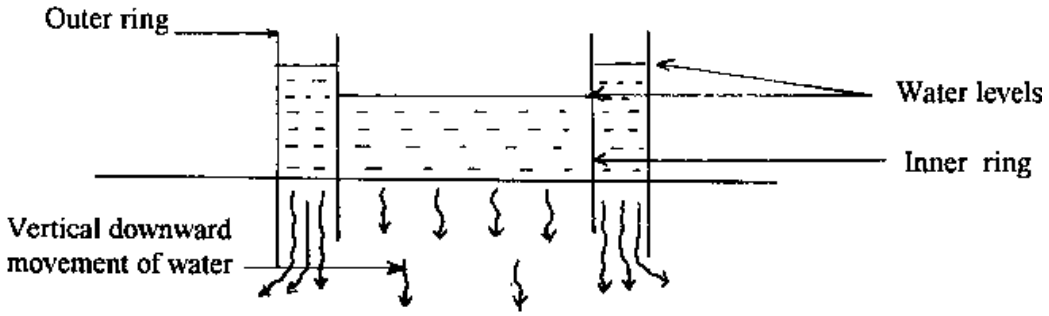

Figure 74: Functioning of double ring infiltrometer (Miller, 1994)

The goal of the infiltrometer test is to determine the hydraulic conductivity of the soil, which is measured by taken the decrease of water height [in meter] over time [in seconds]. According to Darcy's Law as defined in section B.2.1 , the permeability can be defined in this case as the water height decrease per time [in m/s]. This permeability is initially higher due to the low saturation of the soil under the infiltrometer but will over time decrease and reach a steady-state level when the soil also reaches a constant near-saturation condition. The estimation of this steady-state value of the permeability is the goal for this infiltrometer test because this value should be similar to the saturated permeability measured to the GSE lab.
Due to the use of this simplistic measurement self-made infiltrometer, however, the accuracy of the obtained permeability is assumed to smaller than the value measured in the GSE lab. It is therefore chosen to use this infiltrometer test solely as a method to validate the order of magnitude of the value of the permeability measured in the GSE lab.

Materials and method

The handbook *Dubbele ringinfiltrometer* (2019) of the company Eijkelkamp Soil & Water has been used, which describes the background, installation and measuring method of their double ring infiltrometer product. However, the principles and approaches can still be adopted for the self-made infiltrometer.

For this study, the double ring infiltrometer consists of two thin steel rings: the inner ring is 15 cm in diameter and outer ring is 20 cm in diameter. The height of each ring is 12 cm in total (when accounting for the extension on top).
The placement and use of the infiltrometer can be divided into four steps as shown in Figure 75:

- Step 1: Preparation of the test location
  The desired location for the infiltrometer test should be level and even. Vegetation and irregularities (branches, stones, etc.) should be removed so that only the dike cover material is present at the surface.

- Step 2: Placement of both rings
  For the placement of each ring, a wooden plate has been placed on top of the ring before it is hammered into the ground. This is done so to keep the insertion of the ring into the soil even and prevent the ring from damage during hammering. Both rings are hammered into place until they are 4 cm into the soil to limit leakages around the sides.

- Step 3: Measuring the height of the infiltrometer
  The extensions are placed on top of each ring, which makes the measuring height of the infiltrometer 8 cm in total.

- Step 4: Preparation for testing
  Both rings of the infiltrometer are filled initially and the test can begin from this point onward.

The test itself is conducted by filling both rings initially. Every hour, the water height in the inner ring is measured and both rings are refilled to the top again. This process is repeated until the decrease in water height reaches a constant value. The accuracy of the water height measurements of the inner ring are up to 1 mm.

Figure 75: The placement and use of the double ring infiltrometer

Results

The permeability measured by the infiltrometer is presented in Figure 76. The course of the permeability follows the theory: it starts off with a higher permeability and decreases to a (near) steady-state value of $k_s = 3 \cdot 10^{-3}\ \mathrm{m/hr} = 8 \cdot 10^{-7} \mathrm{m/s}$. This value is in the same order of magnitude as the permeability measured in the GSE laboratory, which is $k_s = 7.42 \cdot 10^{-3}\ \mathrm{m/hr} = 2.06 \cdot 10^{-6}\ \mathrm{m/s}$, and is therefore assumed to be accurate enough in its current state.

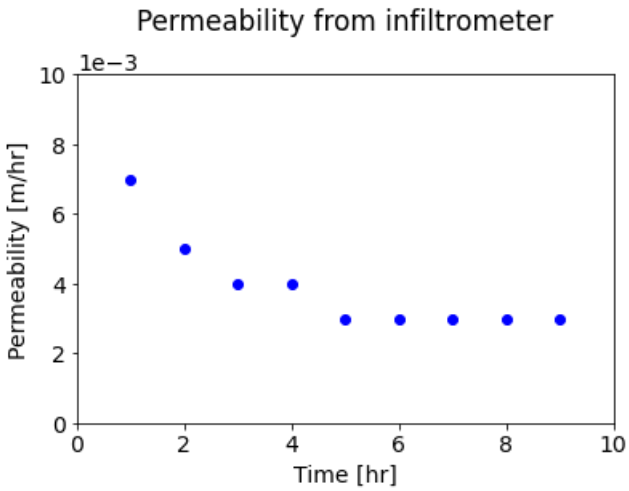

Figure 76: Development of the permeability over time from the infiltrometer test

D. Dike Safety

D.1 Macro stability

D-Stability

As discussed in section 2.1.2 of the theory, macro stability is a relevant failure mechanism to discuss in the safety assessment of a dike. The assessment of macro stability of a dike is a complex process that depends on thorough soil investigation, modelling, and calculations. It is therefore opted for this study to simplify the process by using the numerical software D-Stability. D-Stability has been developed for the design and stability control of embankments on soft ground. Some strong points of this program are listed on the webpage of Deltares:

- The stability of an embankment can be calculated with the Bishop, Spencer and Uplift-Van models.
- It is possible to calculate with both drained and undrained soil behavior.
- The safety factor can be calculated in different (construction) phases, which is beneficial for modelling transient conditions of the phreatic surface.
- D-Stability has a user-friendly user interface.
- The WBI default materials are included.

Method

The goal of this macro stability analysis is to check whether the textile has an effect in terms of failure due macro instability, which can be achieved by comparing the phreatic surface level for textile cases and corresponding reference cases. Over time, the phreatic surface level changes for all cases which leads to a time-varying factor of safety (FoS) for each case. All other parameters are kept constant, which include dike dimensions, soil material, subsurface and calculation methods. The absolute value for the safety factor is not of importance, but the value of the safety factor in relation to the different cases is of great interest.

The dike profile directly behind the center of the textile (described as row 1 in Figure 40) is evaluated since the largest effect of the textile on the phreatic surface is measured at this location (as can be concluded from the height maps from section 5.3). The phreatic line of the D-Stability model is constructed by taking the measurements of sensor 1, 3, 6 from the physical modelling and the boundary conditions of the outside water level at 1.45 m and no water height at the inner toe, which is shown in Figure 77.

The Spencer method has been selected as LEM method since this method uses fixed boundaries for the calculation of the design slip plane. The option to use a single calculation is used to simplify the analysis using a single boundary containing only four specific points in total, which is presented in Figure 78. This boundary is kept constant for all the different cases and is chosen in such way that (1) the model considers large slip planes through the dike core and (2) the model stays stable for lower and higher phreatic lines.

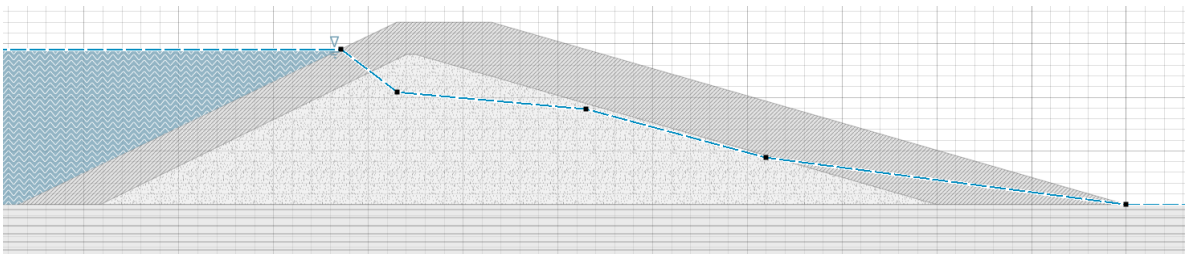

Figure 77: Phreatic line for D-Stability model (for Case 1 at t = 8 hours)

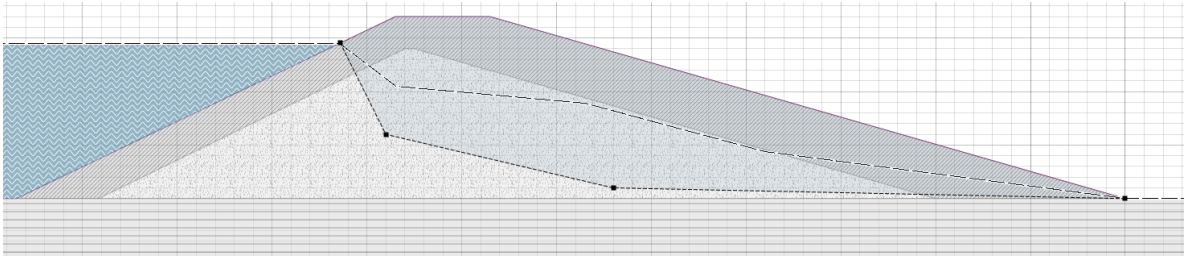

Figure 78: Slip plane boundary for D-Stability model (for Case 1 at t = 8 hours)

D.2 Micro stability

Method

The safety criterium for micro stability is presented in the literature study (Section 2.1.3.2) and is formulated as a safety factor (See Equation 2).

The length measure Δx has an arbitrary value which influences the safety factor besides the phreatic line and soil parameters. The critical value of Δx, which gives the minimal safety factor (SF), can be determined analytically. The value of Δx ranges from zero to $\Delta h/sin\alpha$. The minimum value on this interval can be found by setting the derivative $\mathrm{d}SF/\mathrm{d}\Delta x$ to zero and solve this for Δx. This value of Δx can be used to find the minimal safety factor for micro stability, which is presented below as a set of equations.

$$\Delta x = \frac{-AD \pm \sqrt{A^2D^2 - ABCD}}{BD} \tag{20}$$

$$A = \frac{2c' \cdot d_{klei}}{\gamma_n \cdot \gamma_d \cdot \gamma_{m,c}}$$

$$B = \frac{\rho_g \cdot g \cdot d_{klei}}{\gamma_n \cdot \gamma_d \cdot \gamma_{m,\rho}} \left(\cos\alpha + \sin\alpha \frac{\tan\phi}{\gamma_{m,\phi}} \right)$$

$$C = \Delta h \frac{\rho_w \cdot g}{\gamma_{m,\rho}}$$

$$D = -\frac{1}{2} \cdot \sin\alpha \frac{\rho_w \cdot g}{\gamma_{m,\rho}}$$

$$SF = \frac{A + B\Delta x}{C\Delta x + D\Delta x^2} \tag{21}$$

Where:

$\tan\phi'$	Tangent of the effective angle of internal friction	$[°]$
$\gamma_{m,\phi}$	Partial safety factor for $\tan\varphi'$	$[-]$
c'	Effective cohesion	$[\mathrm{Pa}]$
$\gamma_{m,c}$	Partial safety factor for c'	$[-]$
ρ_g	Volumetric weight of saturated soil	$[\mathrm{kg/m^3}]$
ρ_w	Volumetric weight of water	$[\mathrm{kg/m^3}]$
$\gamma_{m,\rho}$	Partial safety factor for volumetric weight	$[-]$
α	Inner slope angle	$[\mathrm{rad}]$
g	Gravitational acceleration	$[\mathrm{m/s^2}]$
d	Thickness of clay cover	$[\mathrm{m}]$

Δh	$= (h - z)$ Location of the phreatic line in relation to the height of the inner toe	[m]
Δx	Length measure along the inner slope	[m]
γ_d	Model factor	[−]
γ_n	Damage factor	[−]

This approach is straightforward and can be easily programmed. The input variable that changes is the phreatic level at the inner toe Δh which leads to a varying Δx and SF. When the phreatic level at the inner toe changes over time, the factor of safety will change as well.

Parameters

The set of equations from the previous section have been used to find the parameters to find Δx and SF for different cases of the FPH experiments. The only variable that changes for these cases is Δh, which depends on the water level at the inner toe. For the theory of this analytical approach the assumption is made that the water level at this location is horizontal. The measurements taken from sensor 6 are assumed to approximate this parameter the closest, since this sensor is in the row closest to the inner toe and located in the same plane as the hole. During the FPH experiments, the water level changed at this sensor location over time and varied for the different cases. This will ultimately lead to a time-depending safety factor during filling for each test case.
The constant variables for the test cases are presented in Table 19. The soil parameters $c'$and $\phi'$are not measured in this study and are therefore assumed for a tested sand sample.

Table 19: Input parameters for micro stability assessment

	Parameter	Unit	Value
Soil parameters	c'	[Pa]	600
	ϕ'	[°]	35.3
GSE lab	ρ_g	$[\mathrm{kg/m^3}]$	$2 \cdot 10^3$
FPH experiments	ρ_w	$[\mathrm{kg/m^3}]$	$1 \cdot 10^3$
	d	[m]	0.5
	α	[rad]	0.25
	g	$[\mathrm{m/s^2}]$	9.81
Partial safety factors	γ_n	[−]	1.1
	γ_d	[−]	1.1
	$\gamma_{m,c}$	[−]	1.25
	$\gamma_{m,\rho}$	[−]	1.0
	$\gamma_{m,\phi}$	[−]	1.1

E. Flood Proof Holland

E.1 Leakage paths

E.1.1 Tube with sliding door

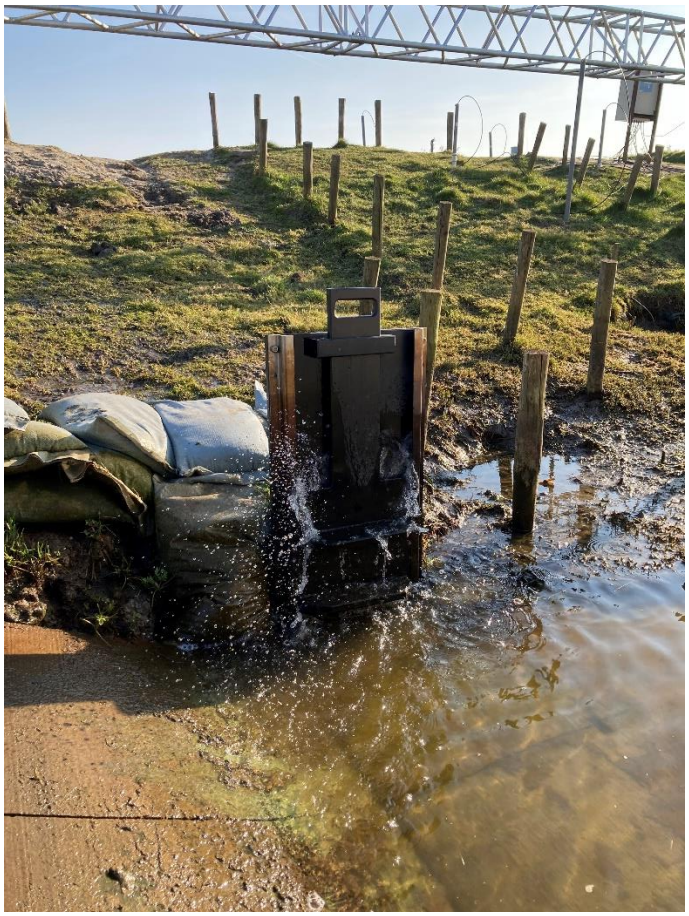

Figure 79: Sliding door of tube which goes through dike. The hydrostatic water pressure from the high-water level in the outer basin causes the sliding door to leak water into the inner basin.

Figure 80: Inner slope of dike where water is present at the dike surface directly above the tube with sliding door

E.1.2 Tubes from previous study

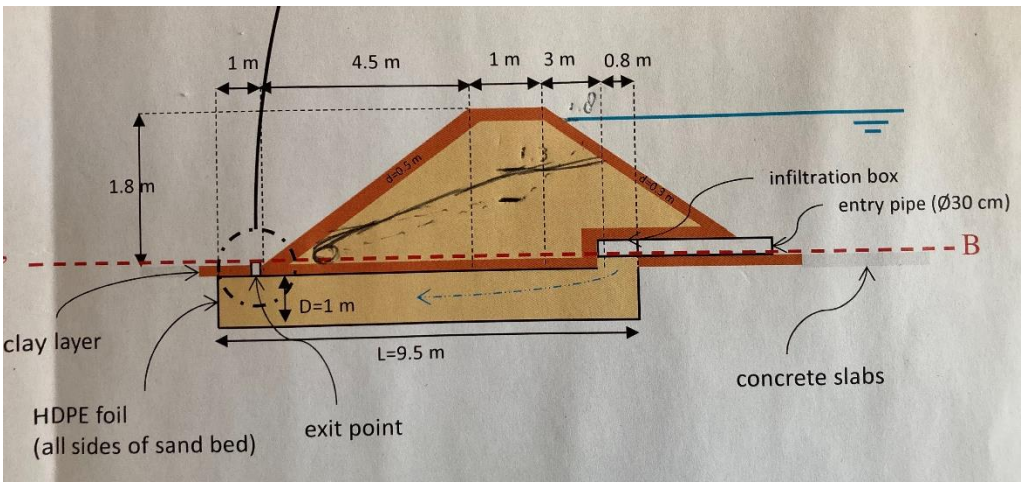

Figure 81: Schematization of previous experiment set-up

Figure 82: Excavated tube with infiltration box

Figure 83: Infiltration box and drain.

E.2 After-construction state of dike

Figure 84: FPH dike right after construction (Picture by Joost Pol)